Impacts of Structural Photomodification of Anthracene Derivatives on the Aquatic Higher Plant *Lemna gibba* (Lemnaceae) Under Actinic Radiation and Modeling of Toxicological Risk

by

Ali Mallakin

A Thesis
Presented to the University of Waterloo
in fulfilment of the
thesis requirement for the degree of
Doctor of Philosophy
in
Biology

Waterloo, Ontario, Canada, 2000

The University of Waterloo requires the signatures of all persons using or photocopying this thesis. Please sign below, and give address and date.

ABSTRACT

The toxicity of polycyclic aromatic hydrocarbons (PAHs) is enhanced by light via photosensitization reactions (production of active oxygen) and photo-modification of the chemicals (e.g., oxidation) to more toxic compounds. Anthracene (ANT) toxicity in particular increases dramatically following photo-modification. The objective of this study was to identify the photooxidation products of ANT and assess the toxicity of selected photoproducts. It was found that PAH photooxidation products likely exist as complex, dynamically changing mixtures in PAH contaminated aquatic environments. High Performance Liquid Chromatography analysis of anthracene photooxidation revealed a complex array of oxidation products; prevalent among these were anthraquinone (ATQ) and hydroxy-anthraquinones (hATQs). Thirteen compounds (ANT, ATQ, a hANT and 10 hATQs) were tested for toxicity reflected by growth inhibition of the duckweed *Lemna gibba* L. G-3. Almost all the ANT photoproducts were directly toxic to *L. gibba*. Light was not a requirement for toxicity of most of the ANT photoproducts. However, in about half the cases, the ATQ compounds were rapidly photooxidized and the resultant photoproducts were more toxic than the parent compounds. Photosynthetic activity was monitored both in vivo and in vitro by measuring chlorophyll *a* (Chl *a*) fluorescence. Impacts on Chl *a* fluorescence were found to correlate with whole organism toxicity for the thirteen compounds used in this study. One Chl *a* fluorescence end point (F_V/F_M, maximal PSII activity) was found to be a measure of acute toxicity. Fluorescence quenching (F_Q/F_M) was found to be a measure of chronic toxicity. Thus, Chl *a* fluorescence was validated as a bioindicator of toxicity of photomodified ANT. Finally, computer analysis was used to determine which shape features of ANT and its photoproducts best correlated with toxicity. It was found that a QSAR could be generated based on computer generated electron density shape maps of the molecules.

ACKNOWLEDGEMENTS

I would like to express my appreciation and gratitude to my supervisory committee, Drs. Bruce Greenberg, George Dixon and Neils Bols for their guidance and assistance throughout this study. I would like to thank Dr. Bruce Greenberg for his comments in editing this thesis.

I would like to acknowledge the information and suggestions gained from Dr. Lynn McCarthy in using computer statistical software in developing the data provided in third Chapter.

Molecular shape study which is presented in Chapter five was performed in collaboration with Dr. Paul G. Mezey and his research group. Extended appreciation goes to Zbigneuf Zimpel for his patience and help in building the structures. My gratitude to Dr. Victor Sniekus and his research group for providing me with the chemicals they synthesized and used in my toxicity studies.

I thank my laboratory colleagues for their collaboration during this study.

A special acknowledgement is given to my parents specially my mother who offered her support throughout my university studies.

TABLE OF CONTENTS

LIST OF TABLES

LIST OF FIGURES

ABBREVIATIONS AND ACRONYMS

$^1O_2$	Singlet state oxygen
$^3O_2$	Ground (triplet) state oxygen
ANT	Anthracene
ASTM	American Society for Testing and Materials
ATQ	Anthraquinone
B[a]P	Benzo [a] Pyrene
BCF	Bioconcentration factor
°C	Degrees Centigrade (Celsius)
chl	Chlorophyll
chl *a*	Chlorophyll a
chl *b*	Chlorophyll b
cm	Centimeter
cyt	cytochrome
d	Day
d	Density
dhATQ	Dihydroxyanthraquinone
DCMU	3-(3,4-dichlorophenyl)-1,1-dimethylurea
DCPIP	2,6-dichlorophenol indophenol
DMSO	Dimethyl sulphoxide
EC_{50}	Concentration of a compound producing an effect in 50% of the exposed organisms
EPA	Environmental Protection Agency
ES	Lowest-energy singlet state
EST	Singlet-triplet splitting energy

ET	Lowest energy triplet state
FLA	Fluoranthene
F_m	Maximum fluorescence
F_v	Variable fluorescence
F_s	Steady state chlorophyll fluorescence
g	Gram
GC	Gas chromatography
>	Greater than
<	Less than
HPLC	High-performance (or high-pressure) liquid chromatography
h	Hour
h_v	Photon
hATQ	hydroxyanthraquinone
kg	Kilogram
K_H	Henry's law constant ($atm.m^3/mol.K$)
K_{oc}	Soil/sediment partition coefficient (organic carbon basis)
K_{ow}	Octanol-water partition coefficient
L	Liter
LC_{50}	Concentration of a compound lethal to 50% of the exposed organisms within a defined period of time
LD_{50}	Dose of a compound lethal to 50% of the exposed organisms within a defined period of time
LOEC	Lowest observed effect concentration
m	Meter
M	Molarity (moles/liter)
mg	Milligram

min	Minute
mL	Milliliter
MW	Molecular weight
NADPH	Nicotinamide adenine dinucleotide phosphate (reduced)
NAF	Naphthalene
NOEC	No observed effect concentration
nm	Nanometer
σ	Sigma
P	Vapour pressure
PAH	Polycyclic aromatic hydrocarbons
Phen	Phenanthrene
ppb	Parts per billion
ppm	Parts per million
PQ	Plastoquinone
PSI	Photosystem I
PSII	Photosystem II
PYR	Pyrene
QA	Primary quinone of PS II
QB	Secondary quinone of PS II
QSAR	Quantitative structure-activity relationship
SSR	Simulated solar radiation
UV	Ultraviolet
UV-A	Ultraviolet at A region [320-400 nm]
UV-B	Ultraviolet at B region [280-320 nm]
Vis	Visible light
V, vol	Volume

Chapter I

Introduction

1.1 Ecotoxicology and Aquatic Environment

The aquatic environment includes several types of ecosystems, such as fresh water streams, lakes, ponds, and rivers, as well as estuaries, coastal zones and deep ocean waters. They have diverse biotic and abiotic components (Rand *et al.*, 1995). The biotic elements consist of combinations of microorganisms, aquatic plants and animals that inhabit specific ecological niches. The abiotic components include physical factors such as water, sediment, and suspended particulate material, all with a range of physico-chemical characteristics. Impacts of xenobiotics and other contaminants on living organisms can be influenced by the physical and chemical properties of aquatic ecosystems. Because aquatic ecosystems involve complex interactions of physical, chemical and biological factors it would be beneficial to understand the relationships among components of these systems. Any environmental assessment will be complicated by the ability of the biotic components to adapt, the diversity of species present in the ecosystem, and the differences in structural and functional responses among the biological components (Drever, 1988; Libes, 1992; Rand *et al.*, 1995).

There is great interest regarding the occurrence of aromatic hydrocarbons in the environment. Among the many classes of aromatic hydrocarbons, polycyclic aromatic hydrocarbons (PAHs) are of particular concern. PAHs (also known as polynuclear aromatic hydrocarbons) include a wide range of naturally occurring and anthropogenic chemicals. Many PAHs are confirmed or suspected carcinogens even at low concentrations (Kennish, 1992; MacKay *et al.*, 1992a). Most PAHs also exhibit significant direct non-carcinogenic cytotoxicity (Huang *et al.*, 1993; Schrimer *et al.*, 1999). Many aquatic organisms can metabolize and detoxify certain PAHs, but some of these compounds become carcinogenic, mutagenic and/or toxic when

metabolically activated (Hawkins *et al.*, 1990). Carcinogenic metabolites have the potential for ecological and human health impacts. PAHs disperse in the water column, concentrate in aquatic biota, and undergo chemical transformation, photochemical oxidation and biodegradation (Katz *et al.*, 1979; Shiaris, 1989; Huang *et al.*, 1995; Mallakin *et al.*, 1999, 2000). Most PAHs in water do not occur in dissolved form but rather are associated with particulate matter. The substantial amount of PAH contamination in the aquatic environment and the potential hazards they pose to the aquatic biosphere motivated this study on their fate, phototoxicity and impacts on aquatic organisms.

Aquatic toxicology is a broad discipline, with concerns for the safety, conservation, and protection of aquatic environments. Researchers in this area study the biological, chemical and physical factors that affect chemical contaminants in the environment to evaluate how potentially toxic agents can act on the biosphere (Butler, 1978; Rand *et al.*, 1995). Contaminants can cause both positive and negative deviations from previously existing conditions, both of which are considered to be adverse in nature. Impacts at the organismal level include both rapid and delayed lethality, as well as sublethal effects on growth, development, reproduction, and tissue structure (Scheehan *et al.*, 1984). Adverse effects at the suborganismal level include induction or inhibition of enzymes, membrane damage, and genetic mutations (Rand *et al.*, 1995). Because exposure to toxic agents may occur via water, sediment, and/or the food chain in the aquatic environment, the quantities and concentrations of toxic agents in these aquatic compartments are of primary concern (Lanno *et al.*, 1989). Furthermore, the sources, transport, distribution, transformation, and ultimate fate of toxic agents in the aquatic environment are important components of aquatic toxicology.

This chapter highlights those aspects of aquatic toxicology pertinent to this thesis, including: the chemical and physical properties of PAHs, the sources and distribution of PAHs, the environmental fate of PAHs, the metabolism of PAHs, the use of plants (particularly *Lemna gibba* L. G-3) as test organisms for toxicity, the role of photoactive PAHs in phytotoxicity, and the use of QSAR relationships to relate biological responses to PAH structure. Finally, the overall objectives of the research reported in this thesis are given.

1.2 Chemical and Physical Properties of Selected PAHs

Polycyclic aromatic hydrocarbons (PAHs) are compounds consisting of two or more fused benzene rings (Neff, 1979). They are normally crystalline solids at room temperature, have high melting and boiling points, and have highly negative resonance energies. Environmental PAHs co-exist with heterocyclic molecules and alkyl substituted homologues. These heteroatomic and substituted compounds are closely related, both chemically and functionally, to PAHs. The relative stability and properties of PAHs are related to their ring arrangement (linear, angular or cluster) and their extensive conjugated π-electron orbital system (Neff, 1979; Cooke and Dennis, 1983; Nakhimovsky, 1989; Mackay *et al.*, 1992a). PAHs are highly hydrophobic and have significant photochemical activity, both of which are key factors in their environmental chemistry. The physical properties of some PAHs have been tabulated (Montgomery and Welkom, 1990) and presented in Table 1.1.

Table 1.1 Physical properties of ANT, ATQ and some hATQs (Montgomery and Welkom, 1990).

Compound	Formula Weight	Solubility in Toluene	Melting Point	Boiling Point	Henry's Law Constants $atm.m^3/mol$	Log Kow	Log Koc	Vapour Pressure	Vapour Density
ANT	178.23	1g/ 100 ml	216-218°C	340°C	2.9×10^{-3}	4.54	4.27	1mmHg/ 145°C	6.15 kg/m^3
ATQ	208.22	0.3 g/ 100 ml	284-286°C	377°C	2.2×10^{-3}	4.69	4.38	1mmHg/ 190°C	7.16 kg/m^3
1-hATQ	224.22	0.08 g/ 100 ml	196-118°C	279°C	1.3×10^{-3}	4.72	4.65	1mmHg/ 195°C	7.96 kg/m^3
1,2-dhATQ	240.21	0.2 g/ 100 ml	279-283°C	430°C	1.2×10^{-3}	4.78	4.40	1mmHg/ 197°C	8.3 kg/m^3
1,4-dhATQ	240.21	0.1 g/ 100 ml	198-199°C	356°C	1.7×10^{-3}	4.23	4.65	1mmHg/ 196°C	8.3 kg/m^3
1,8-dhATQ	240.21	0.1 g/ 100 ml	240.21	345°C	1.1×10^{-3}	4.91	4.72	1mmHg/ 198°C	8.2 kg/m^3
2,6-dhATQ	240.21	0.07 g/ 100 ml	>320°C	330°C	2.0×10^{-3}	4.98	4.69	1mmHg/ 205°C	8.3 kg/m^3
1,2,4-thATQ	226.23	0.18 g/ 100 ml	253-256°C	420°C	1.3×10^{-4}	5.18	4.53	1mmHg/ 199°C	8.0 kg/m^3
1,2,5,8-thATQ	272.21	0.09 g/ 100 ml	>275°C	360°C	2.1×10^{-4}	5.22	5.42	1mmHg/ 210°C	8.5 kg/m^3
1,2,10-thANT	226.23	0.14 g/ 100 ml	279°C	348°C	1.6×10^{-3}	5.16	4.67	1mmHg/ 209°C	8.3 kg/m^3

The vapour pressure of PAH decreases with increasing molecular weight (Neff, 1979; Cook *et al.*, 1983; Mackay *et al.*, 1992a). All PAHs typically demonstrate low aqueous solubilities (e.g. 32 μg/l for naphthalene, 14 μg/l for benzo(a)anthracene) that are inversely related to molecular weight (Montgomery and Welkom, 1990). PAHs with a linear arrangement of aromatic rings are usually less water soluble than those having angular structures. This is illustrated by comparing the solubilities of anthracene (linear 3 ring PAH) and phenanthrene (angular 3 ring PAH), which are 73 μg/l and 1290 μg/l, respectively (Montgomery and Welkom, 1990; Huang *et al.*, 1995). Temperature is an important factor in the solubility of PAHs. The water solubility of anthracene increases from 13 μg/l to 56 μg/l when the temperature is raised from 5°C to 29°C (May *et al.*, 1978). The reduction in aqueous solubility with increasing molecular weight is an important consideration for bioavailability and toxicity of these chemicals in aquatic environment. In numerous studies, low bioavailability has been claimed to be the main factor limiting PAH toxicity and biodegradation (Stucki and Alexander, 1987; Gauger *et al.*, 1990). Selected physical parameters for some PAHs are summarized in Table 1.1.

1.3 Sources and Distribution of PAHs

PAHs are widespread contaminants in natural water bodies (Goerlitz *et al.*, 1985). Production of PAHs results predominantly from the combustion and thermal degradation of organic matter (Suess, 1976; Cook *et al.*, 1983; Morselli and Zappoli, 1988). Sources of PAHs include municipal and industrial effluents, petroleum spills, creosote oil, combustion of fossil fuels, production of steel, and incineration (Cook *et al.*, 1983; Nikolaou *et al.*, 1984). PAHs are present in crude oils, coals and their derived products. The composition of different PAHs in crude oil depends on the source of oil, and usually does not exceed 5% of total hydrocarbons. In contrast, as

much as 85-90% of creosote are PAHs (Nestler, 1974). Although PAHs are released to the environment from natural sources, including forest and grass fires, volcanic activity, as well as seepage from natural oil reservoirs (Bjorseth, 1983), it is generally accepted that anthropogenic sources are responsible for the largest portion of environmental PAHs (Hites *et al.*, 1977). Significant quantities of air-borne PAHs are associated with fine particles, although at high temperatures low molecular weight PAHs may exist in the vapour phase (Bjorseth, 1983). The atmospheric deposition of PAH-containing particles to surface of waters and soils is a significant route of entry for these compounds into the environment. Disposal of aromatic hydrocarbons containing PAHs is another source of environmental contamination by PAHs. For instance wastes from petroleum refining operations and wood-creosoting can enter the environment as a consequence of improper disposal or accidental spillage (Sims and Overcash, 1983; Baek *et al.*, 1991). Overall, industrial impact has resulted in extensive contamination of surface soil and groundwater aquifers with PAHs (Morgan and Watkinson, 1989; Sims *et al.*, 1990).

Another source of PAHs in the environment is biological metabolism. At least some PAHs can be synthesized by bacteria (Knorr and Schenck, 1968; Brisou, 1969), algae (Borneff *et al.*, 1968) and plants (Graef and Diehl, 1966). This phenomenon is not fully elucidated and is considered a minor contribution to total PAH load (Neff, 1979). The formation of a wide variety of quinones and phenols by living organisms has also been reported (Thompson, 1971; Harvey *et al.*, 1985). Production of PAHs by *in situ* chemical aromatization of various cyclic compounds (e.g. terpenoids and pigments) also has been described (Blumer, 1965).

The distribution of PAHs in different environmental compartments has been studied extensively. PAHs have been detected in animal and plant tissues (Blumer,

1976: Jones *et al.*, 1989), sediments (Johnson and Larsen 1985; Lamparczyk *et al.*, 1988, McKee *et al.*, 1990), soils (Wild *et al.*, 1991; Jones *et al.*, 1992), air (Baek *et al.*, 1991; Wild *et al.*, 1992), ground and surface waters (Readman *et al.*, 1984), and consumer products and food (Bjorseth, 1983). PAHs are also present in crude oils, coals and their derived products. PAH compounds associated with oily wastes, such as wastes from petroleum refining operations and waste from wood-creosoting industries, enter the environment as a consequence of improper disposal or accidental spillage. More information on PAH environmental dynamics including sources, distribution patterns, concentration levels is provided in the following comprehensive review papers (Edwards, 1983; Baek *et al.*, 1991).

1.4 Environmental Fate of PAHs

The fate and distribution of PAHs is influenced by many factors including volatilization, sorption, leaching, bioaccumulation, biotransformation and photochemistry. The first four physical processes do not change the structure of PAHs, but concentrate or transfer them to another medium. Chemical transformation of PAHs is often slow without an activating factor such as light.

1.4.1 Transport of PAHs in Air

In aqueous environments, volatilization refers to the transfer of solutes across air-water interfaces into the atmosphere. Many organic compounds can be volatized. The loss of volatile hydrocarbons from water to the atmosphere is a well-known phenomenon, observed especially with oil spills (Readman *et al.*, 1984). The rate of volatilization from the aqueous environment is influenced both by the properties of the compound and environmental factors such as wind, water turbulence and

temperature (Southworth, 1977; Thomas, 1982). Compounds with two benzene rings (e.g. NAF) have a higher vapour pressure relative to PAHs with three or more rings (such as ANT and PYR). For the chemicals that exchange across the air-water interface, there is a point at which volatilization and dissolution rates will be equal. Henry's law describes the ratio of gas- and liquid-phase concentrations under such equilibrium conditions:

$$H_A = [A]_{air}/[A]_{water}$$

Where H_A is the Henry's law constant for solute A. Values of H depend on many environmental parameters, including temperature, wind and current velocity. Values of H increase with increasing temperature in approximate proportion to the increase of the chemical's vapour pressure over the same temperature range. For soluble chemicals, H can be estimated as the ratio of the vapour pressure *(P)* to the water solubility *(S)* of the chemical (i.e. $H \sim P/S$) (Bjorseth, 1983; Mackay, 1991).

For PAHs, Henry's law constants decrease with increasing molecular weight. The rates of volatilization of several PAHs from different aquatic ecosystems have been elucidated (Smith *et al.*, 1978). In general, high molecular weight PAHs such as benzo(a)pyrene and benzo(a)anthracene are relatively non-volatile, with half-lives in water exceeding 100 h, while low molecular weight PAHs such as NAF and ANT are more volatile. Mathematical models are currently available to estimate the rates of volatilization of aromatic hydrocarbons from water. The following equation shows the volatilization flux:

$$N = k\Delta C$$

Where N (mass/area x time) is proportional to the concentration gradient across the

interface, ΔC, and k, which is related to the Henry's law constant and to liquid- and gas-phase mass transfer coefficients (Thomas, 1982).

The mass transfer coefficients reflect both physical and environmental conditions. The former includes molecular diffusion coefficients while the latter describes factors such as wind and current velocity (Thomas, 1982). In many environmental assessments it may be sufficient to determine whether volatilization is an important factor. This may be done by taking field measurements of the air and water concentrations for the chemical of interest and comparing the ratio with measured or estimated values of H (Thomas 1982; Rand *et al.*, 1995). If the field-determined ratio is significantly smaller than H, then the aqueous phase concentration is higher than the equilibrium amount and the chemical will volatilize into the air. If the field-determined ratio is larger than H, the direction of net transport will be from the air to the water. In general it is hard to predict this ratio for PAHs, since they have both low water solubility and volatility. Because of high octanol:water partition coefficients (K_{ow}), adsorption processes are probably more important in determining the fate of PAHs in terrestrial and aquatic systems than volatilization.

1.4.2 Sorption (partition coefficient, K_P)

Considering the relatively high octanol:water partition coefficients (K_{ow}) for most PAHs, sorption to sediments and particles, instead of volatilization, is generally, more important in determining the fate of PAHs in aquatic environments (Bierman, 1990; Ferraro, 1990). The term sorption refers to a variety of processes that result in the transfer of a chemical (A) from the solution phase to solid phase. Sorption is characterized by a partition coefficient (K_p) and the following equation:

$$A_{(solution)} + \text{solid} \leftrightarrows \text{A-solid}$$

Physical adsorption, and several processes involving chemical interaction stated below, are factors in the binding strength of PAHs to particles. As indicated in the equation above, the sorption is an equilibrium process (Lyman, 1995). Sorption of aromatic compounds will be influenced by three processes in the aquatic environment: (1) the transport between the aqueous phase and particulate matter, (2) the electrostatic properties of suspended particles, which affect their aggregation and transport; and (3) the reactivity at surfaces, including dissolution, precipitation onto surfaces, and surface-catalyzed solute reactions.

Sorption characteristics of PAHs can be described as an equilibrium between the aqueous phase and the nonaqueous phase. This can be quantified as a partition coefficient (K_P) for the particular compound (Montgomery and Welkom, 1990). Partition coefficients are related to the physical properties of both the compound and the sorbent material. The ratio of the concentrations in the two phases is the *partition coefficient* of the system. That is, the partition coefficient, K_P, is the equilibrium constant for the equation S (in phase 1)$\leftrightarrows$S (in phase 2) and the partition coefficients is:

$$K_P = [S]_2/[S]_1$$

where $[S]_1$ and $[S]_2$ refer to the concentration of solute in phases 1 and 2 respectively.

PAHs are readily adsorbed to a variety of particulates such as minerals and humic materials (Hinga *et al.*, 1980; Mihelic and Luthy, 1991). High correlations between the sorption of PAHs on to suspended particles and sediments, and the

organic carbon content of the particles have been demonstrated in aquatic systems (Karickhoff *et al.*, 1979; Means *et al.*, 1980). Thus, the concentration of freely dissolved PAHs in natural water columns is normally fairly low, but the total PAH concentration can be quite high if based on the amount bound to suspended particulate matter (Cook *et al.*, 1983; Cooke and Dennis 1983). These bound PAHs generally have high bioavailability in aquatic environments (Rand *et al.*, 1995). Moreover, the PAH concentration in sediment can be very high with concomitant negative effects on benthic biota (Ankley *et al.*, 1994).

1.4.3 Bioaccumulation

All aquatic organisms have the ability to bioconcentrate contaminants (Gobas *et al.*, 1991; Duxbury *et al.*, 1997). Bioconcentration is the process by which chemicals enter organisms and are accumulated or concentrated to levels higher than those in the surrounding environment (Connell, 1988; Rand *et al.*, 1995). Chemicals with low solubility in water (e.g., PAHs) usually have high affinity for biomembranes, and thus can be concentrated in biological tissues to high levels. The bioconcentration factor (BCF) is the ratio of the concentration of a given chemical in a test organism under steady-state conditions relative to its concentration in the water (McCarty *et al.*, 1990; McCarty *et al.*, 1992; Mackay *et al.*, 1992b).

The BCF of organic chemicals is often proportional to their octanol/water partition coefficients (K_{ow}). Thus, this parameter is used as an indicator of the tendency of compounds to distribute between water and biological tissue across cell membranes. The EPA has issued a guideline that a chemical having a log $K_{ow} > 3.5$ which is detected at environmental concentrations > 0.1 μg/l is a concern in terms of bioconcentration (U.S. Code of Federal Regulations, 1991). Since intact PAHs are

hydrophobic with high K_{ow} values, they will rapidly transfer from the aqueous phase into cell membranes until the ratio of the lipid:water concentrations is equal to the equilibrium constant for partitioning between lipid bilayers and aqueous media (Gobas, 1991; Duxbury *et al.*, 1997). Two factors can greatly alter PAH bioaccumulation. First, the high molecular weight PAHs have such low aqueous solubility that they can have limited bioavailability. Secondly, photooxidation of PAHs increases their water solubility and consequently increases bioavailability and bioaccumulation. PAHs have a strong tendency to accumulate in biological membranes and have high BCFs (Duxbury *et al.*, 1997). As well, they can be taken up by biota from sediment phases (Ankley *et al.*, 1994).

1.4.4 Bioavailability of PAHs

Bioavailability is a critical concept in toxicology because toxic agents that are present in the environment but which are not available for assimilation are unlikely to be hazardous. Landrum *et al* (1994) and Rand *et al* (1995) have discussed working definitions for:

Environmental availability is the amount of contaminating chemicals present in the environment or in the part that can be involved in any process. It can be modified by physical, chemical or biological modifying means. In general, this term defines the total amount of a given chemical potentially available for any environmental process.

Environmental bioavailability is the portion of a chemical that an organism actually accumulates when encountering a given environmental medium. This is a measure of an organism's uptake efficiency from the environmentally available

portion of a contaminant. This concept can be viewed as a subset of environmental availability where an organism actually encounters some of the material in question. Thus, environmental bioavailability incorporates the chemical properties and speciation of the chemical, as well as the behaviour and physiology of the organism.

Toxicological bioavailability is the part of the exposure dose or concentration, which is adsorbed and/or absorbed by an organism, and presented to sites of toxic action. Environmental bioavailability and toxicological bioavailability are similar in that both are estimates of an up-take efficiency. Environmental bioavailability addresses the total amount adsorbed by an organism, whereas toxicological bioavailability considers the amount that reaches the site(s) of toxic action.

Mathematical modeling can be used to integrate data on complex mechanisms such as transport and transformation processes, transfer between environmental media, and biological uptake into an effect profile for an environmental contaminant (Jorgensen, 1990; Calamari, 1993; James, 1993). Models may be used to predict the bioavailable concentrations of the chemical in the aquatic environment, the potential exposure areas, and the fate of the chemical (Samiullah 1990; Mackay, 1991). The use of some mathematical models in environmental toxicology is described in more detail below (see Section 1.9).

PAHs generally have high log K_{ow}'s and are therefore subject to rapid accumulation by any given organism. However, due to their low solubility, they have limited availability in the water column. Conversely, there is higher availability to aquatic organisms via sediment and suspended particles. As one would expect, the BCF for PAHs is strongly log K_{ow} dependent (Gobas *et al.*, 1991; Djomo *et al.*, 1996; Duxbury *et al.*, 1997).

1.4.5 Photochemistry of PAHs

The more water-soluble bicyclic and tricyclic PAH are not carcinogenic, but recent studies indicate that light activates these and other PAHs into acutely toxic compounds (Oris and Giesy, 1985; Huang *et al.*, 1993; Krylov *et al.*, 1997; McConkey *et al.*, 1997; Mallakin, *et al.*, 1999). The high energy π-bonding orbital and relatively low energy π^* anti-bonding-orbital of PAHs leads to the strong absorption of UV radiation (200-400 nm) and short wavelength visible light (400-500 nm), with the concomitant transition of an electron from the π- to π^*- orbital (Nakhimovsky, 1989). Excited state PAHs can act as photosensitizers or be photomodified. Both of these processes result in enhanced toxicity of PAHs.

Photosensitization by a chemical can result in formation of highly toxic singlet state oxygen ($^1O_2$) (Foote, 1991; Krylov *et al.*, 1997). The process begins with the molecule absorbing a photon, which elevates it to the excited singlet state. From the singlet excited state the molecule may be converted to the excited triplet state by intersystem crossing (Foote, 1987; Newsted and Giesy, 1987). In this state it can react with ground state triplet oxygen to form excited singlet state oxygen.

In the presence of light, strong oxidants, or certain oxidases (e.g. cytochrome P-450), PAHs are rapidly and efficiently converted to ketones, quinones and diols (Cavalieri, 1990; Huang *et al.*, 1995; Mallakin *et al.*, 1999, 2000). Modified PAHs, being hydrophilic, reactive, soluble, bioavailable and electrophilic, may bind covalently to cellular structures such as proteins and DNA causing long term damage (Kim and Sancar, 1993; Imlay and Fridovich, 1992). Because many modified PAHs are more toxic than intact PAHs, acute toxicity based on intact PAHs alone does not adequately reflect the potential impacts of PAHs in the environment (Huang *et al.*,

1995; McConkey *et al.*, 1997; Mallakin *et al.*, 1999). For instance, ANT was oxidized to ATQ, hATQs, benzoic acid, benzaldehyde and phenols in the presence of actinic light (Figure 1.1). Many of these compounds are toxic (Mallakin *et al.*, 1999, 2000).

Studies in an outdoor model ecosystem indicated that photochemical transformation is an important process for several PAHs (Cook *et al.*, 1983). Both direct and indirect (photosensitized) oxygenation may be important. Direct photooxygenation is initiated through light absorption by the PAHs. Indirect photooxygenation occurs via light absorption by another chemical that is present in addition to the aromatic compound that is oxidized. It has been generally accepted that singlet state oxygen is the key intermediate in photooxygenations of PAHs (Young and Brewer, 1976; Halliwell and Gutteridge, 1985). Most likely the $^1O_2$ that is generated by the excited state PAH in turn is used to oxidize a PAH molecule. Kinetic data for the photooxidation of PAHs in water could be described by a pseudo first-order rate equation (Krylov *et al.*, 1997). The half lives for PAHs in solar radiation range from 15 min for ANT to 2-3 d for B[a]P and FLA (Huang *et al.*, 1995). Oxidation quantum yields, ϕ_{AO2}, were computed from the slopes of the first-order degradation plots (Zepp and Schlotzhauer, 1979; Krylov *et al.*, 1997). Quantum efficiencies can be determined at a wavelength that closely corresponds to that of maximum sunlight absorption by the PAH.

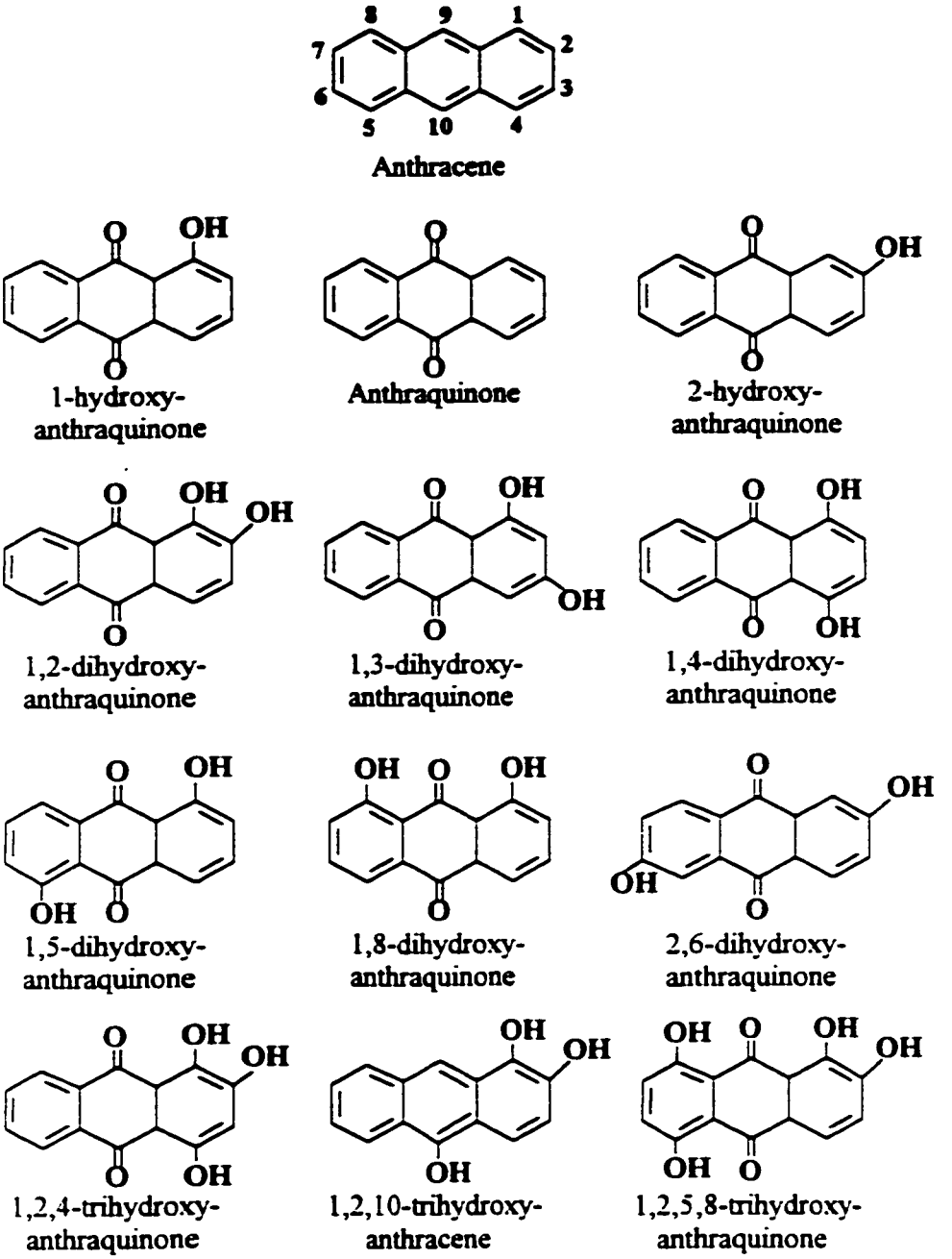

Figure 1.1 Structures of anthracene and its photoproducts used in this study. These compounds were identified in work described in Chapter 2.

Most of the quantum yields were in the 0.001 and 0.01 range (Nakhimovsky, 1989). More detailed wavelength studies were conducted with pyrene and fluoranthene. The disappearance quantum efficiency of pyrene exhibited a wavelength independence. However, ϕ_{AO2} for fluoranthene can drop sharply in going from 300 to 400 nm (Huang *et al.*, 1993; Krylov *et al.*, 1997). The photooxidation of dissolved PAHs appears to be relatively rapid under both laboratory and natural solar radiation, with half-lives ranging from 30 minutes to 23 days, depending upon the compound and the photolytic conditions. Half-lives determined from photooxidation in sunlight irradiation have been reported to be shorter by approximately 20-60% (Huang *et al.*, 1995).

The following equation for quantum yields for photooxidation has been elucidated (Stevens *et al.*, 1974):

$$\phi_{AO2} = \phi_T \{([A] + pB)/([A] + B\}$$

The term ϕ_T is the intersystem crossing efficiency, B is a reactivity index that is inversely proportional to the rate constant for reaction of singlet oxygen with the aromatic compound, and pB is a solvent-dependent constant that approximately equals 8×10^{-5} mole/L in water (Stevens, 1974). Quantum efficiencies for reaction of naphthalene, anthracene, pyrene and naphthacene were observed to be lower in organic solvent than in water, indicating that the observed reaction is dependent on solvent polarity. This solvent effect suggested that the reactions in water may be initiated by electron transfer to oxygen (a "type I" photooxidation) which would be enhanced in polar solvents (Foote, 1991). However, type II photosensitization reactions involving $^1O_2$ are probably as or more important, especially since the rates of photooxidation are proportional to the triplet state quantum yield (Q_Y) (Foote, 1987).

Photochemical reactions of PAHs in the environment appear to represent a major mode of transformation of these chemicals. In the case of PAHs in the atmosphere, photochemical oxidation reactions in the presence of sunlight result in a variety of products, including some of the phenols and quinones shown in Figure 1.1 (Katz, 1979). Recently, the pattern of photooxidation of ANT, B[a]P and other priority PAHs has been studied (Huang *et al.*, 1995; McConkey *et al.*, 1997; Mallakin *et al.*, 2000). Attempts have been made to relate the electronic structure of PAHs to their properties of photooxidation (Mezey *et al.*, 1996). The fundamental electronic properties of PAHs and possible correlations with toxicity and carcinogenecity have been the origin of the K- and L-region structural hypothesis. The prototype of this structural element is the 9,10-carbon bond in phenanthrene, called the K-region of the molecule. The L-region is typified by the 9,10 positions in anthracene. L-region photochemical reactions at the 9,10 positions of anthracene, in the absence of oxygen, give Diels-Alder photoadducts at these positions (Lee *et al.*, 1981). In the presence of oxygen, the L-region photoreacts to form quinones (Figure 1.1). K-region photoreactions in phenanthrene also result in photooxidation to form the 9,10-quinone (Katz *et al.*, 1979; McConkey *et al.*, 1997). L-regions are generally much more photoreactive than the K-regions because they have much lower electron density (Mezey *et al.*, 1996). Thus, if PAHs are present in an environmental compartment exposed to solar radiation, there is the potential for photomodification. Because the toxicity attributable to PAHs is derived from the products of photomodification, hazard assessment of PAHs in the natural environment should be based not only on levels of parent compound, but also on levels of the associated photoproducts.

1.5 Toxicity of Xenobiotics to Plants

Chemical contaminants and habitat loss are major concerns facing our environment today (Brody *et al.*, 1993; McVey *et al.*, 1993). Because of the significant role of plants in the biosphere, it is critical to include plants when assessing the environmental change (Fletcher, 1990; Hinman and Klaine, 1992; Brody *et al.*, 1993; Barnthouse and Brown, 1994). Plants are primary producers, supporting almost all other life forms. They provide an active role in transferring contaminants to higher trophic levels (Manny and Kenaga, 1991; McVey *et al.*, 1993). Plants also influence habitat by providing cover, stabilizing the soil and sediment, and regulating the temperature and flow of water. Whole plant communities can be irreversibly altered when exposed to anthropogenic stressors (Outridge and Noller, 1991). These changes can have significant direct and indirect effects on higher organisms, which may persist after the original stressor has been, attenuated (Lovett Doust *et al.*, 1993; Peterson and Nyholm, 1993). Thus, plants are a relevant kingdom for toxicity assessment of PAHs.

Plants are more sensitive than animals to some xenobiotics (e.g. herbicides) (Wang and Freemark, 1995). Also, within the plant community, plant species differ in their sensitivity to given contaminant classes (Fletcher *et al.*, 1990). The most commonly used group of aquatic plants for phytotoxicity tests are the algae (Benenati, 1990). Because of the ecological relevance of plants and the observed differences in species response to stressors, aquatic plants should be considered when making environmental decisions.

Plants can be used as field biomonitors (Barnthouse and Brown,1994; Outridge and Noller, 1991; Lovett Doust *et al.*, 1994; Weinstein *et al.*, 1990). They readily

lend themselves to bioindicator measurements, such as photosynthetic activity. Use of plants as biomonitors can be divided into two categories. The first group are indigenous organisms, which are the plants that are already present in the field (Chaphekar, 1991; Lovett Doust *et al.*, 1994). Using indigenous species can provide valuable information regarding the distribution of contaminants and how they will act on native environments. The second group of biomonitors consist of organisms that are either cultured in the laboratory or collected from a noncontaminated reference site, and used in contaminated environments or the laboratory for the designated period of time (Chaphekar, 1991; Lovett Doust *et al.*, 1994). The latter type of the system allows for the exposure time and chemical dose to be carefully controlled.

Plants possess many characteristics, that make them good test species for toxicology. Plants, and particularly aquatic plants, are easy to grow and relatively inexpensive to maintain (Wang, 1991). They are also subject to a variety of contaminant exposure routes (Walsh *et al.*, 1991). They can be grown from seed, or clonal colonies (Lovett Doust *et al.*, 1994). Plants provide the necessary amount of tissue for assessment of chemical stress, and plants can be readily used in life-cycle assessment of toxicants (Weinstein *et al.*, 1990; Walsh *et al.*, 1991).

1.6 Use of *Lemna gibba* for Phytotoxicity Assessment

Lemna gibba L.G-3 (common duckweed) was chosen for this research to study the toxicity of PAHs on higher plants. *Lemna gibba* is a member of the Lemnaceae, a group of fast-growing freshwater higher plants (Landolt and Kandeler, 1987). This C-3 monocot has world-wide distribution and is a key component of aquatic food webs (Krull, 1969; Fassett, 1972; Hillman and Culley, 1978). Several genera of the Lemnaceae (*Lemna, Spirodela,* and *Wolfzia*) have been used in laboratory toxicity

assessment studies (Hughes *et al.*, 1988; Wang 1990; Greenberg *et al.*, 1992). Lemnaceae have a high capacity for the assimilation of a wide range of organic chemicals and can represent an important entry point for numerous contaminants into the biosphere (Rodgers *et al.*, 1978; Culley *et al.*, 1981; Tridech *et al.*, 1981; Muir *et al.*, 1985; Greenberg *et al.*, 1992). The high bioconcentration capacity of the Lemnaceae suggests that they could be useful for bioremediation (Greenberg *et al.*, 1992; Duxbury *et al.*, 1997). With *L. gibba*, growth is readily assessed during toxicity tests as production of new leaves. Because the plant naturally propagates clonally, this represents a life-cycle test. *Lemna gibba* can also be used for photosynthetic measures of impacted plants (Huang *et al.*, 1997a; Gensemer *et al.*, 2000).

1.7 Modes of Action and Impacts of Photoactive PAHs to Plants

PAHs strongly absorb blue light and UV radiation, and show enhanced phytotoxicity in the presence of actinic radiation (Schoney *et al.*, 1988; Huang *et al.*, 1993). Photooxidation of the compounds increases the phytotoxicity of the chemicals relative to intact PAHs (Huang *et al.*, 1993, 1997a). The extent that photoactive compounds can be transported in the environment and affect plants is not clear. However, as pollutants are transported through aquatic systems, they will be exposed to solar radiation. Thus, PAHs are likely to photooxidize in aquatic environments and influence plants such as *L. gibba*.

As discussed above, photoinduced toxicity of PAHs to plants involves two photochemical processes: photomodification and photosensitization (Huang *et al.*, 1993; Krylov *et al.*, 1997). Photomodification of PAHs (generally oxidation) results in the formation of new photoproducts that have altered biological activity (Larsen

and Barenbaum, 1988; Huang *et al.*, 1995; Mallakin *et al.*, 1999). Photosensitization results in the formation of highly toxic singlet state oxygen ($^1O_2$) (Larson and Berenbaum, 1988; Foote, 1991). The photosensitization and photomodification processes contribute additively to toxicity of PAHs to *L. gibba* (Krylov *et al.*, 1997). Toxicity studies with *L. gibba* have shown that photooxidized PAHs inhibit growth and photosynthetic activity, and result in chlorosis (Greenberg *et al.*, 1992; Huang *et al.*, 1993). PAHs and oxyPAHs accumulate in plant membranes (Duxbury *et al.*, 1997), which is consistent with their mode of action being predominantly at photosynthesis (Huang *et al.*, 1997a).

1.8 Effect of Xenobiotics on Photosynthetic Activity

Photosynthetic activity is responsive to many changes in environmental conditions, including the effect of xenobiotics. Photosynthesis can be readily measured by $^{14}CO_2$ incorporation, oxygen evolution or Chl *a* fluorescence induction (Jones *et al.*, 1984; Hill *et al.*, 1997). The effects of petroleum hydrocarbons (Gaur and Singh, 1990), metals (Turbak *et al.*, 1986), complex mixed industrial effluents (Delistraty, 1986), PAHs (Huang *et al.*, 1997a) and herbicides (Trebst and Harth, 1974; Jones and Winchel, 1984) on photosynthetic activity have been studied using these techniques. Two key advantages of using photosynthesis for toxicity assessment are the short duration of the test (seconds to minutes), and the short toxicant exposure times required for effects (30 min to 48 h) (Kuivasniemi *et al.*, 1985; Versteeg, 1990). There is interest in the practical application of Chl *a* fluorescence as a rapid, sensitive bioindicator for the determination of different environmental factors on plants (Papageorgiou, 1975; Lavorel and Etienne, 1977; Gensemer *et al.*, 1996). This technique permits the rapid determination of changes in photosynthetic activity before the appearance of visible injury (Baker *et al.*, 1983).

Many studies have demonstrated the potential of Chl *a* fluorescence measurements as a bioassay of xenobiotic impacts (Lower *et al.*, 1984; Judy *et al.*, 1990a,b, 1991; Gensemer *et al.*, 1996; Huang *et al.*, 1997a). Illumination of a dark adapted leaf by light of a proper wavelength gives a characteristic Chl *a* fluorescence emission kinetic, known as the Kautsky effect (Figure 1.2) (Kautsky and Hirsch, 1934). Chl *a* fluorescence induction kinetics give several parameters as follows (Van Kooten and Snel, 1990):

1. F_O is the initial fluorescence level that is reached immediately after illumination. This value characterizes a dark-adapted leaf when most PSII reaction centers are open and the primary acceptor of PSII, quinone A (Q_A), is fully oxidized.
2. F_M is the maximal fluorescence measured when the plastoquinone (PQ) pool becomes fully reduced and thus Q_A is reduced.
3. F_V, variable fluorescence, is the difference between Fo and Fm.
4. F_V/F_M is related to the efficiency with which electrons are passed through PSII It is proportional to maximal PSII activity. It commonly has a value close to 0.7 to 0.8 and drops when PSII is inhibited or damaged.
5. $t_{1/2}$ is half of the length of time required for the fluorescence level to rise from F_O to F_M. It is a measure of the size and accessibility of the electron acceptor pool (PQ pool). It drops when PSII is blocked before the PQ pool, such as at Q_B.
6. F_{SI} is the first intermediate quenching phase (first shoulder). This fluorescence drop is due to electron transport downstream from PSII.
7. F_Q, the fluorescence quenching capacity of the system, is the difference between F_M and F_{SI}.
8. F_Q/F_M measures the utilization of PQH_2 by cytochrome-b6/f and/or PSI; it decreases when electron transport after the PQ pool is blocked.
9. F_T is the terminal steady state Chl *a* fluorescence.

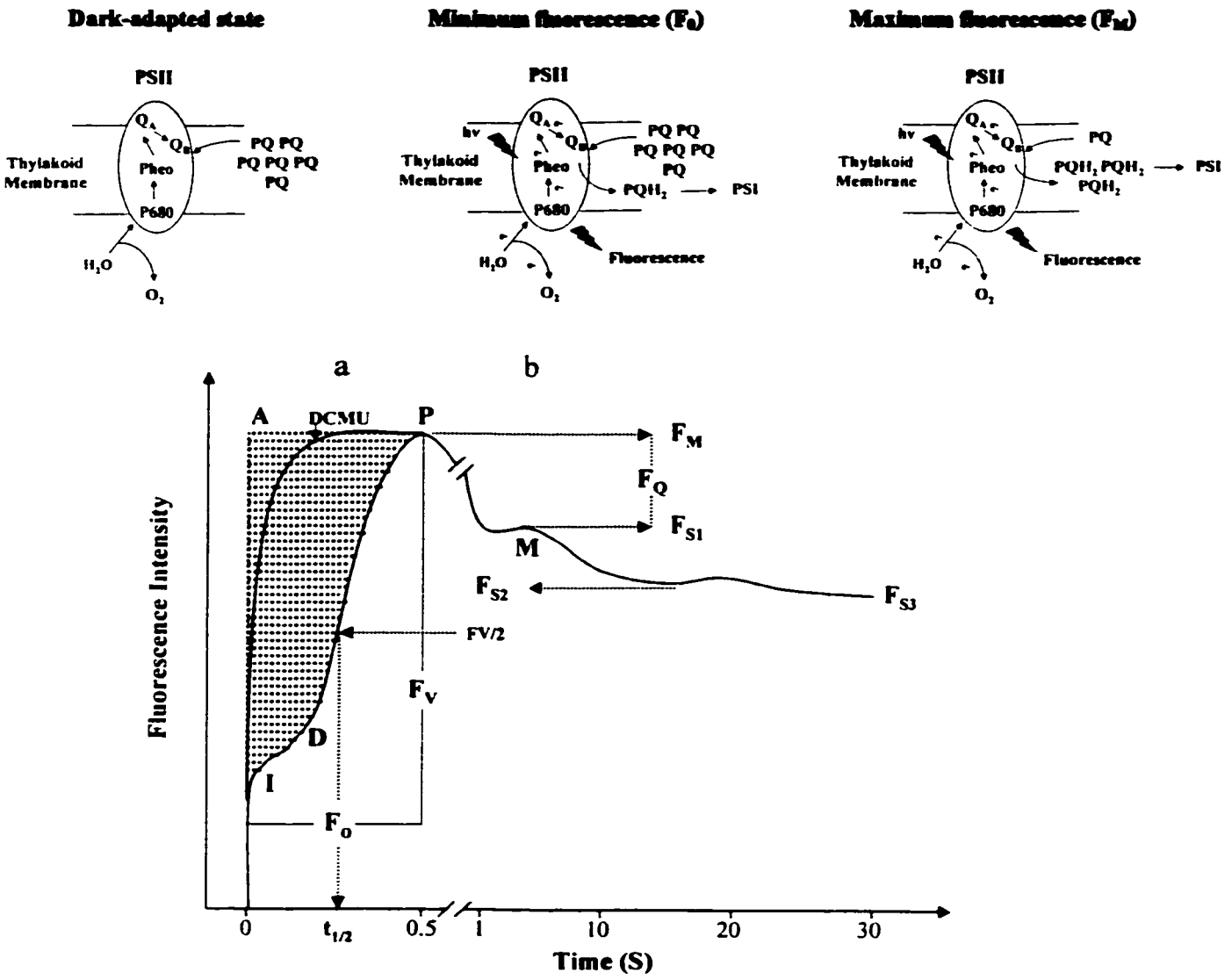

Figure 1.2 A typical Chl *a* fluorescence induction (or Kautsky) curve recorded from a dark-adapted plant. a, fast kinetics; b, slow kinetics; A , area above the curve; F_0, minimal initial fluorescence; I, inflection or intermediate level; D, dip or plateau; P, peak level; F_M, maximal fluorescence at peak; F_V, variable fluorescence; $t_{1/2}$, half rise time from F_O to F_M, M, secondary maximum; DCMU, (3-(3,4-dichlorophenyl)-1,1-dimethylurea) fluorescence scan with DCMU (at 5 μM). The first Fluorescence quenching phase (F_{S1}), and the difference between F_M and F_{S1} (F_Q). The second and third fluorescence quenching (F_{S2} and F_{S3}) are also shown.

10. **The area above the curve between F_O and F_M is proportional to the pool size of the electron acceptors on the reducing side of PS II.**

Any changes in electron transport may be reflected by changes in the Chl *a* fluorescence pattern, and provides information into how well the photosynthetic apparatus is functioning. Inhibitors or stress conditions usually change one or more Chl *a* fluorescence parameters. If electron transport on the oxidizing site of PSII is blocked, the level of fluorescence will decrease. If the electron transport chain is inhibited at the reducing site of PSII, steady fluorescence yield will increase and quenching will be inhibited (Hill *et al.*, 1997). Overall, the site of inhibition within the electron transport chain can be predicted (Krause and Weis 1984; Miles, 1990). Electron transport in chloroplasts proceeds from H_2O through PSII to the plastoquinone (PQ) pool, and then through PSI to nicotinamide adenine dinucleotide phosphate ($NADP^+$) (Hall *et al.*, 1987; Greenberg, 1991). When electron transport downstream from PSII is inhibited, electron transport from PSII to PSI will also be blocked because the PQ pool will be reduced and remain in that state. This will lower $t_{1/2}$ and F_Q/F_M, and will ultimately result in permanent oxidative damage to PSII as a consequence of excitation pressure of chlorophyll without the possibility of transferring the energy into the electron transport chain (Gray *et al.*, 1996; Huang *et al.*, 1997a).

The chemical 3-(3,4-dichlorophenyl)-1,1-dimethylurea (DCMU) blocks electron transport at the Q_B site and the area above the fluorescence curve is strongly decreased because no re-oxidation of Q_A can occur (Anderson *et al.*, 1987). A study with photomodified anthracene revealed that the mechanism of toxicity action starts with inhibition of PSI or the cytochrome-b6/f complex, followed by photooxidative damage to PSII. The effects of modified ANT were discovered by Chl *a* fluorescence

studies (Huang *et al.*, 1997a). Thus, Chl *a* fluorescence was able to detect the impact of a mixture of photomodified ANT products and indicate a possible mechanism of action for the chemicals (Huang *et al.*, 1997a). In this thesis, Chl *a* fluorescence is used to examine the impacts of specific ANT photomodification products.

1.9 Structure-Activity Relationships

The application of quantitative structure activity relationship (QSAR) to environmental toxicology has been reviewed extensively (Kaiser, 1984; Hermens, 1987; Turner *et al.*, 1988; Nendza, 1991). QSARs were initially used in the design and development of new drugs and pesticides (Martin *et al.*, 1990; Tute, 1990; Kubinyi, 1993). QSARs are based on the premise that the structure of a chemical will influence the type and potency of its biological action. Resultant biological effects are the result of interaction between the chemical and one or more receptors within a living system. QSARs relate chemical structure and interaction of a receptor to well-defined biological endpoints (Lipnick *et al.*, 1993). They define the limits of variation in structure of a chemical moiety that are consistent with the production of a specific biological effect, and indicate the ways in which alterations in structure influence toxic potency (Purcell *et al.*, 1973; Albert, 1985).

QSAR models can be used for the estimation of rates of hydrolysis, photolysis, volatilization, soil sorption, and biodegradation, as well as determination of water solubility, octanol-water partition coefficients, acid dissociation constants, bioaccumulation and bioconcentration (Mackay and Paterson, 1990; Shimp et al., 1990; Sabljic, 1990; Dearden and Nicholson, 1991; Chessels et al., 1992; Krylov *et al.*, 1997). Partition coefficients are often related to the toxicity of simple hydrophobic compounds, since they predict how well the compounds will be taken

up by a biological organisms (tissue burdens), a prerequisite for toxicity. As such, partition coefficients are an important descriptor in modelling environmental fate and transport processes. They can be related to water solubility, soil-sediment sorption and bioaccumulation (Tanford, 1980; Valvani and Yalkowsky, 1980; Taylor , 1990). One coefficient, log K_{ow}, is often well correlated with toxicity, especially in the absence of modifying factors (such as light) (Leo *et al.*, 1975).

The development of modern QSAR methods for environmental toxicology was initiated by Hansch *et al* (1989), who regressed the logarithm of the octanol-water partition coefficient (log K_{ow} or log *P*) against enzyme inhibition as well as cellular, and whole-animal toxicity data (Hansch and Leo, 1979; Leo *et al.*, 1991). The general form of the Hansch equation describes the influence of substituents (structure-related parameters for modeling hydrophobic, electronic, and steric properties that influence log K_{ow}) on the biological activity of a parent molecule.

A large number of QSAR models have been used to predict the effects of chemicals on aquatic organisms based on bioaccumulation. The narcotic organic chemicals (e.g. alcohols, ketones, ethers, chlorinated alkanes, and aromatics) are the largest group to which QSARs have been applied to different test species and end points (Lipnick, 1995). The QSAR equations applied to toxicity data have the general form,

$$\text{Log } 1/C = a \log K + b$$

Where *K* is the sole chemical descriptor related to hydrophobicity of the molecule. The constants *a* and *b* are empirically derived constants and *C* is the molar concentration of a chemical that is toxic. The following generalization can be made from the above QSAR equation. The constants *b* is a measure of test species or effect

sensitivity, and describes differences in species sensitivity to chemicals (Call *et al.*, 1985; Hermens *et al.*, 1989). Above a certain K_{ow} toxicity often decreases because very hydrophobic molecules are not bioavailable. In this case results can be modeled using parabolic or bilinear models (Kubinyi and Kehrhahn 1978; Veith *et al.*, 1983; Lipnick *et al.*, 1987a,b).

In developing a QSAR model, it is essential to consider the impacts of the environmental compartments in which the contaminant of interest resides. This will define which physicochemical properties are likely to be most influential in toxicity. Because solar radiation is ubiquitous in the environment and can enhance the toxicity of PAHs, solar radiation is a factor that should be used in QSAR modeling of PAH toxicity (Larson and Berenbaum, 1988; Krylov *et al.*, 1997; Huang *et al.*, 1997b). A detailed model relating structural features of PAHs to their phototoxic strength has been previously demonstrated (Mezey *et al.*, 1998). This latter QSAR approach was applied to PAH toxicology using the electron densities of the molecules, which describe the reactivity of the molecules. Detailed electron shape density maps can be built by computer techniques and they provide an accurate description of the shape of the electron cloud (Mezey, 1995). In this thesis, based on this methodology, three-dimensional electron densities and shape analysis were applied to the toxicity of ANT, ATQ and eleven hATQ molecules to *L. gibba* (Chapter 5).

1.10 Objectives of the Current Study

Toxicity of oxyPAHs is a potentially important environmental phenomenon (Huang *et al.*, 1997a; McConkey *et al.*, 1997; Mallakin *et al.*, 1999). It seems almost certain that oxyPAHs will be present in PAH contaminated environments where sunlight is present. PAHs are oxidized so rapidly in sunlight, that oxyPAHs could be

more abundant than intact PAHs at certain sites (Huang *et al.*, 1995). ANT in particular is very rapidly oxidized to a variety of products (Huang *et al.*, 1997a, Mallakin *et al.*, 1999, 2000). The mechanism of toxicity has been investigated for mixtures of oxyPAHs, and QSAR models explaining and predicting phototoxicity in intact PAHs have been generated (Huang *et al.*, 1997a,b; Krylov *et al.*, 1997). QSAR modeling of the phototoxicity process of PAHs has shown that photooxidation of PAHs is a key factor in describing their phototoxicity. Although, on a relative scale, oxyPAHs are more polar than intact PAHs, they are still hydrophobic and accumulate in biological membranes (Duxbury *et al.*, 1997). It is thus significant that a mixture of ANT photoproducts inhibit photosynthetic electron transport (at cytochrome-b6/f) in chloroplast thylakoid membranes. However, prior to this study specific products of ANT photomodification had not been systematically examined for toxicity.

Because ANT is an abundant PAH, one of the most rapidly photooxidized PAHs and numerous photoproducts are generated (Huang *et al.*, 1997a; Mallakin *et al.*, 1999, 2000), it is highly likely that modified ANT will exist in aquatic environments. Thus, ANT and its photooxidized derivatives were chosen for this study. The specific objective of this thesis was to identify the ANT photooxidation products and probe their toxicity using growth and photosynthetic endpoints with *L. gibba*. In the initial part of this research the photoproducts of ANT were identified and the toxicity of the individual products was determined. The first goal was to study the pathway of ANT photooxidation (Chapter 2). The second goal was to test the toxicity of the identified ANT photooxidation products at the whole organism level (Chapter 3). The third objective was to probe the mechanism of photoinduced toxicity of specific photooxidation products of ANT (Chapter 4). The final objective was to develop computer modeling techniques to explain and predict the toxicity of oxyPAHs, allowing preliminary predictions of the toxicity of untested compounds (Chapter 5).

Chapter II

Pathway of Anthracene Modification Under Simulated Solar Radiation[1]

---

[1] This paper is appeared in *Chemosphere*. 2000, Vol 40(12), 131-137, and authored as Ali Mallakin, D. George Dixon, and Bruce M. Greenberg.

2.1 Introduction

Polycyclic aromatic hydrocarbons (PAHs) are one of the most prevalent groups of aquatic environmental contaminants (Neff, 1979; Cook *et al.*, 1983). Without an external stimulus, PAHs are extremely stable compounds (Neff, 1979; Krylov, *et al.*, 1997), making them a persistent environmental problem (Basu and Saxena, 1978). Due to their extensive π-orbital systems, PAHs absorb sunlight in the visible (400-700 nm) and the ultraviolet regions (290-400 nm) of the solar spectrum (Nikolaou *et al.*, 1984; Huang *et al.*, 1993). Photooxidation of PAHs is a potentially important pathway for PAH modification in the environment (Katz *et al.*, 1979; Huang *et al.*, 1993). Upon absorbing sunlight, a PAH can be rapidly transformed to a variety of compounds, most of which are oxidation products. Compounding the problem, the photooxidation products of PAHs are in many cases as or more toxic than, the parent compounds (Krylov *et al.*, 1997; McConkey *et al.*, 1997; Mallakin *et al.*, 1999). Clearly, it is important that the modification pathways of PAHs are well understood. This will indicate which by-products are likely to accumulate in the environment allowing for more realistic analysis of the environmental implications of PAH loads.

In this study, anthracene (ANT) was chosen for a detailed investigation of a PAH photomodification pathway. Upon exposure to natural or simulated solar radiation, ANT undergoes rapid photooxidation with high quantum efficiency (Katz *et al.*, 1979; Krylov *et al.*, 1997). This is because it absorbs strongly in the UV-B (290-320 nm) and UV-A (320-400 nm) spectral regions found in sunlight, and its central ring has low π-orbital stability, making it susceptible to attack by O_2 (Mezey *et al.*, 1998). Further, the ANT photomodification pathway results in many toxic products (Huang *et al.*, 1997a; Mallakin *et al.*, 1999). Indeed, we recently found that several specific photoproducts of ANT (anthraquinone and hydroxyanthraquinones)

to be as toxic as ANT (Mallakin *et al.*, 1999). In this study, we characterized the photooxidation products of ANT to derive a complete environmentally relevant photomodification pathway based on kinetic data for ANT photooxidation and product formation. It was found that ANT is modified to 9,10-anthraquinone (ATQ) likely via an endoperoxide intermediate. ATQ is then hydroxylated forming hydroxyATQs (hATQs), and ATQ, along with some of the hATQs, are subject to ring fission to form a complex mixture of various phenols, benzaldehydes and benzoic acids. This work represents the most complete analysis of a PAH photomodification pathway to date.

2.2 Material and Methods

2.2.1 Chemicals

The structures of anthracene and the identified photoproducts along with their abbreviations are given in Figure 2.1. ANT was purchased in high purity (Sigma Chemical Co., St. Louis, MO) and used as received. The other compounds were purchased (Aldrich, Milwaukee, WI; or Sigma Chemical Co., St. Louis, MO) or synthesized as previously described (Mallakin *et al.*, 1999). Solvents employed were HPLC-grade acetonitrile (Aldrich, Milwaukee, WI) and reagent-grade dimethyl sulphoxide (BDH Inc., Toronto, Ontario). Water was purified by reverse osmosis (RO) (Barnstead, Dubuque, IO). Reagent-grade phosphoric acid was used to adjust pH.

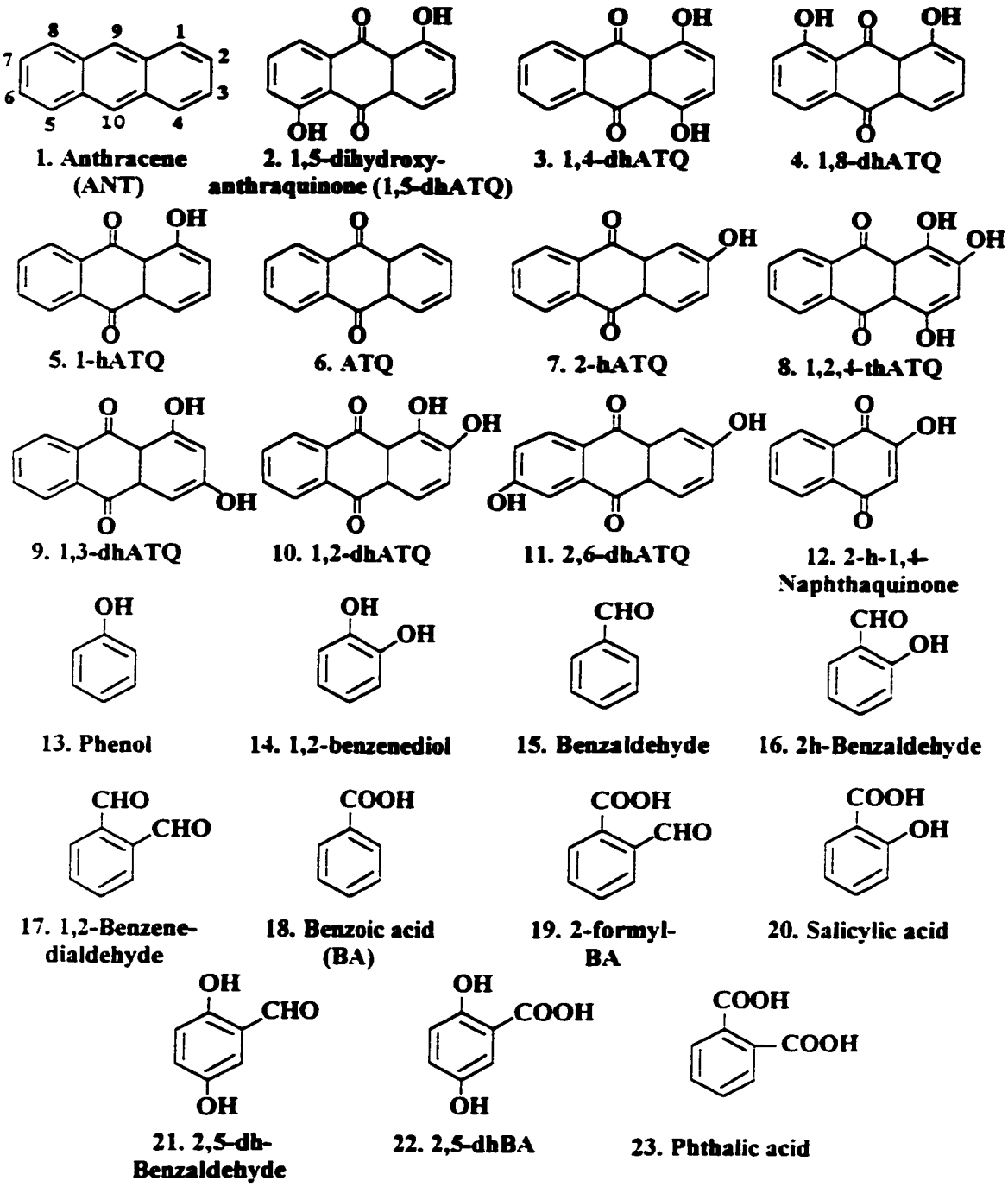

Figure 2.1 Products formed from photomodification of ANT in SSR. Compounds are numbered according to the peaks in Figure 2.2. Abbreviations, where appropriate, are given.

2.2.2 Photooxidation of ANT

Photooxidation of ANT was carried out in aqueous solution under simulated solar radiation (SSR). ANT was dissolved in DMSO to 5 mg mL^{-1}, and 10 µL of this solution was transferred to 10 mL of RO water to give a final concentration of 5µg mL^{-1}. This results in an emulsified solution of ANT. Nonetheless, we have found that the kinetics of photooxidation are rapid and not multi-phasic under these conditions (Huang *et al.*, 1993; Krylov *et al.*, 1997), indicating all of the ANT is fully available for photoreaction. DMSO was used as a delivery solvent because it has been shown to not affect ANT toxicity or ANT photomodification (Huang *et al.*, 1993; Mallakin *et al.*, 1999). The 10 mL aqueous solution containing ANT was exposed to 100 µmol m^{-2} s^{-1} of SSR for 10 h. Samples were taken for analysis every hour. The SSR source is described elsewhere (Huang *et al.*, 1993). The spectral output of the SSR source following passage through a polystyrene petri dish top (polystyrene petri dish tops absorb UV-C exposure) had a PAR: UV-A: UV-B ratio of 100: 10: 1, based on the number of photons (Mallakin *et al.*, 1999).

2.2.3 Analysis of ANT Photooxidation Products by HPLC

A high performance liquid chromatograph (HPLC) with diode array detector (Shimadzu, Columbia, MD, USA) was used to examine the purity of intact ANT and detect the products of photooxidation (McConkey *et al.*, 1997; Mallakin *et al.*, 1999). Samples of 400 µl of the aqueous photooxidized solutions were loaded onto a HPLC column using an auto injector (Shimadzu Inc., Columbia, MD). The columns used were a Supelco LC-18 column (25 cm x 4.6 mm ID, 5-µm particle size; Supelco, Mississauga, ON), a Phenomenex Envirosep-PP column (125 x 3.20mm ID, 120-µm particle size; Phenomenex, Torrance, CA), or a Supelcosil LC-PAH column (25.0cm

x 4.6mm, 5 μm particle size; Supelco, Mississauga, ON). All gave similar separation profiles. The method for elution of ANT and the photoproducts from the column was an acetonitrile-water gradient: isocratic at 1% acetonitrile for 2 min, increased linearly to 90% acetonitrile over 32 min, and isocratic at 90% acetonitrile for 20 min (McConkey *et al.*, 1997; Mallakin *et al.*, 1999). The pH of the water was adjusted with phosphoric acid to pH = 2.8. The flow rate was 1 ml/min. A diode array detection system allowed simultaneous identification and quantification of the ANT photoproducts. Data from the system were collected and evaluated using Shimadzu EZ-chrome software. Identification of photoproducts was achieved via comparison to the retention times and absorbance spectra of authentic material. Identification was considered positive only when both parameters matched.

2.3 Results

2.3.1 Photomodification of ANT and Identification of the Photooxidation Products

ANT in aqueous solution was exposed to SSR for various lengths of time. The HPLC analysis of the product profile is shown for four time points (Figure 2.2). In SSR, ANT was consumed with a concomitant appearance of photoproducts. Initially ATQ and hATQs were formed. After longer time exposures to SSR various benzoic acids, benzaldehydes and phenols derivatives dominated the product spectrum. After 9 h of light exposure, more than 20 distinct compounds had formed and little ANT remained (Figure 2.2). The parent compound and 22 photomodified products were identified by comparison to authentic material (Figures 2.1 and 2.2).

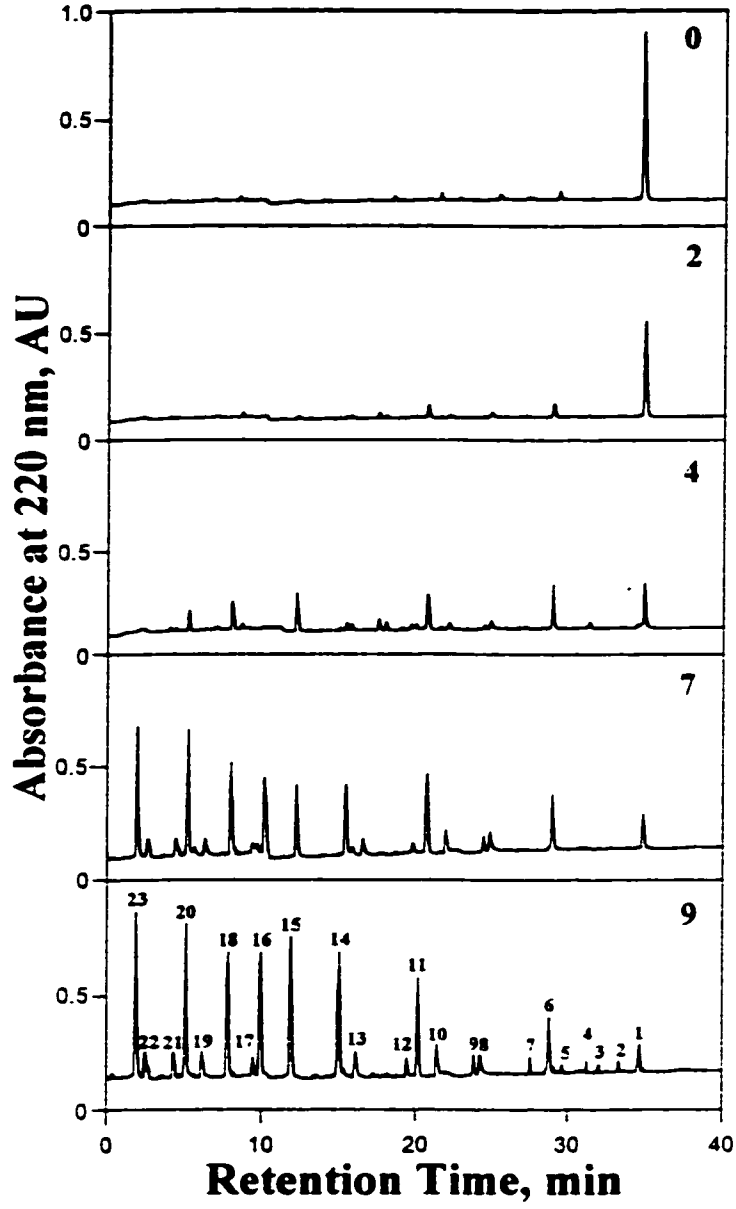

Figure 2.2 High-performance liquid chromatography (HPLC) analysis of ANT photooxidation. Photooxidation was carried out in RO water under 100 μmol m^{-2} s^{-1} of SSR. Samples were taken for analysis at 0, 2, 4, 7 and 9 h. A 400-μl aliquot of each sample was analyzed by HPLC equipped with a diode array detector. The chromatographs show the relative absorbance at 220 nm. Identities of peaks (numbered in Figure 2.1) are based on comparison of retention times and spectra of authentic samples.

2.3.2 Kinetics of ANT Photooxidation

The photooxidation of ANT under SSR was investigated in more detail to assess the kinetics of photooxidation (Figure 2.3). The photochemical reaction was carried out under 100 μmol m^{-2} s^{-1} of SSR in distilled water and monitored by HPLC as above. The kinetics of consumption of ANT was fitted to an exponential decay curve (Figure 2.3) according to the following equation:

$$[ANT]_t = [ANT]_0 e^{k_P t} \quad (1)$$

Where

$[ANT]_t$ = ANT concentration at time t

$[ANT]_0$ = ANT concentration at time 0

k_P = pseudo first-order rate constant

The curve fit for exponential loss of ANT gave a k_p of 0.314 h^{-1} (r^2=0.96 and $p<0.05$).

The first detectable product, ATQ, appeared after a 2 h lag time (Figure 2.3). During this period approximately 50% of the ANT was consumed. This indicates there was an undetected intermediate in the ANT to ATQ photooxidation reaction. The ATQ concentration reached a maximum level after about 6h in SSR, at which point it started to be depleted. As ATQ was depleted hATQs, benzoic acids, benzaldehydes and phenols started to form. Some of the hATQs (e.g. 2,6-dhATQ) were formed after the single ring aromatics started to appear (e.g. phthalic acid) (Figure 2.3). This indicates that ATQ can be cleaved directly to single ring compounds. As well, some of the hATQs are photolabile (Table 2.1), and are therefore also sources of single ring aromatics. Interestingly, other hATQs are photostable (e.g. 2-hATQ) and some of these were found to be toxic (Mallakin *et al.*,

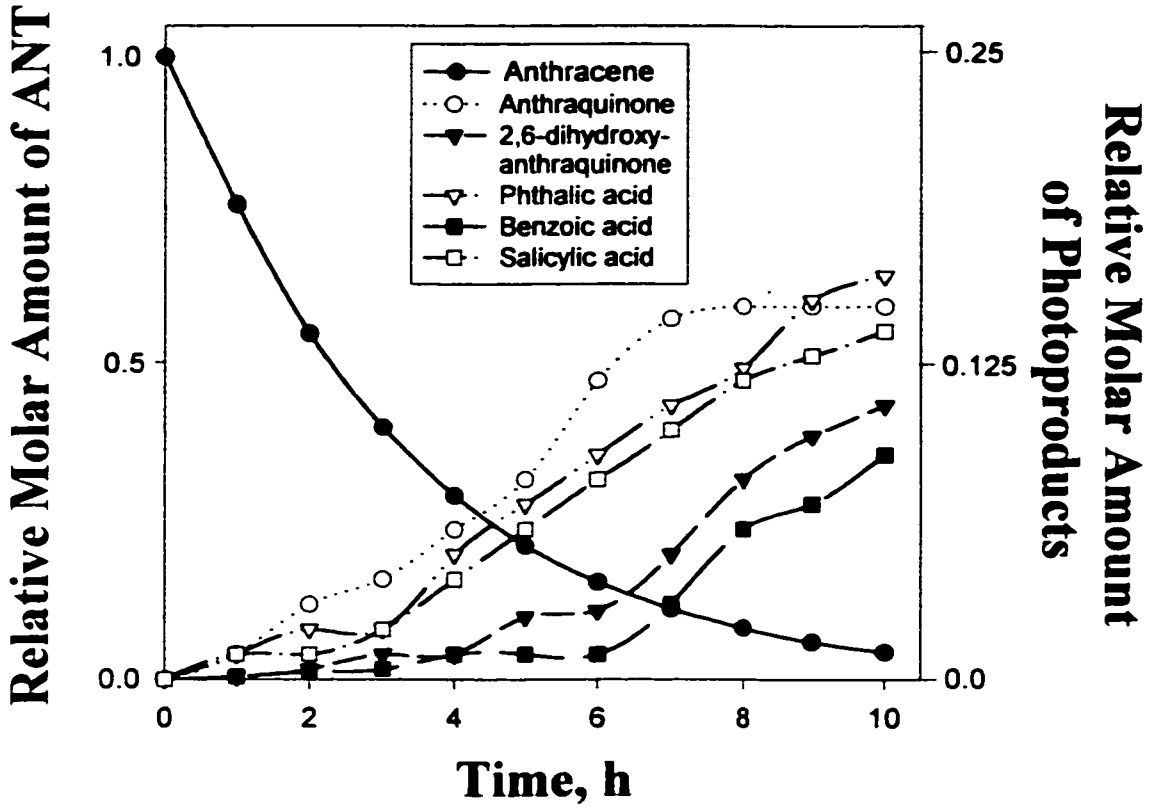

Figure 2.3 Kinetics of ANT photooxidation due to exposure to 100 μmol m^{-2} s^{-1} of SSR. HPLC analysis was as in Figure 2.2. The amount of intact ANT remaining and production of ATQ, 2,6-dhATQ, phthalic acid, Salicylic acid and benzoic acid were quantified by HPLC and plotted against time. Loss of ANT was adequately described by an exponential decay function (r^2=0.96; $p<0.05$). [ANT] at t_0 was: 28.05 μmol. The relative molar amount of the photoproducts is based on the data in Table 2.1.

Table 2.1 Representatives ANT photooxidation products quantified by calibration to external standard method (ESTD). Photomodification was performed under SSR for 9 hours. Molar yields ratio and standard error of triplicate samples are presented.

Compound	Yield[a]	$t_{1/2}$, h in SSR
ANT	0.006 ± 0.008	2
ATQ	0.146 ± 0.018	1.8
1-hATQ	0.018 ± 0.002	EP
2-hATQ	0.062 ± 0.003	EP
1,2-dhATQ	0.027 ± 0.002	3.0
1,4-dhATQ	0.077 ± 0.006	6.0
1,5-dhATQ	0.010 ± 0.001	EP
1,8-dhATQ	0.080 ± 0.018	EP
2,6-dhATQ	0.105 ± 0.015	EP
Phthalic acid	0.148 ± 0.006	EP
Salicylic acid	0.140 ± 0.025	EP
Benzoic acid	0.090 ± 0.020	EP

a) μmoles of compound at (t = 9h) in SSR
b) EP = End Products

1999). Thus, these products are specifically expected to accumulate in the environment and would represent a potential hazard. Indeed, in recent work some ANT photoproducts were detected at significant levels in PAH contaminated sediments (Greenberg *et al.*, unpublished observations).

2.3.3 Pathway of ANT Photomodification

Based on the kinetics for photomodification of ANT and product formation, a photomodification pathway can be proposed (Figure 2.4). ANT is converted to ATQ via an intermediate, most likely the 9,10-endoperoxide of ANT. This molecule would subsequently be oxidized to ATQ with the concomitant generation of hydrogen peroxide (Figure 2.4). ATQ is then hydroxylated or its central ring is cleaved. We assume ATQ can form one-ring aromatics directly as they form with a time frame similar to or faster than hATQ formation (see Figures 2.2 and 2.3). Three of the hATQs (1,2-dhATQ, 1,4-dhATQ and 1,2,4-thATQ) also are subject to ring fission forming benzoic acids, benzaldehydes and phenols. The single ring aromatics and some of the hATQs products are photochemically stable and can therefore be classified as end-products.

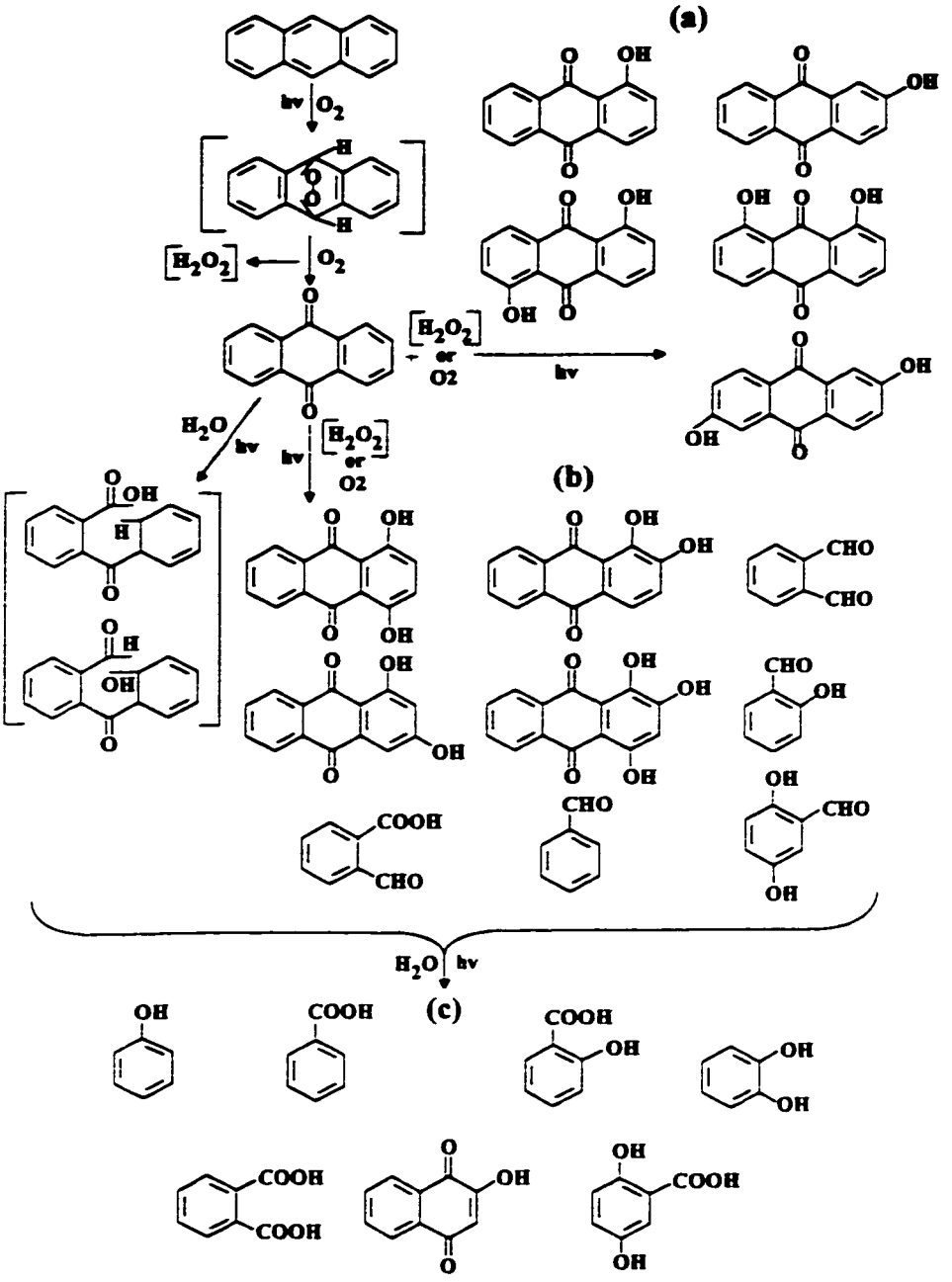

Figure 2.4 Proposed pathway of anthracene photooxidation in simulated solar radiation. The generalized mechanism is based on the identified products and kinetics of their appearance. The brackets indicate unidentified intermediates. (a): Photostable hATQs. (b): Photolabile hATQs. (c): One ring aromatic end products.

2.4 Discussion

In this study, we have shown that ANT was oxidized to ATQ, hATQs, benzoic acid, benzaldehyde and phenols in the presence of SSR. Photooxidation of PAHs and product formation have been described in previous studies (Katz *et al.*, 1979; Ren *et al.*, 1994; McConkey *et al.*, 1997; Mallakin *et al.*, 1999). This study is consistent with previous work which demonstrated that PAHs can be photomodified via oxidation reactions (Katz *et al.*, 1979; Ren *et al.*, 1994; McConkey *et al.*, 1997; Huang *et al.*, 1997). However, this research greatly expanded on the number of identified products and presents a full photooxidation pathway for the first time. Many of the photoproducts identified are intermediates and subject to further photooxidation. The action of light on PAHs can also result in the formation of active oxygen species including hydrogen peroxide, singlet oxygen, superoxide ion and organo-peroxy radicals (Larson and Berenbaum, 1988). In particular, based on the proposed photomodification pathway of ANT, hydrogen peroxide is a likely by-product. Interestingly, hydrogen peroxide has been shown to be at higher levels in aquatic environments exposed to sunlight (Scully *et al.*, 1995), and our work shows one way in which it can be formed.

In solution, there are two possible routes of photomodification of PAHs; type II and type I photosensitization reactions (Foote, 1979). In type II photosensitization, after absorption of a photon, ground-state ANT goes to the excited triplet-state (^{3}ANT) via intersystem crossing from the excited singlet-state ^{1}ANT. The experimental solution was open to the air, so the main quencher of ^{3}ANT would be ground triplet-state oxygen $^3O_2$. This is because the concentration of ^{3}ANT would be low in the aqueous medium relative to the $^3O_2$ concentration (0.25 mM) (Robinson *et al.*, 1970; Krylov *et al.*, 1997). This means the rate of reaction of ^{3}ANT with $^3O_2$ should be

diffusion limited with an average interval of less than 10^{-6} s between collisions (Krylov *et al.*, 1997). Because the ANT excited triplet state is relatively long lived (10^{-6} to 10^{-3} s), the majority of the excited ^{3}ANT should be quenched by oxygen, generating singlet-state oxygen $^1O_2$ (Lakowics, 1983). These singlet $^1O_2$ molecules could then react with ANT forming the endo-peroxide. In type I photosensitization reactions, as in type II reactions, after absorbance of a photon, ANT goes to ^{3}ANT via intersystem crossing from the excited singlet state. The ^{3}ANT does not react with $^3O_2$, but instead with another PAH or solvent molecule to generate a PAH free radical or solvent free radical. These PAH radicals would also be reactive with O_2, forming oxidation products. Assuming the 9,10-endoperoxide of ANT is the initial oxidation reaction, a type II photosensitization mechanism is more likely.

Our studies show that the initial $^1O_2$ attack is exclusively at the 9,10 position in the central ring of ANT. The electron density of this ANT central ring is very low (Mezey *et al.*, 1998), explaining why the initial reaction is so specific to this position. This low electron density of the central ANT ring is also a key factor in the very rapid rate of photooxidation.

The initial ANT concentration used in this study (5 μg/ml) is well above its solubility limit. This was necessary so we would have sufficient material for analysis. Interestingly, the ANT did not precipitate, but rather formed an emulsion. Further, the kinetics of photooxidation were pseudo first-order, mono-phasic and rapid. From this we conclude that PAHs do not have to be fully solublized to be subject to photomodification. This has environmental implications, as PAHs in aquatic environments are often bound to suspended particulate matter. Our data suggest that under these conditions photomodification can occur.

Chapter III

Impacts of Structural Photomodification on the Toxicity of Environmental Contaminants: Anthracene Photooxidation Products[1]

---

[1] This paper is appeared in *Ecotoxicology and Environmental Safety*. 1999. Vol 43, 204-212, available on line at http://www.idealibrary.com, and authored as Ali Mallakin, Brendan J. McConkey, Goubin Miao, Brian Mckibben, Victor Sniekus, D. George Dixon, and Bruce M. Greenberg.

3.1 Introduction

The aquatic environment is a site of high photochemical activity, particularly in shallow waters. Irradiation of chromophores in the presence of oxygen can result in the production of biologically damaging active oxygen species (Larson and Barenbaum, 1988; Foote, 1991). If the chromophore is within an organism, the resultant active oxygen can cause biological damage (Halliwell and Gutteridge, 1985; Larson and Barenbaum, 1988). Other light-absorbing molecules are subject to photomodification (photooxidation and photolysis), with the photolytic products having different biological activities than the parent compounds (Larson and Barenbaum, 1988). Polycyclic aromatic hydrocarbons (PAHs) are one of the best examples of a group of photoactive environmental contaminants (Cook *et al.*, 1983; Newsted and Giesy, 1987; Hall and Oris, 1991; Huang *et al.*, 1993, 1997b; Mekenyan *et al.*, 1994; Arfsten *et al.*, 1996; Krylov *et al.*, 1997). By virtue of their large, highly conjugated π-orbital systems, PAHs strongly absorb in the UV spectral region of natural sunlight. Upon absorbing a photon, PAHs reach excited triplet states with high quantum yields. This can lead to the photosensitized production of biologically damaging singlet state oxygen ($^1O_2$) (Newsted and Giesy, 1987; Hall and Oris, 1991; Huang *et al.*, 1993; Mekenyan *et al.*, 1994; Arfsten *et al.*, 1996; Krylov *et al.*, 1997; Huang *et al.*, 1997a). Absorbance of a photon by a PAH can lead to rapid photomodification (generally by oxidation) to new chemical species (Katz *et al.*, 1979; Huang *et al.*, 1993, 1995, 1997a; Krylov *et al.*, 1997; McConkey *et al.*, 1997). In many instances, it was found that photomodified PAHs are more toxic than the parent PAHs (Huang *et al.*, 1995, 1997b; Krylov *et al.*, 1997; McConkey *et al.*, 1997), most likely due to a combination of increased solubility, bioavailability and reactivity (Duxbury *et al.*, 1997; McConkey *et al.*, 1997; Huang *et al.*, 1997a,b).

Photomodification of any given PAH leads to a wide variety of products (Katz *et al.*, 1979; Neff, 1979; Duxbury *et al.*, 1997; Huang *et al.*, 1997a; McConkey *et al.*, 1997). Since the mixtures of photoproducts are often more toxic than the intact starting material (Huang *et al.*, 1995, 1997b; Krylov *et al.*, 1997; McConkey *et al.*, 1997), it is important to determine which photoproducts in the mixture are making the most significant contributions to toxicity. It was recently demonstrated that phenanthrenequinone, the major photoproduct of phenanthrene, is more toxic to *Lemna gibba* and *Photobacterium phosphoreum* than phenanthrene (McConkey *et al.*, 1997). It was further demonstrated in that study that the increased toxicity of phenanthrene following its photomodification was explained almost entirely by the presence of phenanthrenequinone. Phenanthrene represents a fairly simple example, since phenanthrenequinone is its only abundant photomodification product (McConkey *et al.*, 1997). Commonly, PAH photomodification results in complex mixtures of products (Katz *et al.*, 1979; Duxbury *et al.*, 1997; Huang *et al.*, 1997a) with potentially variable levels of biological activity. The work reported here attempts to explore a more complex case than phenanthrene.

Anthracene (ANT) consistently has been found to be one of the most toxic PAHs following photomodification (Huang *et al.*, 1993, 1995; 1997a,b). ANT photomodification results in the formation of a complex mixture of more than 20 products, including anthraquinones (ATQs), hydroxyanthraquinones (hATQs), benzoic acids and phenols (Katz *et al.*, 1979; Huang *et al.*, 1997a; Chapter 2). It is not known which of these photoproducts are contributing to the high toxicity of photomodified ANT. To begin to assess the toxicity of specific ANT photooxidation products we compared the toxicity of ATQ and 11 different hATQs to ANT. The compounds chosen were either found in the mixture of compounds derived from ANT photooxidation or are structurally related to one or more of those compounds.

Toxicity was measured as growth inhibition using the duckweed *Lemna gibba*. *Lemna gibba* was chosen for this study because it has been used extensively for photoinduced toxicity of PAHs. Moreover, it is an accepted standard test of toxicity and an environmentally relevant plant species (American Society for Testing and Materials, 1991). Growth inhibition was determined under photosynthetically active radiation (PAR) and simulated solar radiation (SSR) to assess whether toxicity was photoinduced in a manner similar to that of ANT. ATQ and about half the hATQs tested were found to have toxic activities similar to or greater than that of ANT.

3.2 Materials and Methods

3.2.1 Chemicals, Chemical Analysis, and Photomodification of Chemicals

The 13 chemicals used in this study were (abbreviations used throughout the text follow the name, common names are also provided): anthracene (ANT), anthraquinone (ATQ), 1-hydroxyATQ (1-hATQ), 2-hydroxyATQ (2-hATQ), 1,2-dihydroxyATQ (1,2-dhATQ; alizarin), 1,3-dihydroxyATQ (1,3-dhATQ), 1,4-dihydroxyATQ (1,4-dhATQ; quinizarin), 1,5-dihydroxyATQ (1,5-dhATQ; anthrarufin), 1,8-dihydroxyATQ (1,8-dhATQ), 2,6-dihydroxyATQ (2,6-dhATQ; anthraflavic acid), 1,2,4-trihydroxyATQ (1,2,4-thATQ; purpurin), 1,2,5,8-tetrahydroxyATQ (1,2,5,8-thATQ; quinalizarin), 1,2,10-trihydroxyANT (1,2,10-thANT; anthrarobin). The structure of these chemicals and their absorption spectra are given in Figure 3.1. Chemicals were purchased in high purity (Sigma Chemical Co., St. Louis, MO and Aldrich, Milwaukee, WI), except for 1-hATQ, 2-hATQ and 1,3-dhATQ, which were synthesized by established procedures in our laboratory (Wang and Snieckus, 1990). High performance liquid chromatography (HPLC, Shimadzu, Inc., Columbia, MD) was used to confirm the purity of all compounds (Huang *et al.*, 1997a,b; McConkey

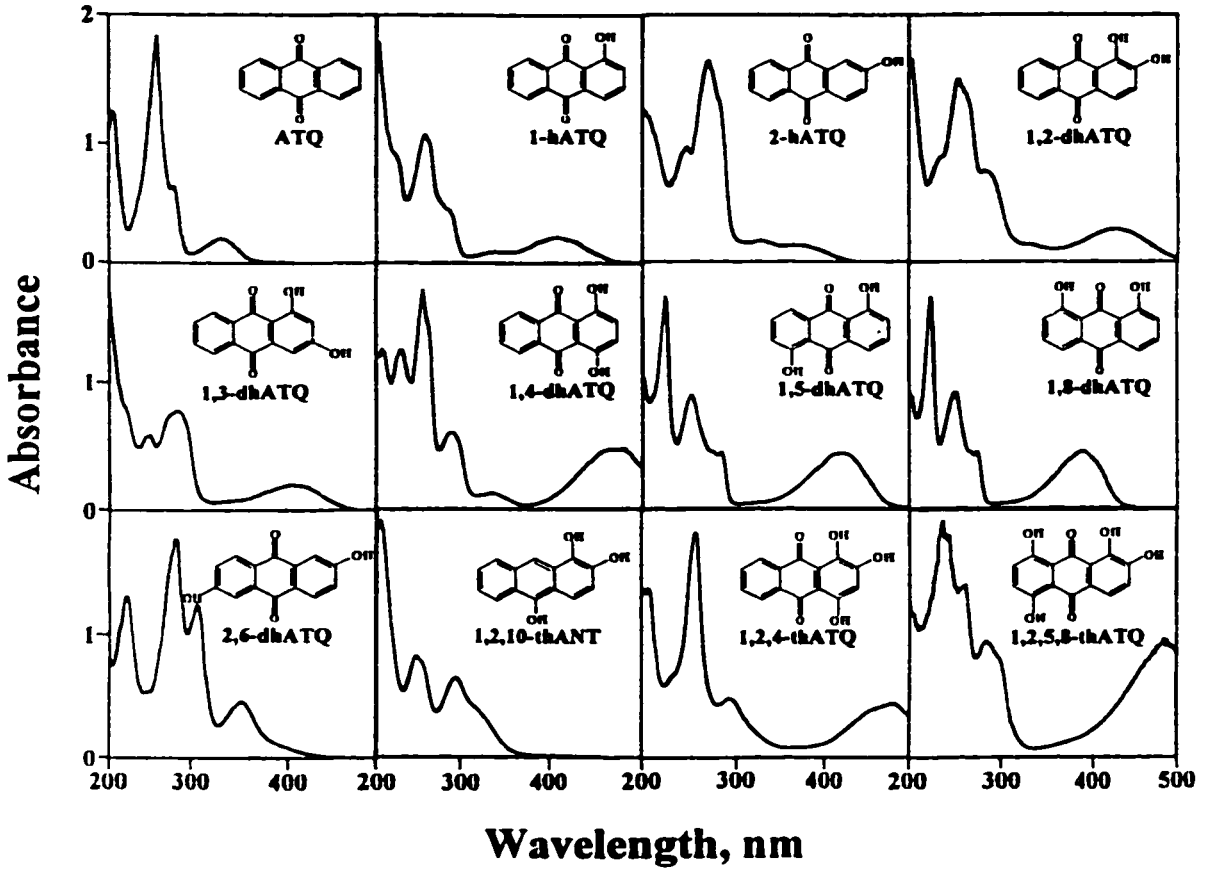

Figure 3.1 Chemical structures and absorbance spectra of anthraquinone and the oxygenated anthracene derivatives used in this study. The chemicals at 2 μg ml^{-1} in chloroform were scanned with a UV/VIS spectrophotometer. Abbreviations of chemical names are as given in materials and methods. An absorbance spectrum of anthracene can be found in Foote (1991).

et al., 1997). Either a Supelco LC-18 column (25cm x 4.6cm ID, 5-μm particles, Supelco, Mississauga, ON) or a Phenomenex Envirosep-PP column (125 x 3.20 mm ID, 120-μm particles, Phenomenex, Torrance, CA) were used. Samples of 400μl (2 mg ml^{-1} in DMSO) were applied to the column with an autoinjector, and separation was carried out with a water (pH 3, adjusted with phosphoric acid) and acetonitrile gradient. HPLC grade solvents were used (VWR/Canlab, Toronto, ON). The acetonitrile-water gradient was: isocratic at 1% acetonitrile for 2 min, increased linearly to 90% acetonitrile over 32 min, and isocratic at 90% acetonitrile for 20 min. The flow rate used was generally 1 ml/min, although 0.5 ml/min was used when greater peak resolution was required. The compounds were detected with a diode array detector (Shimadzu, Inc.) linked to a computer running Shimadzu EZ-Chrome software.

To examine the photomodification reactions of ANT, ATQ and the hATQs, the chemicals were delivered in DMSO by 1000-fold dilution to 10 ml of *L. gibba* growth medium to a final concentration of 5 μg ml^{-1} and exposed to SSR (Huang *et al.*, 1993; 1997a). At various time points, 400 μl of the aqueous photochemical reaction mixture was removed for HPLC analysis. The kinetics of photomodification and product profiles for ANT, ATQ and the hATQs were determined by HPLC using the method described above. Photomodification products were identified by comparison to authentic materials based on coincident HPLC retention time and matching diode array absorbance spectra using the library function of the HPLC software (Shimadzu, Inc).

3.2.2 Light Conditions, Plant Growth, and Toxicity Assessment

Prior to toxicity testing, *Lemna gibba* L. G-3 were transferred from sucrose-containing growth medium to sucrose-free growth medium and cultured aseptically for

2 weeks in a controlled environment chamber under 60 μmol m^{-2} sec^{-1} of continuous PAR (cool-white fluorescent, 400 nm to 700 nm) generated with cool-white fluorescent lamps (American Society for Testing and Materials, 1995; Huang *et al.*, 1993, 1995). The irradiation sources for plant growth during chemical treatments were either PAR or SSR (100 μmol m^{-2} s^{-1}). The spectral output of the SSR source following passage through a polystyrene petri dish top (polystyrene petri dish tops absorb UV-C exposure) covering the plants had a PAR: UV-A: UV-B ratio of 100: 10: 1, based on the number of photons. Construction of the SSR source is described in detail elsewhere (Huang *et al.*, 1993; American Society for Testing and Materials, 1995). The spectral outputs (Figure 3.2) and integrated fluence rates of the light sources were measured with a calibrated spectroradiameter (Huang *et al.*, 1995; American Society for Testing and Materials, 1995). The spectral output of the SSR source has a UV to PAR ratio parallel to that of sunlight from mid spring to mid fall in latitudes corresponding to southern Canada and the northern United States (Henderson, 1977; American Society for Testing and Materials, 1995).

Plants were placed on 10 ml of fresh half-strength Hutner's medium in a 5-cm diameter polystyrene petri dish (Figure 3.3). Chemicals were delivered to the growth medium by 1000-fold dilution of DMSO stock solutions to final concentrations ranging from 0.01 to 10 μg ml^{-1} in a logarithmic dilution series. A DMSO (0.1 % v/v) solvent control sample was performed for each experiment. This concentration of DMSO has no impact on *L. gibba* growth or PAH toxicity tests, and it does not effect net uptake of intact or modified PAHs by *L. gibba* (Greenberg *et al.*, 1992; Huang *et al.*, 1993; Duxbury *et al.*, 1997). A 10 μg ml^{-1} upper limit for the exposure concentration range allowed full dose responses to be observed for each chemical; 10 μg ml^{-1} is an environmentally relevant concentration for the hATQs, which are much more water soluble than ANT. The accuracy of chemical delivery and PAH

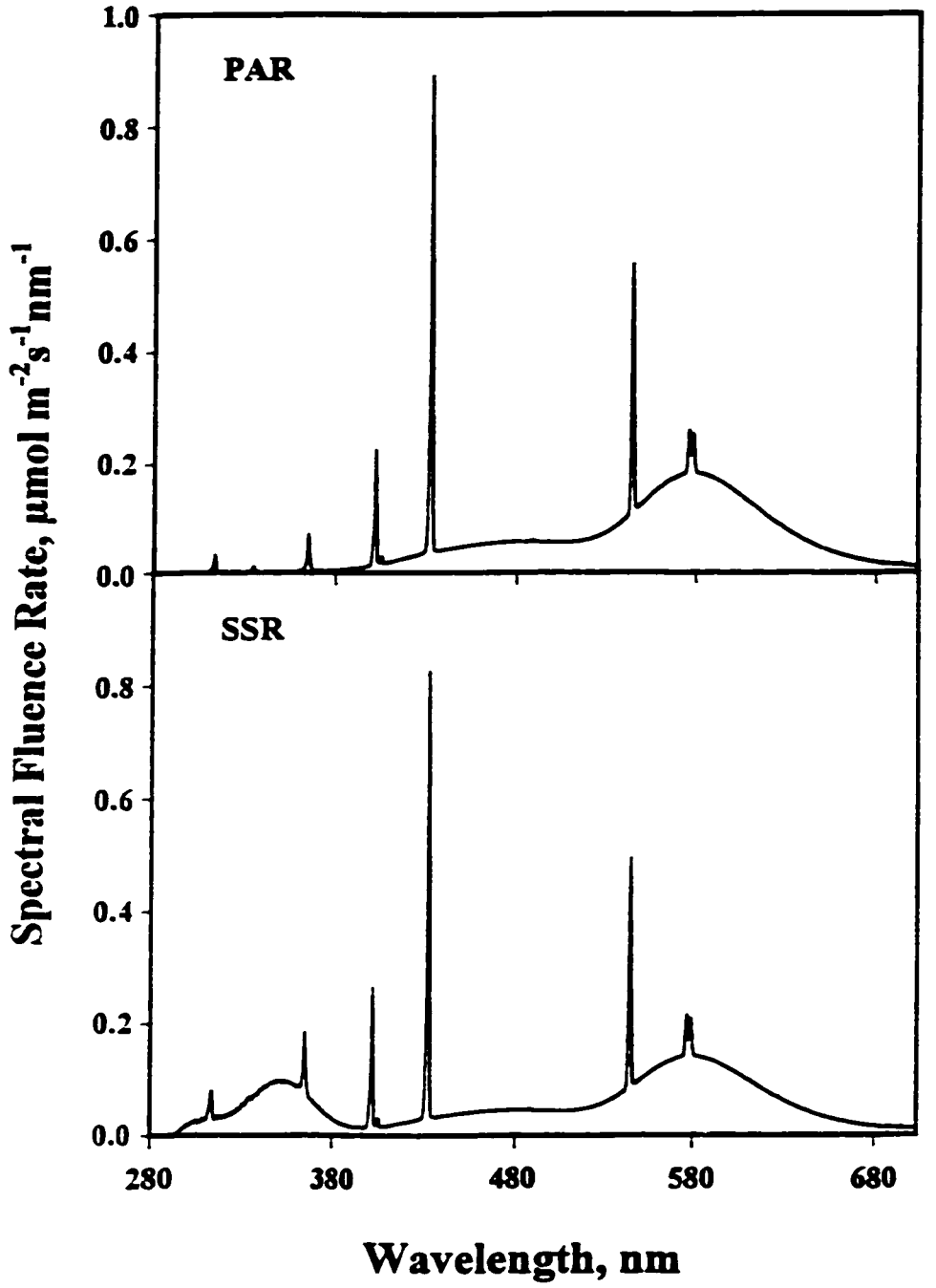

Figure 3.2 The spectral outputs of the simulated solar radiation (SSR) and the photosynthetically active radiation (PAR) sources. Light sources and Spectro-radiometric measurements are described in materials and methods. All data are given in relative units based on photon fluence rates.

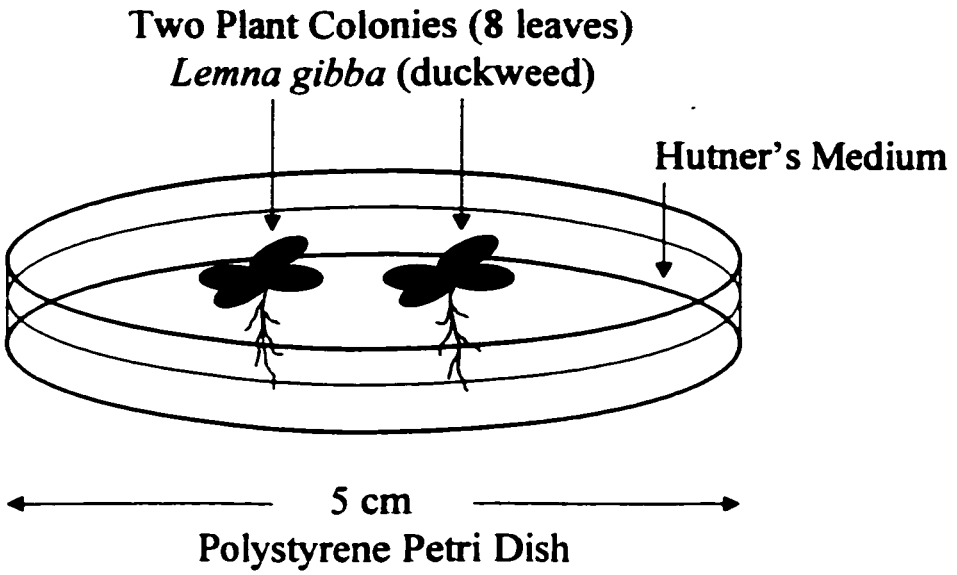

Figure 3.3 Experimental design to determine the toxicity of chemicals to aquatic plant (*Lemna gibba*). Toxicity tests started with two plant colonies per treatment replicate (8 leaves); growth was monitored over an 8-day period by counting leaves.

concentrations in the media were determined by HPLC analysis as above. The media-chemical mixture was replenished by static renewal every 48 h to keep the chemical concentration and nutrient levels somewhat constant. Toxicity of chemicals was assessed based on growth inhibition (American Society for Testing and Materials, 1991; Greenberg *et al.*, 1992; Huang *et al.*, 1993). Toxicity tests started with two plant colonies per treatment replicate (8 leaves); growth was monitored over an 8-day period by counting leaves and converting the data to instantaneous growth rates. Leaf counts are a highly reliable and representative method of assessing PAH toxicity to *L. gibba* (Greenberg *et al.*, 1992; Huang *et al.*, 1997a). The control plants doubled about every 48h under both of the light conditions used in this study. Toxicity data were fit to the sigmoidal function:

$$I = \frac{100}{1 + \exp\ B(x - \mu)}$$

Where I is percent of growth inhibition, x is the logarithm of the chemical concentration, μ is the logarithm of the EC_{50}, and B is chemical-dependent slope parameter (McConkey *et al.*, 1997). Standard errors were calculated for all EC_{50}s using the data from three independent experiments. All toxicity tests were performed in triplicate with a minimum of three independent replicates per test ($n = 3$).

For toxicity tests of photomodified PAHs, intact ANT, ATQ and the hATQs were delivered in DMSO to growth medium to final concentration ranging from 0.01 to 10 $\mu g\ ml^{-1}$. They were incubated in SSR for 7 days; after about 4 days the mixture stabilized as a composite of benzoic acids, thus a 7-d exposure assured photomodification to a mixture that would not change during a toxicity test. In the case of the non-photomodifiable hATQs, there were no changes to the chemical over

this 7-d period. The control plants were also exposed to medium containing 0.1 % DMSO that was preincubated for 7 days under SSR. Toxicity data were fit to a sigmoidal function and standard errors were calculated as above.

3.3 Results

3.3.1 Photomodification of ANT and Identification of Products by HPLC

When ANT is exposed to light, it is rapidly photooxidized to complex mixtures of products that are more toxic than the parent compound (Huang *et al.*, 1993, 1995, 1997a). Most of the photoproducts have not been identified. To identify these photooxidation products, ANT was photomodified under SSR for 9h and HPLC analysis was performed (Figure 3.4). A large number of products were observed; more than 25 peaks could be resolved by HPLC. A similar product profile was observed when ANT was exposed to UVB only (data not provided). When anthracene was left in the dark for the same length of time, no oxidation of ANT was observed and the compound was quantitatively recovered (data not provided). Thus, the observed peaks were attributable to photomodification of the parent compound. The identified photoproducts were ATQ, 1-hATQ, 2-hATQ, 1,2-dhATQ, 1,4-dhATQ, 1,5-dhATQ, 1,8-dhATQ, 2,6-dhATQ, phthalic acid, salicylic acid, and benzoic acid. Unidentified peaks in Figure 3.3 with retention times of 20 to 30 min were also assumed to be hATQs, but these compounds were not successfully identified.

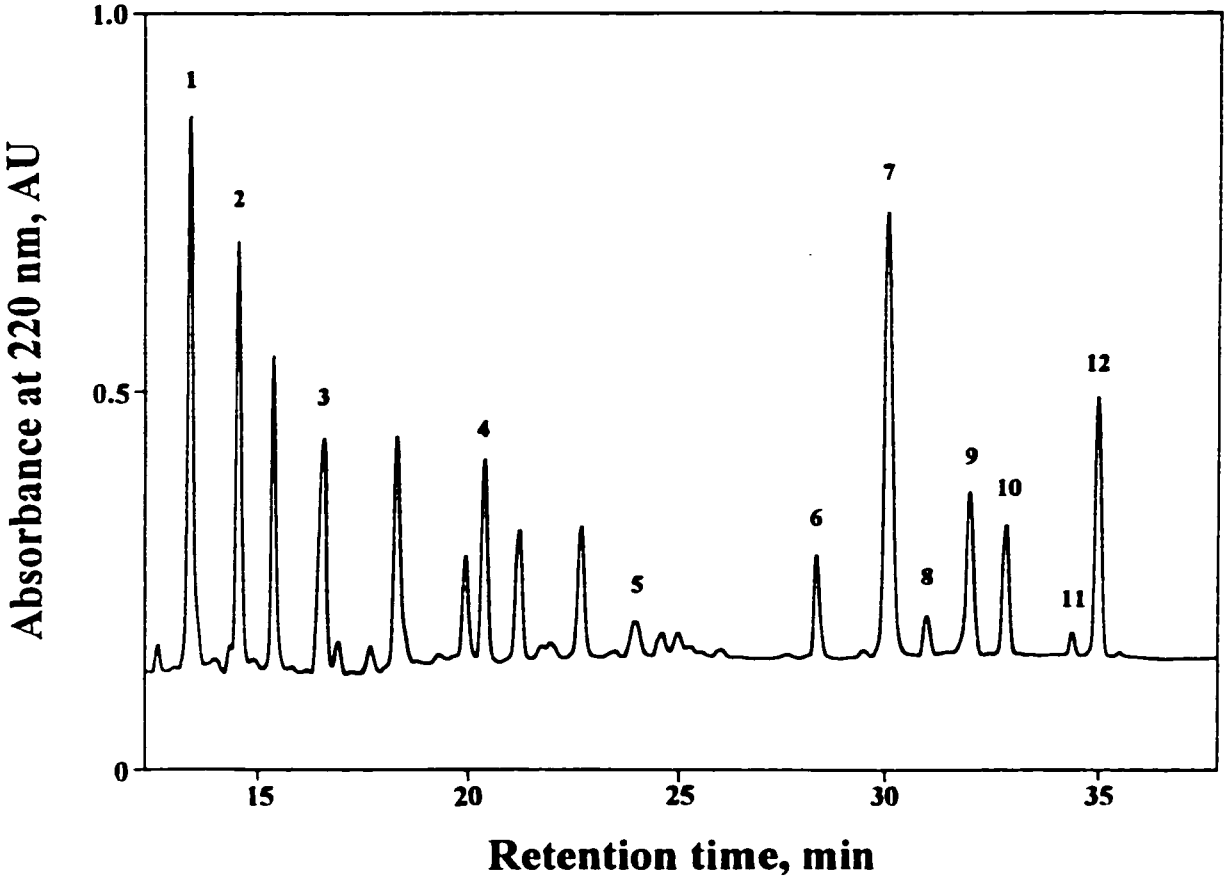

Figure 3.4 HPLC analysis of anthracene photomodification. Anthracene was delivered in DMSO to the growth medium to a final concentration of 5 μg ml^{-1} and exposed to SSR for 9h. Compounds identified are: Anthracene (peak 12), anthraquinone (peak 7), 1-hATQ (peak 8), 2-hATQ (peak 6), 1,2-dhATQ (peak 5), 1,4-dhATQ (peak 10), 1,5-dhATQ (peak 11), 1,8-dhATQ (peak 9), 2,6 dhATQ (peak 4), phthalic acid (peak 1), salicylic acid (peak 2) and benzoic acid (peak 3). Based on retention times and searches of the diode array absorbance spectra library, other peaks with retention times between 13 and 18 min were tentatively identified as hydroxylated derivatives of benzoic acid, and other peaks between 20 and 30 min were probably hydroxylated ATQs.

3.3.2 Photomodification of ATQ and Hydroxylated ATQs

Because ATQ and hATQs were prevalent products of ANT photooxidation, we chose this class of compounds for assessment of toxicological impacts on *L. gibba*. Eight of the compounds selected for testing (Figure 3.1) were positively identified as ANT photoproducts (Figure 3.4), and the others are structurally related to those identified. The latter were chosen for two reasons: to give a larger sampling of compounds for future QSAR modelling, and because under varied environmental conditions other photoproducts could form. Other photooxidation products such as the benzoic acids, are being tested in the scope of another study. First, the rates of photomodification of these compounds (ATQ and the eleven selected hydroxyATQs) were measured in SSR (100 μmol m^{-2} s^{-1}). The HPLC traces for the photooxidation reactions of two typical hydroxyATQs (1,2-dhATQ and 1,8-dhATQ) are shown (Figure 3.5). 1,8-dhATQ was found to be stable in SSR, while 1,2-dhATQ was rapidly photooxidized to various benzoic acids (Figure 3.5). These benzoic acid derivatives are similar to those formed from photooxidation of ANT (c.f. Figures 3.4 and 3.5). No photooxidation was observed for 1-hATQ, 2-hATQ, 1,5-dhATQ, 1,8-dhATQ, 2,6-dhATQ, or 1,2,5,8-thATQ. The compounds found to be subject to photooxidation, in addition to ANT and 1,2-dhATQ, were ATQ, 1,3-dhATQ, 1,4-dhATQ, 1,2,4-thATQ, 1,2,10-thANT. They had half-lives in SSR ranging from 1.8 to 7.3 h (Table 3.1).

3.3.3 Toxicity of ANT, ATQ and the hATQs to *L. gibba*

Photoinduced toxicity to *L.gibba* was determined for ANT, ATQ and the eleven hATQs (Table 3.1 and Figure 3.6). The products chosen for testing were either identified in the mixture of photoproducts derived from ANT or highly related to those products. Other photooxidation products, such as the benzoic acids, are being tested

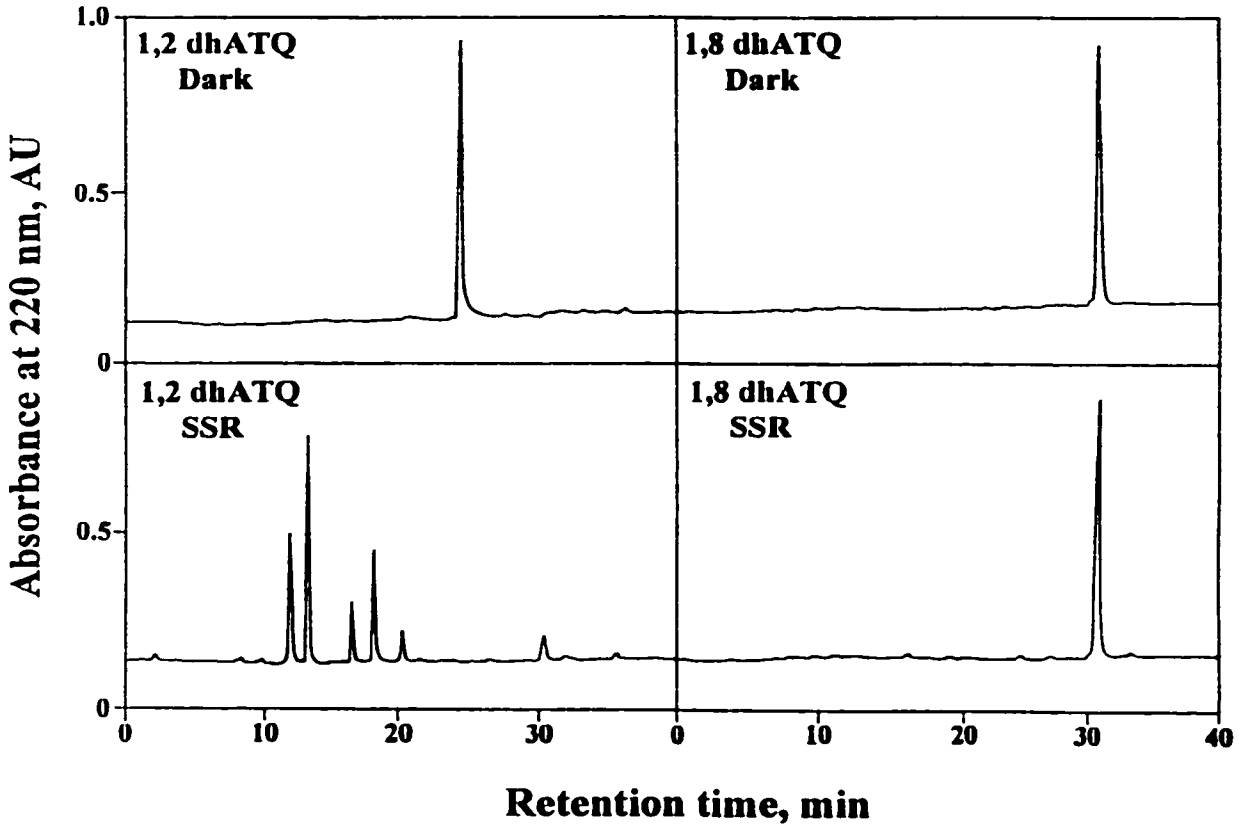

Figure 3.5 HPLC analysis of intact and photomodified hATQs. HPLC traces of 1,2-dhATQ and 1,8-dhATQ exposed to darkness or SSR for 7 days. The peaks with retention times of 10 to 20 minutes were identified as phthalic acid, salicylic acid and benzoic acid products as in Figure 3.4.

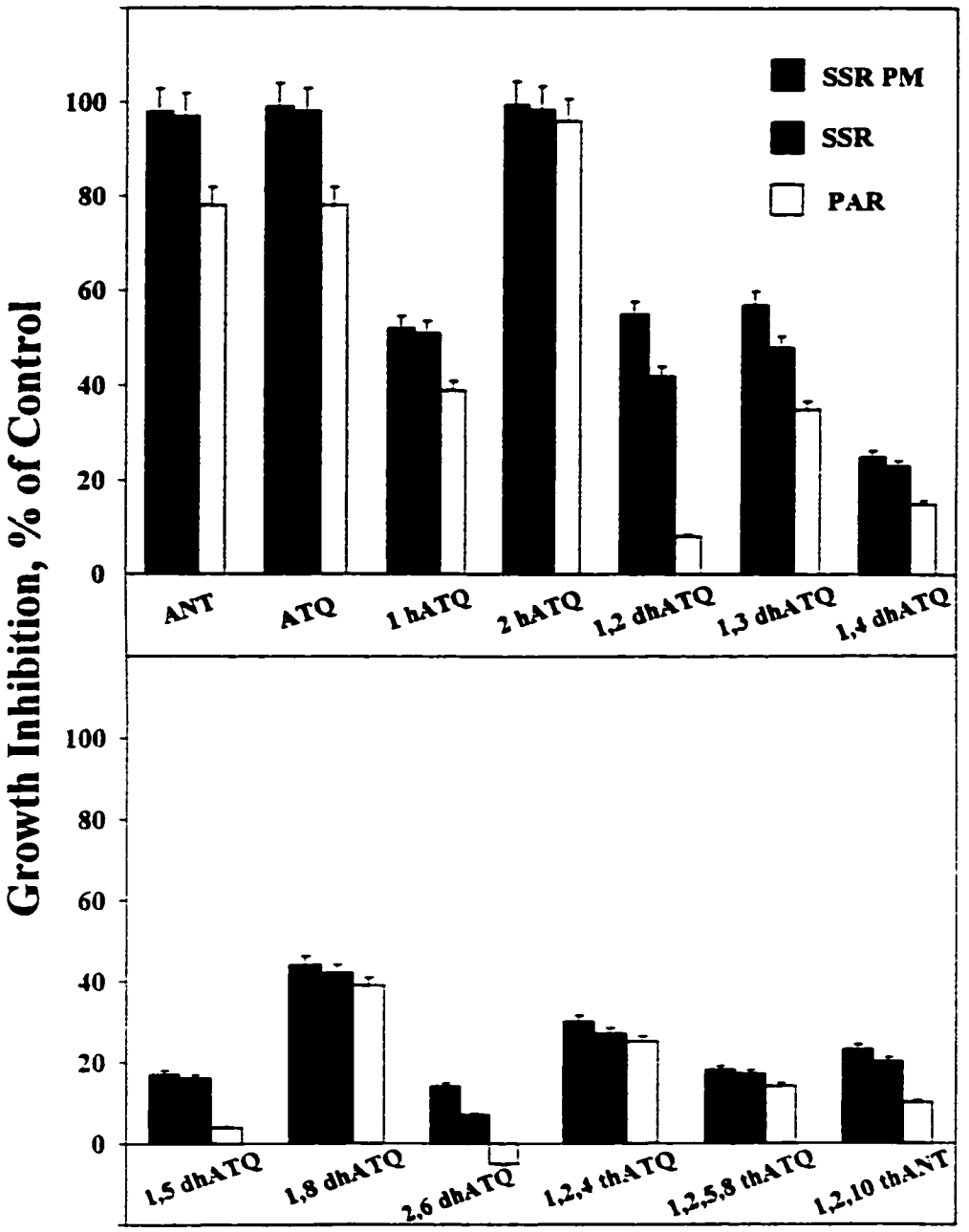

Figure 3.6 Photoinduced toxicity of ANT, ATQ and hATQs applied to *L. gibba* in intact and photomodified (PM) form. Growth was monitored by counting leaves and toxicity is presented as percent inhibition of growth relative to the control plants. Toxicity tests were performed in PAR and SSR. All chemicals were at 2 $\mu g\ ml^{-1}$ based on amount of the parent compound.

Table 3.1 Half lives in SSR and EC_{50} values in PAR and SSR for ANT, ATQ and hATQs.

Chemical	$t_{1/2}$, h in SSR[a]	Toxicity of Intact (PAR)			Toxicity of Intact (SSR)			Toxicity after PM		
		EC_{50} (mg l^{-1})	B[b]	LOEC (mg l^{-1})	EC_{50} (mg l^{-1})	B	LOEC (mg l^{-1})	EC_{50} (mg l^{-1})	B	LOEC (mg l^{-1})
ANT	2.0	1.3±0.14	1.48	0.06	0.8±0.57	1.68	0.01	0.27±0.02	1.71	0.01
ATQ	1.8	1.5±0.20	1.83	0.06	0.5±0.02	1.60	0.01	0.19±0.02	1.23	0.01
1 hATQ	NO PM[c]	2.5±0.12	0.43	0.07	2.4±0.38	0.44	0.01	2.0±0.12	0.69	0.01
2 hATQ	NO PM	0.2±0.02	0.95	0.01	0.05±0.01	0.99	0.01	0.02±0.01	1.31	0.01
1,2 dhATQ	3.0	5.5±0.14	3.36	0.05	2.8±0.57	1.27	0.09	1.5±0.28	0.94	0.01
1,3 dhATQ	7.3	10±1.4	1.67	0.08	2.5±0.09	1.23	0.06	1.5±0.19	0.87	0.02
1,4 dhATQ	6.0	>10	1.12	0.4	6.5±0.95	0.96	0.17	5.9±0.20	0.87	0.02
1,5 dhATQ	NO PM	>10	0.76	1	>10	0.62	0.35	>10	0.54	0.05
1,8 dhATQ	NO PM	3.0±0.20	1.31	0.3	2.5±0.08	1.44	0.15	0.5±0.08	1.21	0.01
2,6 dhATQ	NO PM	NOE[d]	-0.005	....	>10	1.39	2	>10	1.34	1.6
1,2,4 thATQ	5.0	>10	0.92	0.5	6.0±0.63	0.66	0.3	3.0±0.61	0.78	0.03
1,2,5,8 thATQ	NO PM	>10	0.75	0.4	9.5±1.2	0.81	0.2	6.3±0.89	0.74	0.02
1,2,10 thANT	4.4	>10	0.88	0.6	>10	0.51	0.32	9.5±1.3	0.52	0.01

a The half-lives of the chemicals in SSR. The compounds were incubated in SSR (100 μmol m^{-2} s^{-1}), the amount of intact chemicals remaining and photomodified products produced were assayed by HPLC.

b B is a chemical dependent slope parameter solved by fitting the toxicity data to the sigmoidal function $I = 100/[1+\exp B(x-\mu)]$ where I is percent of growth inhibition, x is the logarithm of the chemical concentration and μ is the logarithm of the EC50.

c No Observed Photomodification (NO PM)

d No Observable Effect (NOE)

Example of Toxicity Test Results with Intact and Photomodified Anthracene

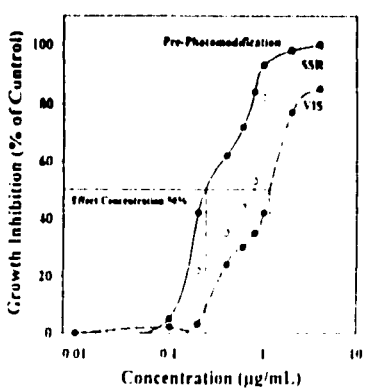

in the scope of another study. The compounds were applied to *L. gibba* in intact form at several concentrations, and growth was measured in SSR and PAR. ANT and 11 of the oxygenated ANTs were found to be toxic. The most toxic of the modified ANTs was 2-hATQ (EC_{50}=0.05μg ml^{-1} in SSR, Table 3.1). Several of the modified ANTs had toxicities at a level similar to ANT (an EC_{50} within a factor of 3). The rest were substantially less toxic than ANT. The only compound found not to show toxic activity in SSR or PAR was 2,6-dhATQ.

In most cases, the compounds tested were more toxic in SSR than PAR (Table 3.1 and Figure 3.5). For example, with the chemicals at 2 mg L^{-1}, and comparing plant performance in PAR and SSR respectively, growth inhibition was 78% and 97% for ATQ, 8% and 42% for 1,2-dhATQ, and 5% and 17% for 1,5-dhATQ. Moreover, in most cases the EC_{50}s for growth inhibition were significantly lower in SSR relative to PAR (Table 3.1). The only chemicals that did not show any increase in toxicity in SSR compared to PAR were 1,5-dhATQ and 1,2,10-thATQ. Interestingly, 2,6-dhATQ which had no impact under SSR, actually promoted leaf production in PAR (Figure 3.5). Because all the chemicals absorb UV radiation more strongly than PAR, and SSR contains UV radiation, this implies that the ANT derivatives with elevated toxicity in SSR are phototoxic.

3.3.4 Toxicity of Photomodified ANT Derivatives to Plants

Because ANT toxicity increases upon photomodification (Huang *et al.*, 1993, 1995; Krylov *et al.*, 1997), it was important to test if the toxicity of the oxygenated ANTs also increased after pretreatment in SSR. For each chemical that was found to be photomodified (ANT, ATQ, 1,2-dhATQ, 1,4-dhATQ, 1,2,4-thATQ, 1,2,10-thANT), the photomodified chemicals were more toxic than the non-pretreated

chemicals (Table 3.1 and Figure 3.5). Since mixtures of benzoic acid derivatives are generated upon photomodification of these chemicals, it implies that such mixtures are somewhat toxic. The hATQs that were not subject to photomodification were also tested for toxicity following pretreatment in SSR (1-hATQ, 2-hATQ, 1,3-dhATQ, 1,5-dhATQ, 1,8-dhATQ, 2,6-dhATQ, 1,2,5,8-thATQ). In general, these compounds did not exhibit a significant increase in toxicity following pretreatment in SSR. Two exceptions were 2-hATQ and 1,8-dhATQ: they were not photomodified in SSR but increased in toxicity when applied to the plant after pretreatment in SSR. Higher toxicity of these two compounds following exposure of SSR may be due photo-generation of stable active oxygen species such as hydrogen peroxide.

3.4 Discussion

Based on this study and previous work (Huang *et al.*, 1993, 1995; 1997a; Krylov *et al.*, 1997; McConkey *et al.*, 1997), it is clear that a significant part of the photoinduced toxicity of PAHs can be attributed to the photomodification products. Application of different light conditions shows that the toxicity of the photoproducts of ANT can also be photoinduced. This is in contrast to the major photoproduct of phenanthrene, phenanthrenequinone, which is more toxic than phenanthrene, although its toxicity is not greatly photoinduced (McConkey *et al.*, 1997). Certain ANT photoproducts are themselves subject to photooxidation, with a concomitant increase in toxicity. Conversely, some of the photoproducts of ANT (2-hATQ), while not readily photooxidized are nonetheless phototoxic, indicating photosensitization activity.

Upon exposure to UV light, ANT is rapidly photooxidized to a mixture of photoproducts that are more toxic than the parent compound (Huang *et al.*, 1993, 1997

a,b). The first primary product ATQ, is subject to further modification resulting in the production of several hATQs and benzoic acids (Figure 3.3). Of the ATQ and hATQs tested, ATQ, 1,2-dhATQ, 1,3-dhATQ, 1,4-dhATQ, 1,2,4-thATQ and 1,2,10-thANT, are subject to photomodification, while the other hATQs are light stable. HPLC analysis of the photomodification products revealed that similar mixtures of benzoic acids are generated when ATQ and hATQs are photomodified. It is unclear at this time why certain hATQs are photostable.

Because the ANT photooxidation products are more water soluble than ANT, their concentrations in the water column could be higher, resulting in increased bioavailability. Furthermore, these oxygenated ANTs are still sufficiently lipophilic to partition into biological membranes (Duxbury *et al.*, 1997). This combination of good bioavailability and high bioconcentration potential suggests that photomodified ANTs present a real risk when they are present in the environment. The extent of this risk is currently unknown, however, because ANT photoproducts have never been included in environmental surveillance programs.

The EC_{50}s for the ANT photoproducts ranged from 0.05 to >10 $\mu g\ ml^{-1}$ (Table 3.1). 2,6-dhATQ was the least toxic, with no observable effect in SSR and actually accelerating growth in PAR. In contrast, 2-hATQ was the most toxic (EC_{50}= 0.05 $\mu g\ ml^{-1}$ in SSR and EC_{50}= 0.2 $\mu g\ ml^{-1}$ in PAR). Interestingly, since both 2,6-dhATQ and 2-hATQ are photostable compounds, they would not be sources of toxic photoproducts. This explains 2,6-dhATQ's lack of toxic activity. 2-hATQ, however, is toxic in PAR (where it has almost no absorbance) and has enhanced toxicity in SSR (where it absorbs UV strongly). This suggests that it can have negative interactions via direct biological receptors, and via photosensitization generating singlet oxygen. Interestingly, when 2-hATQ was pretreated in SSR before toxicity testing, its toxicity

increased modestly. It is possible that in the plant growth medium 2-hATQ can photochemically generate active oxygen leading to kinetically stable toxic oxygen species such as hydrogen peroxide (Halliwell and Gutteridge, 1985; Foote, 1991). When the plants are subsequently added, toxicity would be due to the combined effects of 2-hATQ and hydrogen peroxide.

It is suggested that the combination of high toxicity and photostability shown by 2-hATQ may have significant environmental ramifications. First, 2-hATQ is a prevalent photoproduct, which forms at detectable concentrations when ANT is exposed to SSR (Figure 3.3). Therefore, it is likely to be generated in environmental samples wherever ANT and sunlight coexist. Second, it is both stable and toxic, and its toxicity does not require further photoactivation. As such, it will be persistent and would present a risk in any environmental compartment to which it partitions. Thus, it is believed that comprehensive PAH loading assessments should include 2-hATQ as an indicator of the presence of hazardous PAH photooxidation products.

The photooxidation of all the photomodifiable hATQs resulted in dominant production of phthalic acid, salicylic acid, benzoic acid and several other phenol and benzoic acid derivatives. The half-lives of these chemicals ranged from 1.8 h to 7.3 h (Table 3.1), rates that are rapid enough for the photoproducts to contribute to toxicity in an 8-day toxicity test with 2 day static renewal. As well, the half lives are short enough to be environmentally relevant. Thus, many of hATQs may be altered chemically in the environment, and the products are apparently hazardous. Since the benzoic acid mixtures showed moderate to high toxicity, it implies that complex mixtures of these one ring aromatics can have high toxic activity (EC_{50}s of 1.5 to 9 mg L^{-1} for mixtures derived from the hATQs, and 0.2 mg L^{-1} for those derived from ANT and ATQ). Interestingly, the benzoic acids individually are generally less toxic than

in the mixtures found in our study (Pierce *et al.*, 1980; Hobson *et al.*, 1984). Probably ANT and ATQ are more toxic after photomodification than the hATQs, because they can form 2-hATQ upon photomodification, while 2-hATQ can not be derived from the other hATQs. Furthermore, PAHs photomodified in the environment will certainly exist as complex mixtures. This indicates that the toxicity of relevant mixtures should be examined in detail.

For ATQ and the hATQs that are subject to photomodification, toxicity increased following photomodification. The impacts of these chemicals in SSR will be, to some degree, dependent on the rate of photomodification and the composition of the mixture of photoproducts. Nonetheless, many of the chemicals had significant toxic impact in PAR where photomodification is much slower. This implies that the chemicals have a direct negative physiological impact on the plants just as 2-hATQ does. Indeed it was found that photomodified ANT directly inhibits photosynthesis (Huang *et al.*, 1997a), and more recent work has indicated that some of the compounds under investigation here are direct inhibitors of photosynthetic electron transport (Mallakin, Babu, Marder and Greenberg, unpublished observations). Thus, the mechanism of toxicity of these compounds is likely to be multifaceted, with perhaps different mechanisms dominating depending on the specific environmental conditions and the extent of photomodification.

In addition to the ANT photoproducts revealing direct toxic activity in PAR, their toxicity could also have a photoinduced component in PAR (Morgan *et al.*, 1977; Newsted and Giesy, 1987; Larson and Barenbaum, 1988; Huang *et al.*, 1997b; Krylov *et al.*, 1997). Most of the compounds absorb in the long wavelength UV and short wavelength visible regions (370-450 nm) (Figure 3.1), and these spectral regions are in the PAR source (Figure 3.2). However, the absorbance by the chemicals in these

regions is lower than in shorter wavelength UV, so the frequency of photochemical events will be lower in PAR than SSR. Moreover, many of the ATQs have an excited state transition corresponding to absorbance peaks at about 400 nm. This would be the first excited state, S_1 (see Figure 3.1). There is another transition corresponding to peaks at about 300 nm. This is a higher excited state, S_2. Thus, the chemical would reach a higher excited state in SSR relative to PAR, consistent with the greater toxicity observed in SSR.

The differences in toxicity of the oxygenated ANTs will be dependent on the hydroxy substitution pattern. For instance, the molecules with rotational symmetry (2,6-dhATQ and 1,5-dhATQ) were less toxic than the compounds with mirror symmetry (1,4-dhATQ and 1,8-dhATQ) or no symmetry (e.g. 2-hATQ and 1,3-dhATQ). Clearly, it would be a valuable exercise to build a detailed model relating the structural features of oxygenated ANTs to their toxic strength. This would not only provide a better explanation of why various hATQs are hazardous, but might also allow predication of toxicity of other PAH photooxidation products. A powerful method for describing the detailed structures of organics is computational modeling of the molecules. Mezey (1995) has demonstrated that detailed electron shape density maps can be built by computer techniques and that these provide an accurate mathematical description of the shape of the electron cloud (the reactive part of organic molecules). Computer analysis is then used to determine which shape features correlate with a given property of a group of molecules. Indeed, in the case of 16 intact PAHs, detailed electron density shape maps were constructed to accurately describe the photoinduced toxicity of these PAHs (Mezey *et al.*, 1996). Shape analysis is now being performed for oxygenated ANTs.

This study, taken with previous work on phenanthrene /phenanthrenequinone

toxicity (McConkey *et al.*, 1997), clearly demonstrates that photomodified PAHs are hazardous. Specific photoproducts can now be identified which are more toxic than the parent PAHs. Moreover, the relative stabilities of 2-hATQ (Table 3.1) and phenanthrenequinone (McConkey *et al.*, 1997) indicate that these compounds will be generated and persist wherever PAHs and sunlight are present. It is suggested that environmental load studies on PAHs should now include oxygenated PAHs.

3.5 Conclusions

Anthracene photooxidation revealed a complex array of oxidation products. Several of these compounds were identified. Prevalent among the ANT photooxidation products were ATQ and hATQs. Eleven of these compounds were tested for toxicity using growth inhibition of the duckweed *Lemna gibba* L. G-3. All but one of the compounds tested were found to be toxic. When UV radiation was present in the light source toxicity was generally enhanced, indicating the ANT photoproducts are phototoxic. The chemicals were also irradiated under SSR prior to toxicity testing. In about half the cases, the ATQ compounds were rapidly photooxidized and the resultant photoproducts were more toxic than the parent compounds. Interestingly, 2-hATQ, which was not subject to photooxidation, was the most toxic of the compounds tested. As a light stable compound it presents the risk of a persistent environmental hazard.

Chapter IV

Mechanisms of Toxicity of Specific Photooxidation Products of Anthracene to Higher Plants: Inhibition of Photosynthetic Activity and Electron Transport in *Lemna gibba* L. G-3 (duckweed)[1]

---

[1] This paper is for submission to *Ecotoxicology and Environmental Safety*, and authored as Ali Mallakin, T. Sudhakar Babu, D. George Dixon, and Bruce M. Greenberg.

4.1 Introduction

Polycyclic aromatic hydrocarbons (PAHs) become more reactive and hazardous following photomodification (Huang *et al.*, 1997a; McConkey *et al.*, 1997; Mallakin *et al.*, 1999). Due to photomodification, PAHs are structurally altered to a variety of compounds, mainly oxygenation products, and these products are often more toxic than the parent compounds (Huang *et al.*, 1995; McConkey *et al.*, 1997; Mallakin *et al.*, 1999). ANT is a rapidly photooxidized PAH whose photomodification pathway has been determined. The products formed are ATQ, hydroxyATQs and benzoic acid derivatives (Chapter two; Mallakin *et al.*, 2000). These products are toxic to plants (Chapter three; Mallakin *et al.*, 1999), and mixtures of ANT photoproducts have been shown to inhibit photosynthesis (Huang *et al.*, 1997a). The objective of this chapter is to examine the impacts of specific ANT photoproducts on the photosynthetic apparatus. Both in vivo and in vitro studies showed that electron transport downstream from PSII was affected with the primary site of action probably being the cytochrome-b6/f complex.

A common mechanism of toxic action is inhibition of biological pathways such as photosynthesis and mitochondrial electron transport. Plant productivity depends on the conversion of light energy into stable chemical energy (Greenberg, 1991; Krause and Weis, 1991). If the photosynthetic apparatus is inhibited by environmental contaminants, changes in plant cell physiology, growth and biomass yield are inevitable. As well, it has been shown that inhibition of photosynthesis is a reliable assay of the potential toxicity of xenobiotic contaminants (Draber and Trebst, 1986; Lichtenthaler and Rinderle, 1987; Huang *et al.*, 1997a). Chemical stressors may interrupt electron transport activity in PSII, cytochrome-b6/f or PSI. They may also alter the structure of chloroplasts, lower chlorophyll concentrations or inhibit the

Calvin cycle (Krause and Weis, 1991; Hill *et al.*, 1993, 1997; Huang *et al.*, 1997a). Duxbury et al (1997) showed that intact and modified PAHs accumulate in thylakoid membranes of plants. In addition, recent work has shown that photosynthetic electron transport is inhibited by mixtures of oxyPAHs at lower concentrations than either growth or CO_2 fixation (Huang *et al.*, 1995, 1997a). However, little is known about which specific PAH photoproducts inhibit photosynthesis and if this correlates with their toxicity.

To increase our knowledge of the adverse effects of environmental hazards on biological pathways, it is beneficial to understand the mechanisms of toxic action. In this chapter the mechanisms by which PAHs and oxyPAHs influenced aquatic plants was examined to determine if inhibition of photosynthesis correlates with inhibition of growth. The inhibition of photosynthesis at PSII can be observed by monitoring the induction kinetics of endogenous chlorophyll *a* (Chl *a*) fluorescence (Bolhar-Nordenkampf and Oquist, 1993). There is interest in the practical application of Chl *a* fluorescence as a rapid and sensitive bioindicator of plant stress in response to different physical and chemical factors (Baker *et al.*, 1983; Schreiber 1986; Huang *et al.*, 1997a). An advantage of this technique is that it permits in vivo non-destructive determination of changes in the photosynthetic apparatus much earlier than the appearance of visible injury. Portable fluorometers with microcomputers capable of measuring several parameters of Chl *a* fluorescence are available (Schreiber *et al.*, 1975; Orgen and Baker, 1985; Schreiber, 1986). These features make this technique readily applicable both as a laboratory test and an environmental bioassay under field conditions (Oquist and Wass 1988, Greaves *et al.*, 1992). Thus, the use of Chl *a* fluorescence as a bioindicator has great potential. In this chapter, Chl *a* fluorescence was applied to the ANT photoproducts to determine if inhibition of photosynthesis by these compounds could be correlated to the whole organism toxicity determined in

Chapter three.

4.2 Materials and Methods

4.2.1 Plant Growth Conditions

Prior to chemical exposure, *L. gibba* L.G-3 was cultured aseptically on half-strength Hutner's medium (*L. gibba* growth medium) under 60 μmol m^{-2} s^{-1} of continuous cool-white fluorescent light as described earlier (Huang *et al.*, 1993; Mallakin *et al.*, 1999). Chemicals were applied to the plants for 6 h, after which Chl *a* fluorescence was measured. Chemicals were dissolved in DMSO and delivered to the plants via the growth medium as described in Chapter three. The irradiation source for the plants during chemical treatment was simulated solar radiation (SSR) as described previously (Huang *et al.*, 1993; American Society for Testing and Materials, 1995; Mallakin *et al.*, 1999, 2000). SSR has a PAR: UV-A: UV-B ratio of 100:10:1, and a total fluence rate of 100 μmol m^{-2} s^{-1}. Fluence rates and spectral output of the light sources were measured with a photodiode array spectroradiometer calibrated with a 1-kW quartz halogen lamp (Oriel, Stratford, CT, USA).

4.2.2 Chemicals and Chemical Exposure of Plants to PAHs

The chemicals used in this study were abbreviated as outlined in Figures 1.1 and 2.1. For chemical exposure, plants were placed on 10 mL of fresh, half-strength Hutner's medium in 5-cm diameter petri dishes (Huang *et al.*, 1993; Mallakin *et al.*, 1999). ANT, ATQ and hATQs were dissolved in dimethylsulfoxide (DMSO) and delivered to the medium by 1000-fold dilution of DMSO stock solutions to final concentrations ranging from 0 to 10 μg/ml. ANT and its derivatives have low solubility in water (Pearlman *et al.*, 1984), so delivery with DMSO was required to

achieve concentrations necessary for full concentration-response curves. Chemical purity and the accuracy of chemical delivery were assayed by high-performance liquid chromatography (HPLC) as discussed previously (Huang *et al.*, 1993; McConkey *et al.*, 1997; Mallakin *et al*, 1999, 2000). Prior to measurement of Chl *a* fluorescence, plants were incubated with chemicals in SSR for 6 h.

For application of photomodified ANT and ATQ to *L. gibba*, the intact chemicals were delivered to the growth medium to a final concentration of 10 μg/ml. The growth medium containing chemicals was covered with polyethylene film and incubated in UV-B (20 μmol m^{-2} s^{-1}, comparable to the total UV-B in full sunlight) for 7 d. The extent of the photomodification reaction was monitored by HPLC analysis as described previously (Mallakin *et al.*, 1999, 2000). HPLC conditions were the same as those used in Chapter 2.

4.2.3 Chlorophyll *a* Fluorescence Induction

After treatment of plants with a given chemical for 6 h, they were dark adapted for 30 min. A whole leaf was removed from the plants, placed on a probe and put in a spectrofluorometer with millisecond time resolution (Photon Technology International Inc., S. Brunswick, N.J.). A dark adaptation period of 20-30 min is usually enough to reverse all nonphotochemical fluorescence quenching provided that photoinhibition of photosynthesis is not involved (Powles, 1984). Chl *a* fluorescence induction was measured by excitation at 435 nm (70 μmol m^{-2} s^{-1}) and detection of fluorescence at 685 nm. A typical fluorescence induction curve shown in Figure 4.1. The time constant was 1 ms and Chl *a* fluorescence was measured temporally for 10 sec to detect PSII activity, and 60 sec to determine electron transport downstream from PSII. After illumination of a dark-adapted plant leaf, there is an immediate rise in

fluorescence to a minimal level (F_0). Because this state lasts for only picoseconds to nanoseconds, an electromagnetic shutter (Uniblitz, model D122, shutter driver) in conjunction with a computer software package (Photon Technology International Inc., S. Brunswick, N.J.) was used to achieve a good approximation of F_0. After F_0 is reached, fluorescence gradually rises to a maximum level of fluorescence (F_M). This takes about 1 sec when photosynthesis is not inhibited. It takes much less time if electron transport is inhibited. Previous work has shown that 70 μmol m^{-2} s^{-1} of 435 nm light is sufficient to reach F_M in *L. gibba* (Huang *et al.*, 1997a).

Variable fluorescence (F_V) is the difference between F_M and F_0. To measure PSII activity, F_V/F_M and $t_{1/2}$ (the half time for the rise from F_0 to F_M) were used. The ratio of F_V/F_M for *L. gibba* has a typical range of 0.7-0.75. After F_M is reached, fluorescence slowly drops to a transient plateau (F_{SI}). This quenching, $F_Q=(F_M-F_{SI})$ can be used as a measure of electron transport down stream from PSII (Malkin *et al.*, 1994). F_Q/F_M is usually about 0.25 in a healthy plant and drops if photosynthesis has been impaired. The theoretical basis of the above parameters is given in Chapter one (Section 1.8).

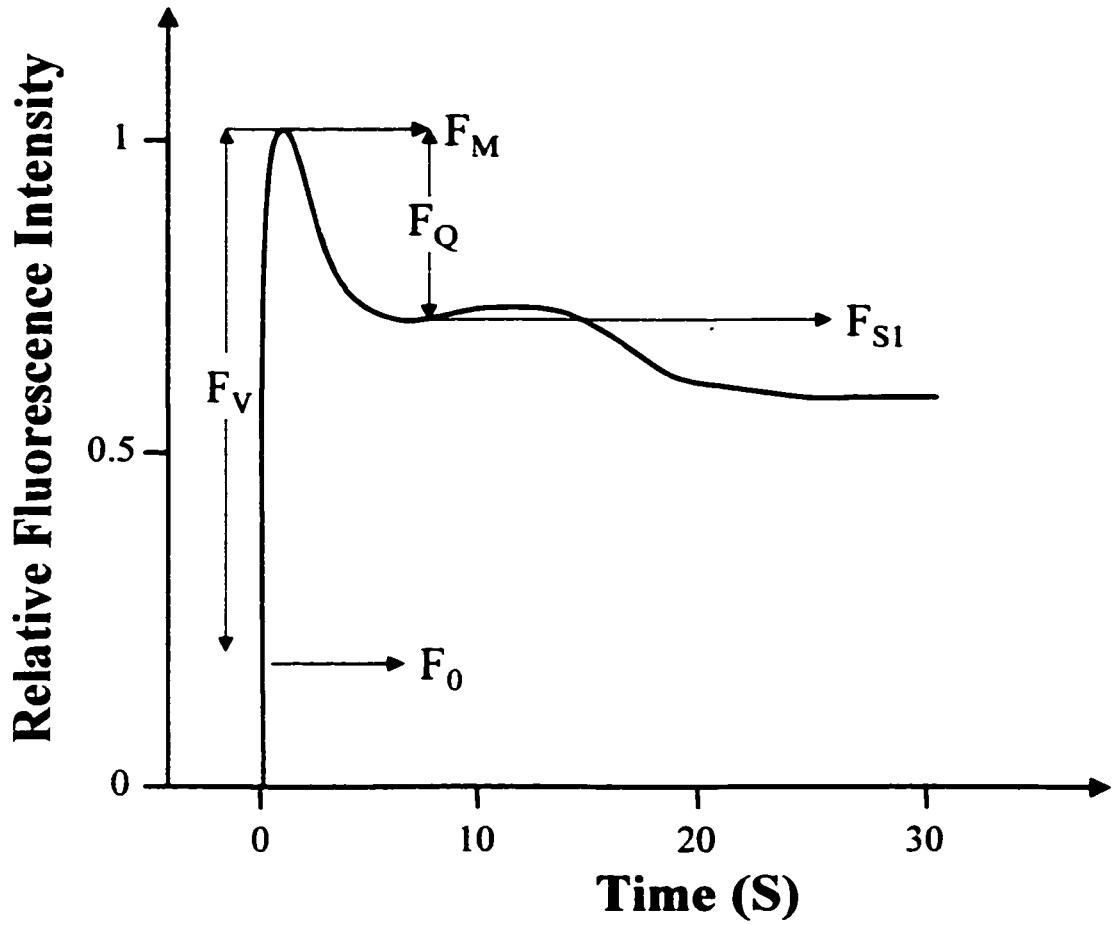

Figure 4.1 A characteristic chlorophyll *a* fluorescence induction curve of a control *L .gibba* leaf. A plant leaf that had been dark adapted for 30 min was illuminated with light at a wavelength of 435 nm, inducing an increase in fluorescence intensity from the initial level F_0 to the maximum level F_M. Light intensity was 70 μmol m^{-2} s^{-1}, and the temperature was 25°C. F_0 was resolved with the aid of the computer software for the fluorometer. F_Q and F_{S1} are as defined in the text.

4.2.4 Pulse Amplitude Modulated (PAM) Fluorescence Measurements

A PAM fluorometer was also used to assess ANT and oxyANT impacts. A typical Chl *a* fluorescence trace using a PAM fluorometer is shown in Figure 4.2. This method is described in detail elsewhere (Schreiber *et al.*, 1986). Dark-adapted *L. gibba* plants were placed under the PAM light guide and the modulated measuring light was switched on to record F_0. The addition of a brief (0.8 sec) saturating non-modulated light pulse (2000 μmol m^{-2} s^{-1} of PAR) to the modulated beam causes fluorescence to rise to F_M (Figure 4.2) and F_V (F_M-F_0) can be calculated. An actinic light (non-modulated; 150 μmol m^{-2} s^{-1}) is then applied which causes a brief rise in fluorescence followed by drop over about 3 min to a steady state level of fluorescence, F_T. Saturating pulses applied with the actinic light on gives F_M' which is a measure of the fraction of reaction centers that are open during steady state photosynthesis. Saturating light pulses were applied during this period with a frequency of 60 second to measure photochemical quenching (q_P) and non-photochemical quenching (q_N). The parameters obtained were: F_V/F_M, maximal PSII photochemical efficiency; Yield [(F_M'-F_T)/F_M'], a measure of steady state electron transport or energy storage; photochemical quenching, $qP = [(F_M'-F_T)/(F_M'-F_0)]$, a measure of quenching for photochemical purposes relative to total light energy absorbed by PSII; and non-photochemical quenching, $qN = [1-(F_M'-F_0)/(F_M-F_0)]$, fluorescence quenching by non-photochemical mechanisms.

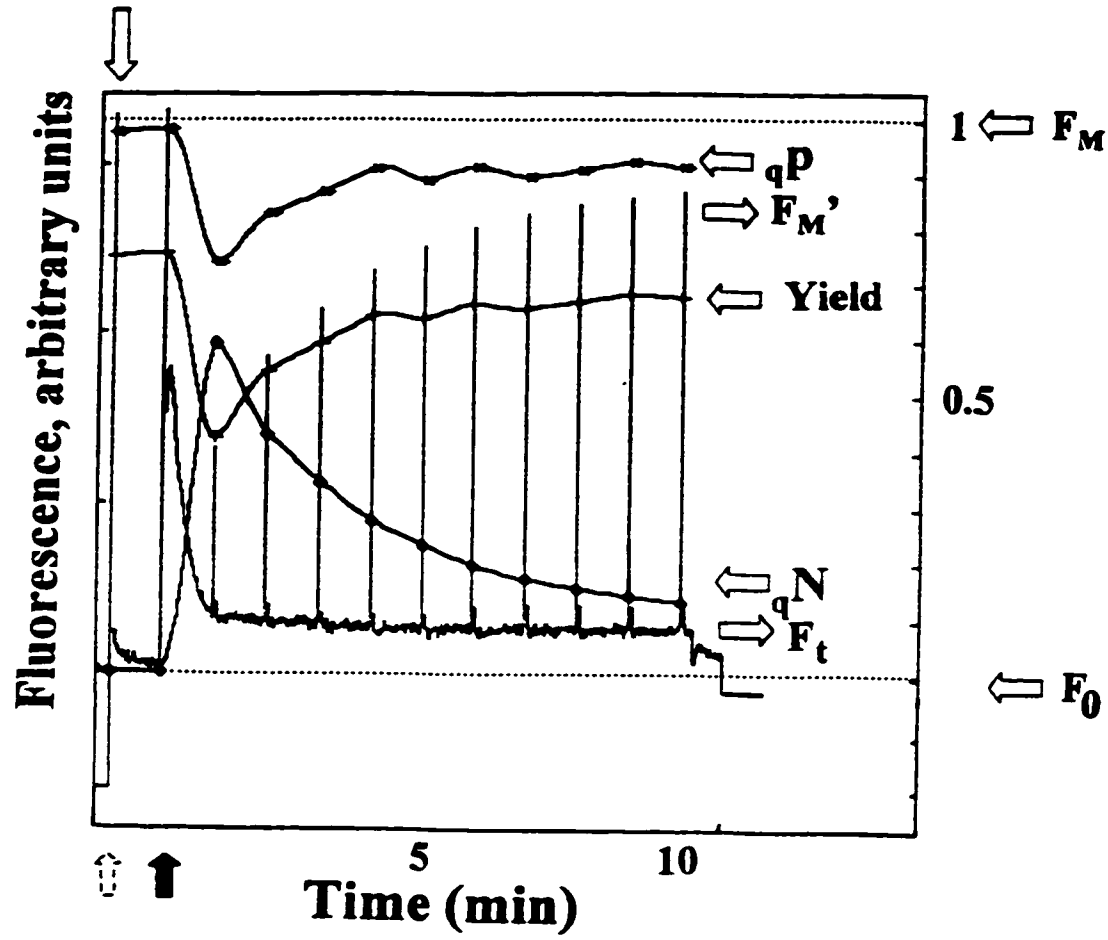

Figure 4.2 A typical PAM fluorometer trace for a dark adapted control leaf. The modulated light is applied (⇧) to give F_0. A single saturating pulse (⇩) is applied to give F_M and F_V. Application of the actinic light (⬆) and saturating pulses (at 1 min intervals) allows F_T and F_M' to be determined after approximately 10 minutes. F_V/F_M, qP, qN and yield are then derived as described in the text.

4.2.5 Isolation of Thylakoid membranes for Measurement of PSI and PSII

Thylakoid membranes were isolated and treated according to the procedures of Nakatani and Barber (1977) and Babu et al (1992), with some modifications. *Lemna gibba* leafs (5 g fresh weight) were washed with deionized water and homogenized in a cold mortar and pestle using 5 ml of buffer A (50 mM Hepes-NaOH pH: 7.5, 0.3 M sucrose, 20 mM NaCl, and 5 mM $MgCl_2$). The homogenate was filtered through one layer of Miracloth® (Fisher Scientific, Mississauga, ON, Canada) and centrifuged at 3,000 g for 5 min. The supernatant was discarded, and the pellet containing chloroplasts was resuspended in 5 mL of buffer B (20 mM Hepes-NaOH pH 7.5, 5 mM $MgCl_2$, 150 mM NaCl) and left on ice for 1-2 min. The homogenate was filtered again and centrifuged at 3,000 g for 5 min. The pellet was resuspended in buffer A and kept at 4°C in the dark until use. The amount of thylakoid membranes was quantified by measuring Chl concentration (Lichtenthaler, 1987). The membranes were diluted with buffer C (20 mM Hepes-NaOH pH: 7.5, 10 mM NaCl, 5 mM $MgCl_2$). Thylakoids equivalent to a final Chl concentration of 10 μg/mL were used in all the chemical treatments. Oxygen evolution and consumption was measured with an oxygen electrode.

Different concentrations of ANT and selected photoproducts were added to the thylakoid membranes (Chl = 10 μg/mL). They were added by 1000-fold dilution from DMSO stock solution. The solutions were incubated in darkness for 20 min at 4 °C and electron transport was measured at room temperature. Electron transport was measured with oxygen electrode (Hansatech Instruments LTD., Kings Lynn, England) at 25°C under a saturating light intensity of 2000 μmol m^{-2} s^{-1}. PSII mediated oxygen evolution activity was measured with 0.5 mM parabenzoquinone (pBQ) as an electron acceptor and H_2O as the electron donor in a 1 mL reaction buffer of 25 mM Hepes-

NaOH (pH 7.5) (Figure 4.3). 10 µl of a treated thylakoid membrane sample was added to the reaction tube and the reaction was initiated by turning on the actinic light (2000 µmol m^{-2} s^{-1}).

The PSI assay mixture contained 25 mM Hepes-NaOH buffer (pH 7.5), 2 mM sodium azide, 0.01 mM 3-(3, 4-dichlorophenyl)-1,1-dimethyl urea (DCMU), 1 mM methyl viologen (MV) and 0.1 mM reduced 2, 6-dichlorophenol indophenol (DCPIP). 10 µl of a treated thylakoid membrane sample was added to the reaction mixture. The DCPIP was reduced by the addition of 10 µl of 5 mM sodium ascorbate adjusted to pH 7.5. The reaction was initiated by turning on the actinic light, and electron transport was measured as O_2 consumption. For the PSI assay it was necessary to eliminate competing PSII activity. To achieve this, DCMU, a PSII inhibitor was used. DCPIP (0.1 mM) with ascorbate (5 mM) were the electron donor couple, allowing measurement of PSI activity via ascorbate –> DCPIP –> PSI –> MV –> O2 (Figure 4.3).

4.2.6 Statistical Analysis

Log-linear regressions were fit to concentration-response data over the linear portion of the curves. Accordingly, the F_V/F_M values for hATQs were normalized to their mean (normalized value = data point % mean of the data set) and related to chemical concentration using linear regression analysis (SYSTAT 8.0 for Windows; Systat Inc., Evanston, IL, USA). The factors used were treatment (intact and photomodified hATQs) and log of concentration, depending on the experiment.

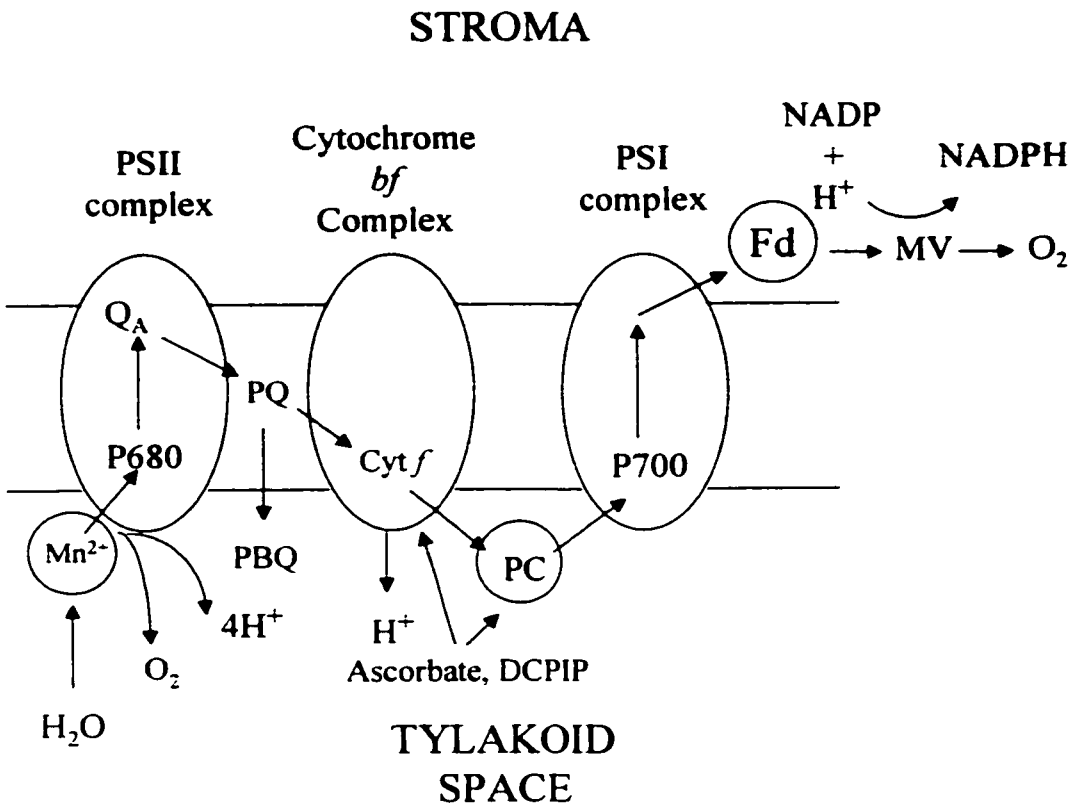

Figure 4.3 Schematic representation of photosynthesis in plants. Both photosystems use the energy of absorbed light to move electrons through thylakoid membranes. Non-cyclic electron transport from water to two electron-acceptors is shown (PBQ and MV). PBQ was used to measure PSII and MV was used to measure PSI. The electron donor 2,6-Dichlorophenol- indophenol (DCPIP) was used as a source of electrons for PSI.

4.3 Results

4.3.1 Effects of Intact and Photomodified ANT and ATQ on Chl *a* Fluorescence Induction in *L. gibba*

To study the effects of intact and photomodified ANT on photosynthesis, a concentration range for in vivo inhibition of photosynthesis in *L. gibba* was established. Chl *a* fluorescence induction was measured following treatment of the plants with the chemicals for 6 h in SSR (Figure 4.4). For both intact and photomodified ANT, F_V/F_M was diminished in a concentration dependent manner (Figure 4.4). A comparison of the response to intact and photomodified ANT revealed that the slopes of the log-linear regressions were not significantly different from each other ($p = 0.21$). Similarly the EC50s for loss of F_V/F_M were reasonably close to each other (EC50s =1.8 ± (0.16) mg/L and 1.0 ± (0.14) mg/L) for intact and photomodified ANT, respectively (Figure 4.4). This could imply that ANT (half-life in SSR of 2 h) is being converted to the photoproducts and then the photoproducts act on photosynthesis. Conversely, ANT and PM ANT could simply have similar potencies.

The effects of specific photoproducts of ANT on photosynthesis were tested. As a first step, the ANT primary photoproduct ATQ was examined for inhibition of photosynthesis. For intact and photomodified ATQ, diminishment of F_V/F_M was dependent on chemical concentration. The concentration responses for both intact and photomodified ATQ were quite similar. Both sets of data fit a log-linear regression ($r^2 = 0.954$ and $r^2 = 0.986$ for intact and photomodified ATQ, respectively) and the two data sets were not significantly different from each other ($p = 0.23$). The EC50s for diminishment of F_V/F_M were 1.6 ± (0.21) mg/L and 0.8 ± (0.19) mg/L respectively, which were also reasonably close to each other and comparable to the EC50's for

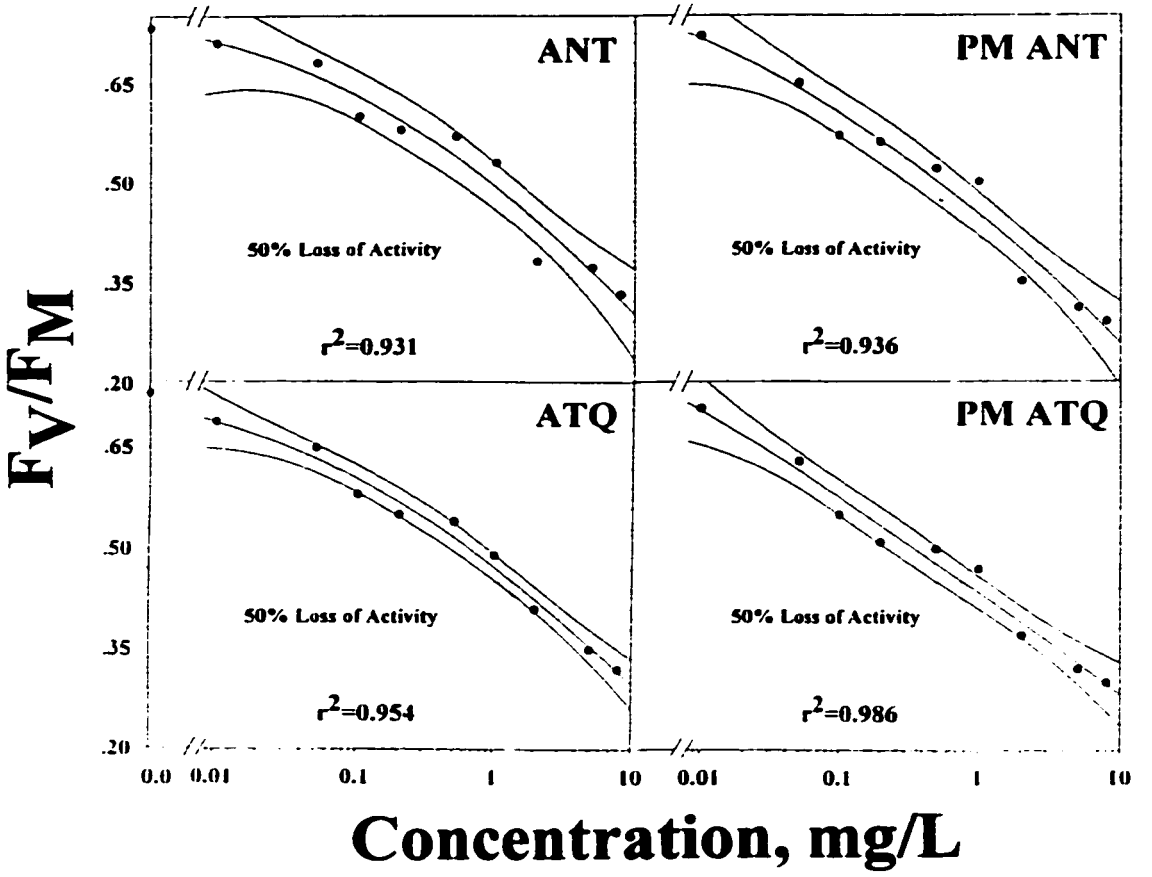

Figure 4.4 Maximal photosystem II efficiency (F_V/F_M) for *Lemna gibba* treated with intact ANT and ATQ. *L. gibba* plants were treated with various concentrations of intact ANT, ATQ, and their respective photomodified (PM) products. After incubation for 6 h, the plants were placed in darkness for 30 min and Chl *a* fluorescence induction was measured for determination of F_V/F_M. Concentration was plotted on a log scale. Each data point represents an average from three independent experiments. A maximal F_V/F_M of 0.7 and a minimal F_V/F_M of 0.2 were used for calculating 50% loss of activity.

growth inhibition (Chapter three). As was the case with ANT, one possible explanation for the similar effects of intact or photomodified ATQ on F_V/F_M (Figure 4.4) is that ATQ is being further photomodified ($t_{1/2}$ = 1.8 h in 100 μmol m^{-2} s^{-1} of SSR) (Mallakin *et al.*, 1999) during the course of the experiment and subsequently inhibiting the photosynthesis in a manner similar to externally photomodified ATQ.

The EC50s for loss of F_V/F_M for intact ANT and ATQ were not significantly different from each other (EC50s = 1.8 ± (0.16) mg/L and 1.6 ± (0.21) mg/L for intact ANT and ATQ) (Table 4.1). This is consistent with the fact that the main photoproduct of ANT is ATQ. The concentration responses for intact ANT and ATQ were also similar; they both fit log-linear regressions (r^2 = 0.931 and 0.954 for intact ANT and ATQ) and the two data sets were not significantly different from each other (p = 0.25).

The above shows that ANT and ATQ, whether applied in intact or photomodified form, can result in inhibition of PSII. However, this can come about via a direct effect on PSII, or via inhibition of downstream electron transport followed by damage to PSII when electron transport backs up. Indeed, Huang *et al* (1997a) showed that electron transport downstream from PSII is inhibited by a mixture of photomodified ANT products. To assess if there was damage downstream from PSII, F_Q/F_M was measured. For plants treated in SSR with ANT or ATQ, F_Q/F_M was diminished (Figure 4.5). For plants treated with intact ANT and ATQ the EC50 values for F_Q/F_M were 0.09 ± 0.02 mg/L and 0.025 ± 0.01 mg/L in SSR, much lower than the EC50s for F_V/F_M (Table 4.1).

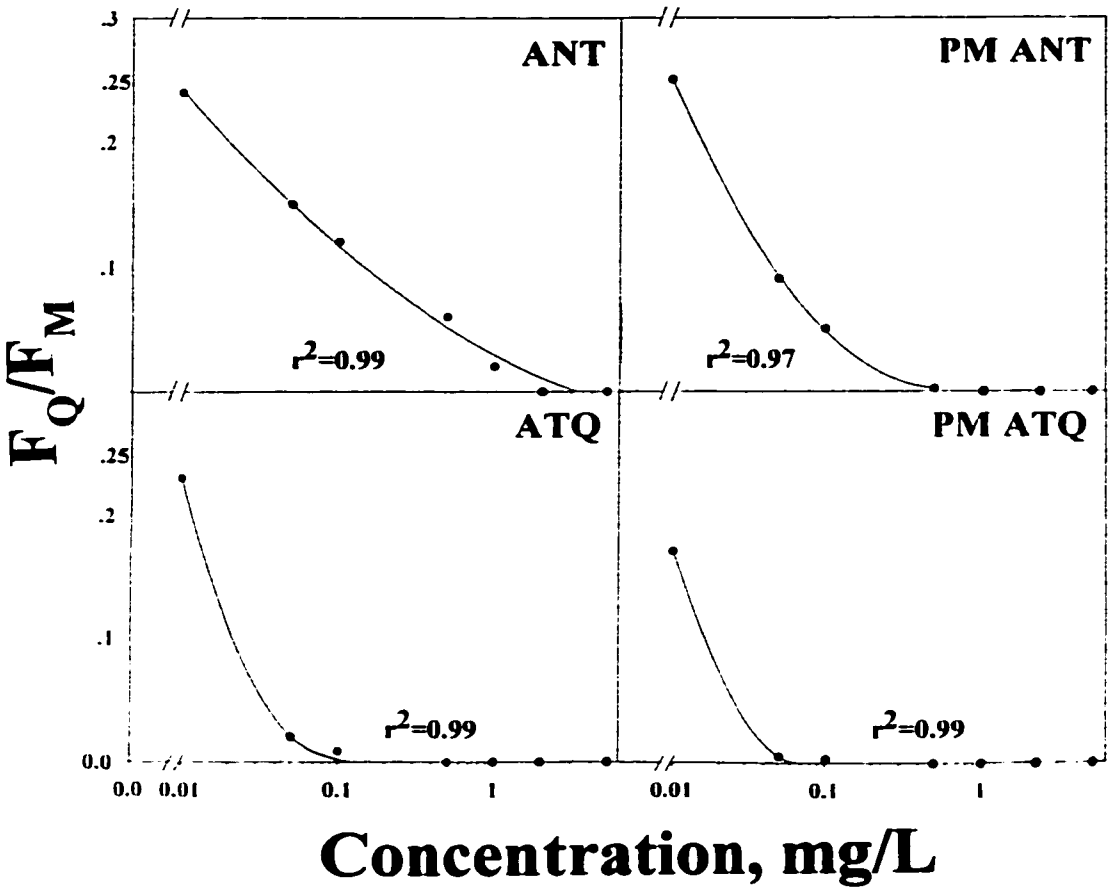

Figure 4.5 In vivo measurements for F_Q/F_M in *Lemna gibba* treated with ANT and ATQ. Intact and photomodified (PM) ANT and ATQ were used. *L. gibba* plants were treated with various concentrations of the indicated chemicals. After incubation for 6 h, the plants were placed in darkness for 30 min and chlorophyll *a* fluorescence induction was measured for determination of F_Q/F_M. Chemical concentration was plotted on a log scale. Each data point represents an average from three independent experiments.

Table 4.1 EC_{50} values for F_V/F_M, F_Q/F_M and $t_{1/2}$.

Chemicals Examined	EC_{50}s (F_V/F_M) µg/mL	EC_{50}s (F_Q/F_M) µg/mL	EC_{50}s ($t_{1/2}$) µg/mL
ANT	1.8 ± (0.16)	0.09 ± (0.02)	1.2 ± (0.01)
ATQ	1.6 ± (0.21)	0.03 ± (0.01)	0.9 ± (0.25)
1-hATQ	3.4 ± (0.14)	0.06 ± (0.04)	2.1 ± (0.04)
2-hATQ	0.4 ± (0.38)	0.02 ± (0.02)	0.8 ± (0.32)
1,2-dhATQ	1.7 ± (0.46)	0.6 ± (0.19)	0.9 ± (0.14)
1,3-dhATQ	3.5 ± (0.20)	0.15 ± (0.03)	2.1 ± (0.02)
1,4-dhATQ	20.0± (0.91)	20.0 ± (0.01)	3.4 ± (0.05)
1,5-dhATQ	13.0± (0.64)	13.0 ± (0.20)	3.2 ± (0.23)
1,8-dhATQ	16.0± (0.28)	8.0 ± (0.01)	3.0 ± (0.12)
2,6-dhATQ	15.0± (0.12)	7.0 ± (0.21)	2.7 ± (0.05)
1,2,4-thATQ	7.0 ± (0.02)	0.55 ± (0.31)	1.4 ± (0.10)
1,2,5,8-thATQ	10.0± (0.25)	1.00 ± (0.43)	2.2 ± (0.38)
1,2,10-thANT	5.0 ± (0.08)	1.00 ± (0.09)	2.5 ± (0.41)

For ANT, the diminishment of F_Q/F_M increased upon photomodification, but for ATQ the difference was not significant (Figure 4.5). The EC50s for diminishment of F_Q/F_M for intact ANT and PM ANT were significantly different from each other (EC50s = 0.1 ± (0.14) mg/L and 0.03 ± (0.01) mg/L for intact ANT and PM ANT; p = 0.05) (Figure 4.5). Conversely the concentration responses for F_Q/F_M both intact and photomodified ATQ were quite similar. Both sets of data fit a log-linear regression (r^2 = 0.99 and r^2 = 0.99 for intact and photomodified ATQ, respectively) and the two data sets were not significantly different from each other (p = 0.22). As well, the concentration responses for loss of F_Q/F_M for intact ANT and ATQ were significantly different (EC50 = 0.9 mg/L and EC50 = 0.02 mg/L, respectively; p = 0.02) (Figure 4.5).

4.3.2 Effects of ANT Photoproducts on Chl *a* Fluorescence Induction in *L. gibba*

Having found that ANT and ATQ inhibit photosynthesis and that the more sensitive measure was F_Q/F_M, it was of interest to determine if other oxyANTs behaved in the same way. Because the above responses to the intact and photomodified chemicals were similar for the most part, only the intact chemicals were applied. Dose responses for F_V/F_M for 1,2-dhATQ, 1,4-dhATQ, 2,6-dhATQ and 2-hATQ are shown in Figure 4.6. 2-hATQ, caused diminishment of F_V/F_M at very low concentrations. 1,2-dhATQ also diminished F_V/F_M, but less so than 2-hATQ. 2,6-dhATQ and 1,4-dhATQ had little or no effect on F_V/F_M fluorescence (Figure 4.6). Interestingly, at the whole organism level 2-hATQ was highly toxic, 1,2-dhATQ had intermediate toxicity, and 2,6-dhATQ was not toxic (see Table 3.1). The only deviation was 1,4-dhATQ, which was toxic but did not inhibit the photosynthesis (Figure 4.6 and Table 3.1).

The effects of 1,2-dhATQ, 1,4-dhATQ, 2,6-dhATQ and 2-hATQ on Chl *a*

fluorescence quenching (F_Q/F_M) were also examined (Figure 4.7). As was the case for ANT and ATQ, F_Q/F_M was a more sensitive measure of effect than F_V/F_M. In fact, 2,6-dhATQ significantly inhibited photosynthesis by this indicator of effect. The dose response curve for 2-hATQ gave a very low EC50 of 0.015 μg/ml (Table 4.1). Once again, 1,4-dhATQ almost had no effect on photosynthesis as measured by F_Q/F_M (Figure 4.7), even though it has moderate whole organism toxicity. For 2-hATQ, 1,2-dhATQ and 2,6-dhATQ, F_Q/F_M was predictive of their relative toxic strengths (c.f. Table 3.1 and Table 4.1). Because F_Q/F_M was more sensitive than F_V/F_M, it may be assumed that the initial effects of 1,2-dhATQ, 2,6-dhATQ and 2-hATQ are downstream from PSII, either at cytochrome-b6/f or PSI.

To further study the effects of oxyANTs on photosynthesis in vivo, the EC50s for F_V/F_M and F_Q/F_M for seven additional compounds were determined (Table 4.1). The EC50s for diminishment of F_Q/F_M for all 13 chemicals were lower than those for F_V/F_M. This clearly shows that F_Q/F_M was a more sensitive indicator than F_V/F_M for ANT and its photoproducts.

For plants treated with ANT, ATQ and hATQs the EC50's for diminishment of $t_{1/2}$ were determined (Table 4.1). As was the case for F_V/F_M, the EC50s for loss of $t_{1/2}$ for intact ANT and ATQ were similar to each other (EC50s = 1.2 μg/ml and 0.9 μg/ml, respectively) (Table 4.1). Treatment of plants with 2-hATQ resulted in decrease of EC_{50}s for $t_{1/2}$ (EC50 = 0.8 ± 0.32 μg/ml). This indicates that the electron acceptor pool and the photochemical reactions of PSII were inhibited by this chemical. The EC50s for loss of $t_{1/2}$ in many cases were between F_V/F_M and F_Q/F_M values. This may suggest that $t_{1/2}$ may be used as an intermediate indicator of effect.

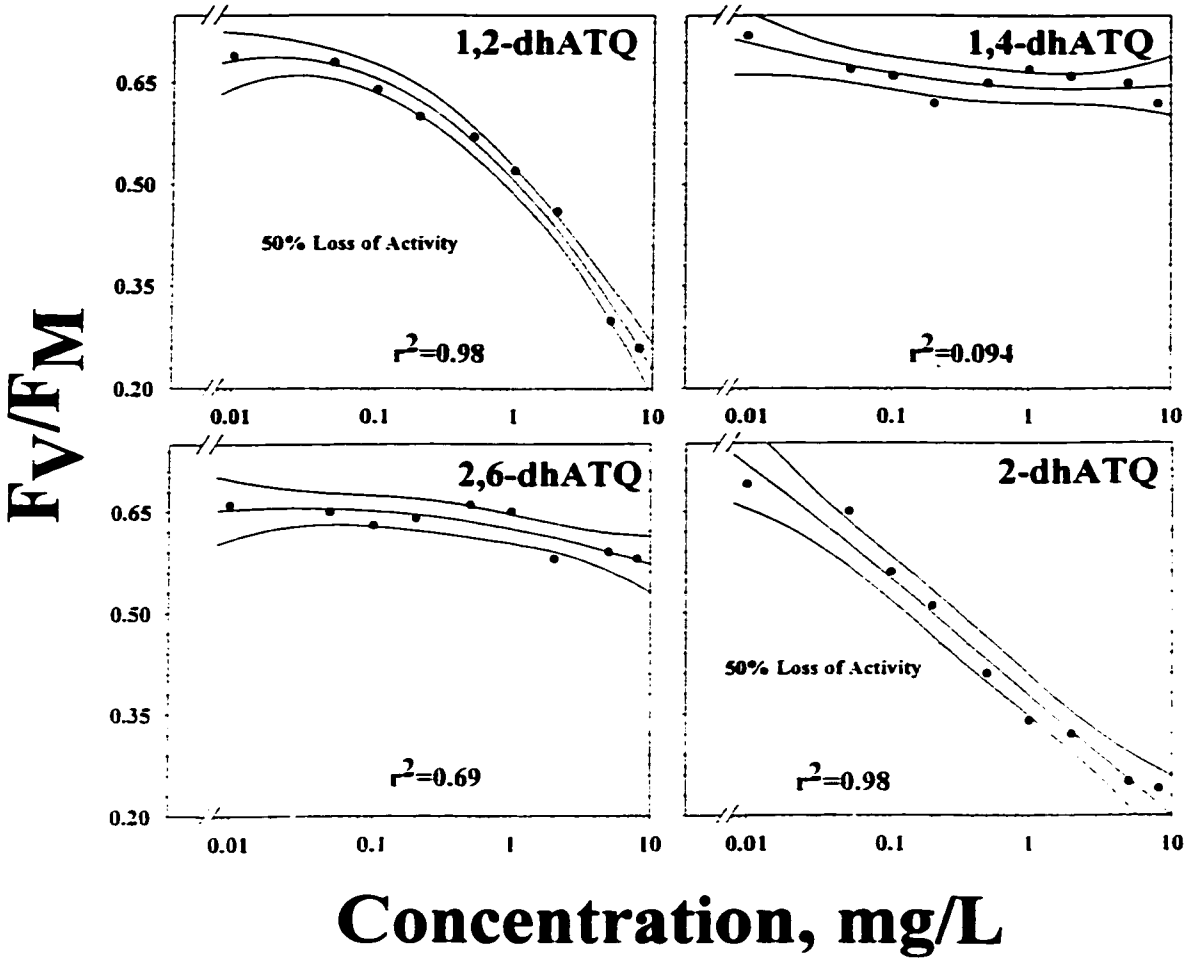

Figure 4.6 Maximal photosystem II efficiency (F_V/F_M) for *Lemna gibba* treated with intact 1,2-dhATQ, 1,4-dhATQ, 2,6-dhATQ and 2-hATQ. *L. gibba* plants were treated with various concentrations of these compounds. After incubation for 6 h, the plants were placed in darkness for 30 min and chlorophyll *a* fluorescence induction was measured for determination of F_V/F_M. Concentration was plotted on a log scale. Each data point represents an average from three independent experiments. A maximal F_V/F_M of 0.7 and a minimal F_V/F_M of 0.2 were used for calculating 50% loss of activity.

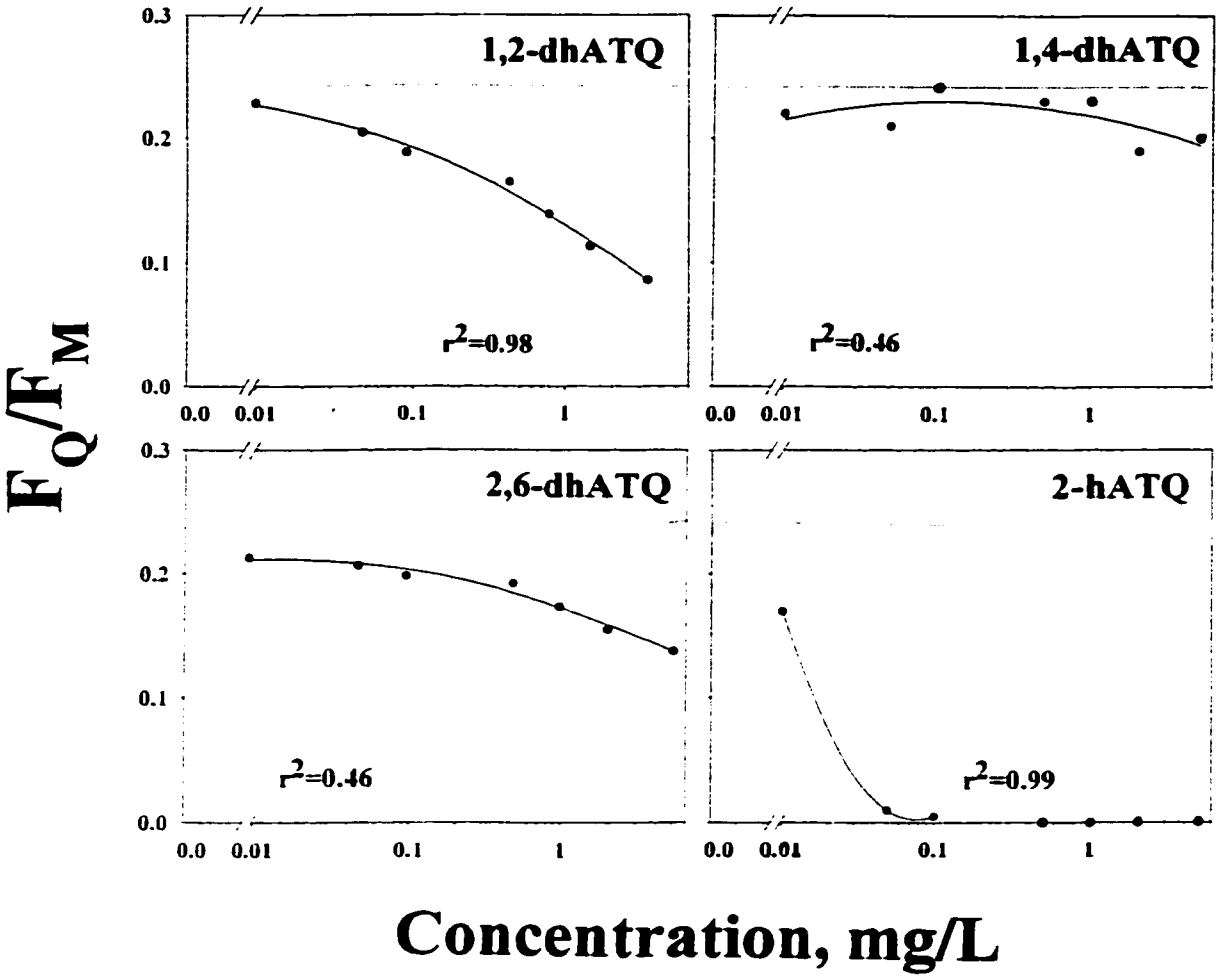

Figure 4.7 In vivo measurements for F_Q/F_M in *Lemna gibba* treated with 1,2-dhATQ, 1,4-dhATQ, 2,6-dhATQ and 2-hATQ. *L. gibba* plants were treated with various concentrations of the indicated chemicals. After incubation for 6 h, the plants were placed in darkness for 30 min and chlorophyll *a* fluorescence induction was measured for determination of F_Q/F_M. Concentration was plotted on a log scale. Each data point represents an average from three independent experiments.

4.3.3 Correlation Between EC50s for Inhibition of Growth and Photosynthetic Activity

Correlations between inhibition of growth and photosynthetic activity were examined. Because it was shown that ANT derivatives inhibited downstream from PSII electron transport in vivo, it may be assumed that a correlation between toxicity and photosynthetic activity will be found. There were good correlations between the EC50s for inhibition of growth (Chapter Three, Table 3.1) and the EC50s for both F_V/F_M and F_Q/F_M (Figure 4.8). Nonetheless correlations for F_Q/F_M (proportional to cytochrome-b6/f and/or PSI activity) and F_V/F_M (proportional to PSII activity) vs the EC50s for growth inhibition were different. The quality of the log linear regressions (r^2 = 0.67 and 0.78 for F_Q/F_M and F_V/F_M, respectively) showed F_V/F_M to correlate better with whole organism toxicity. However, F_Q/F_M was a more sensitive measure of toxicity (the EC50s for F_Q/F_M were lower than the EC50s for growth). Interestingly, when the non-toxic chemicals were removed from the regression for F_Q/F_M and growth (EC50s > 5 μg/ml for both measured), the correlation was improved (r^2 = 0.75). Thus, F_Q/F_M seems to be both a sensitive and predictive bioindicator of ANT and PM ANT toxicity.

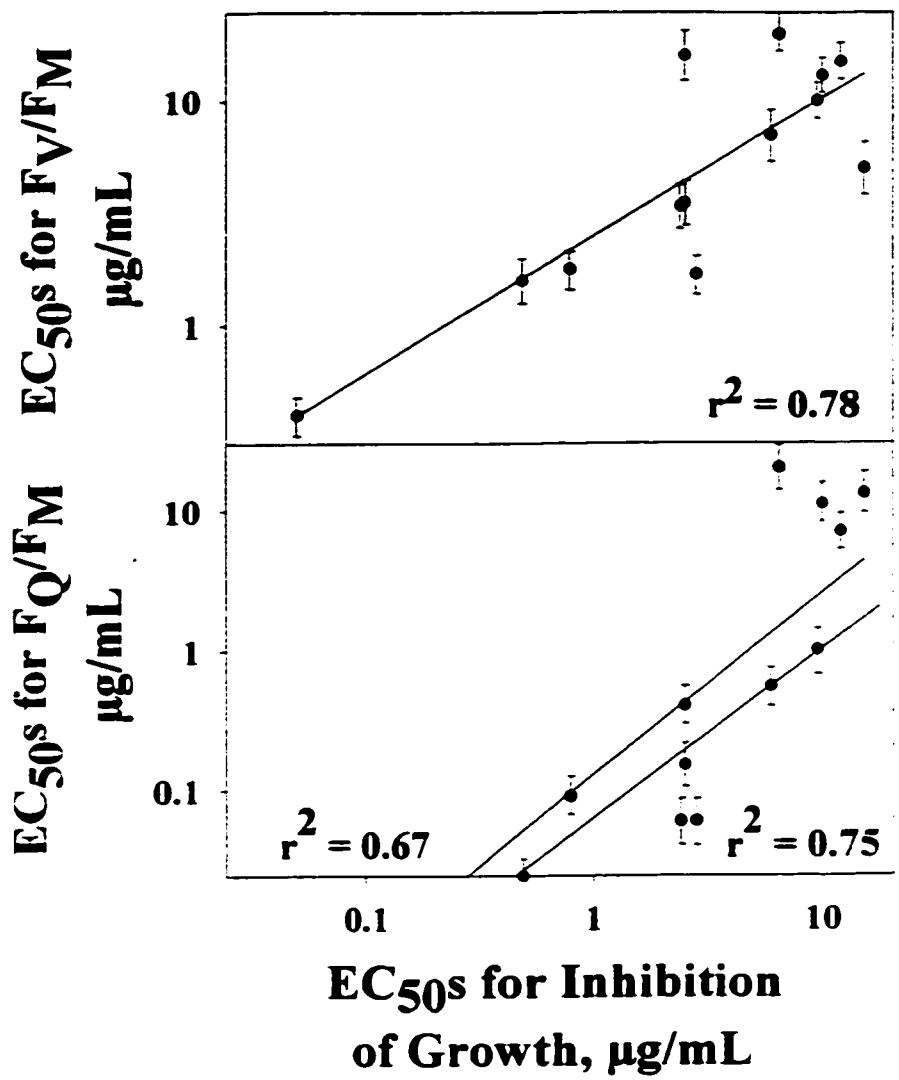

Figure 4.8 EC50s for in vivo diminishment of F_V/F_M and F_Q/F_M by chemicals plotted vs the EC50s for growth. Fluorescence induction was measured for determination of F_V/F_M and F_Q/F_M and expressed as EC50 values. EC50s for growth inhibition are from Table 3.1. EC50s for F_V/F_M and F_Q/F_M are from Table 4.1. All data were plotted on log scales. Each data point represents an average from three independent experiments. Log-log regressions were performed with SYSTAT. All regressions were significant ($p<0.05$). The correlation for F_Q/F_M vs growth inhibition was improved, when the non-toxic chemicals were removed from the regression ($r^2 = 0.75$).

4.3.4 Fluorescence kinetics measured with PAM fluorometer

Photosynthesis was also measured with a PAM fluorometer (see Figure 4.2). This was done to better define the site of inhibition. Full PAM traces were made and the quantitative measures derived from the traces were photochemical quenching (qP), non-photochemical quenching (qN), and Yield (Figure 4.2). Photochemical quenching is the fraction of absorbed energy used to reduce the PQ pool, non-photochemical quenching is the amount of energy dissipated due to the pH gradient, photoinhibition, and other processes. Yield is a measure of steady state energy storage by photosynthesis (Van Kooten and Snel, 1990).

After incubation of *L. gibba* with ANT and hATQs, Chl *a* fluorescence was measured with PAM fluorometer. Full scans at three concentrations are shown for 2-hATQ and 2,6-dhATQ, to compare a low impact compound to a high impact compound, respectively (Figures 4.9 and Figure 4.10). For 2-hATQ (Figure 4.9), as the concentration was increased, F_T gradually rises while F_M' drops only slightly. Relative to the control, this is reflected as large drops in qP and Yield, while qN does not change a great deal. This implies that the plastoquinone pool is remaining reduced during steady-state photosynthesis (i.e. loss of photochemistry), but PSII is relatively undamaged (i.e. no photoinhibition). This is in accord with the above finding that F_Q/F_M is diminished at lower concentrations than F_V/F_M. As would be predicted from the above photosynthesis data, 2,6-dhATQ had little effect on Chl *a* fluorescence as measured with the PAM fluorometer. The only effect was that F_M' was slightly depressed.

The PAM fluorescence kinetics data for plants treated with 1 µg/ml ANT, 1,2-dhATQ, 1,8-dhATQ and ATQ were measured (Figure 4.11). For ANT (Figure 4.11)

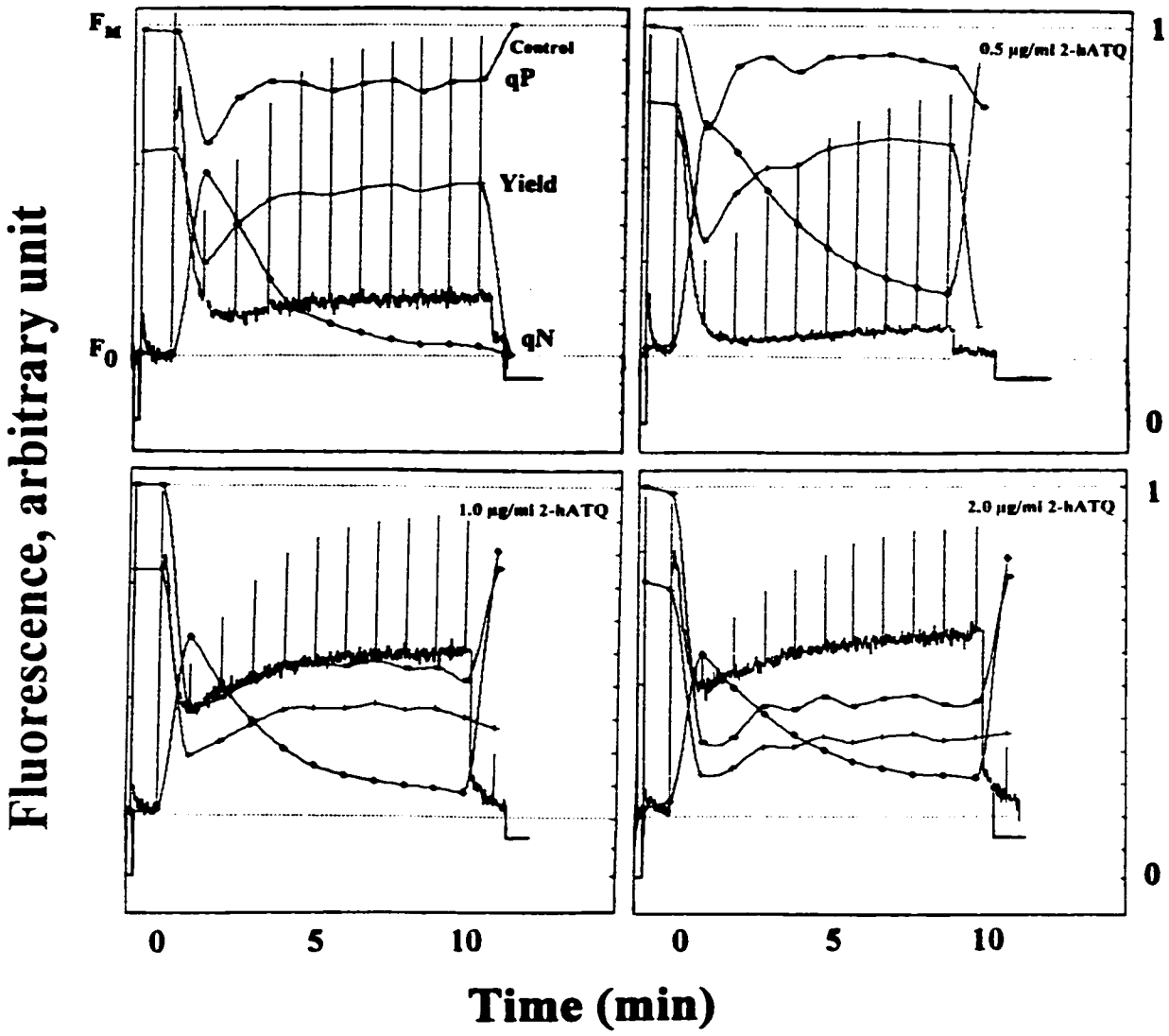

Figure 4.9 PAM Chl *a* fluorescence scans of *L. gibba* plants exposed to different concentrations of 2-hATQ. F_0, F_M, F_M' and F_T are as described in material and methods. qP, qN and yield were calculated after each saturating pulse.

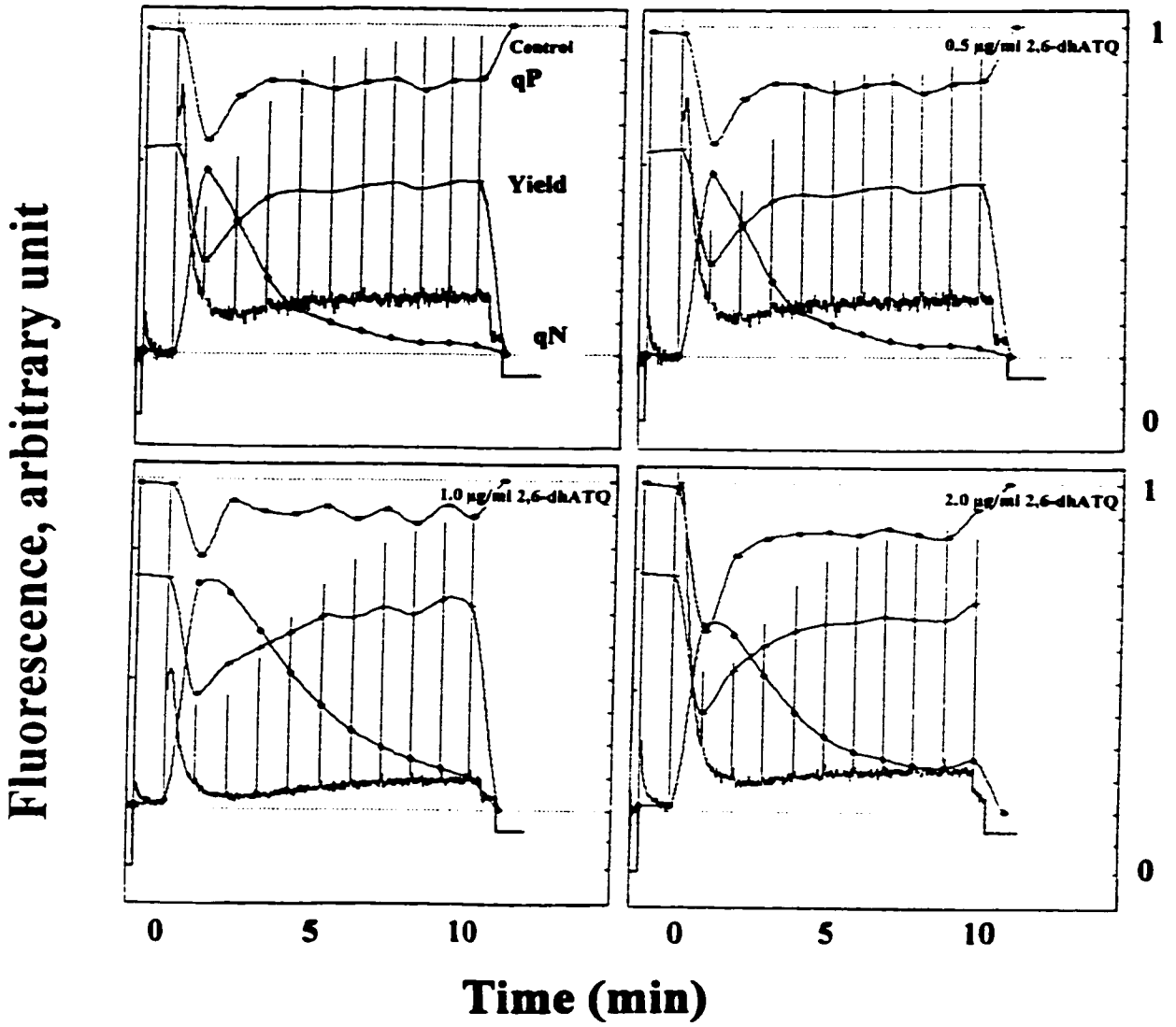

Figure 4.10 PAM Chl *a* fluorescence scans of *L. gibba* plants exposed to different concentrations of 2,6-dhATQ. F_0, F_M, F_M' and F_T are as described in material and methods. qP, qN and yield were calculated after each saturating pulse.

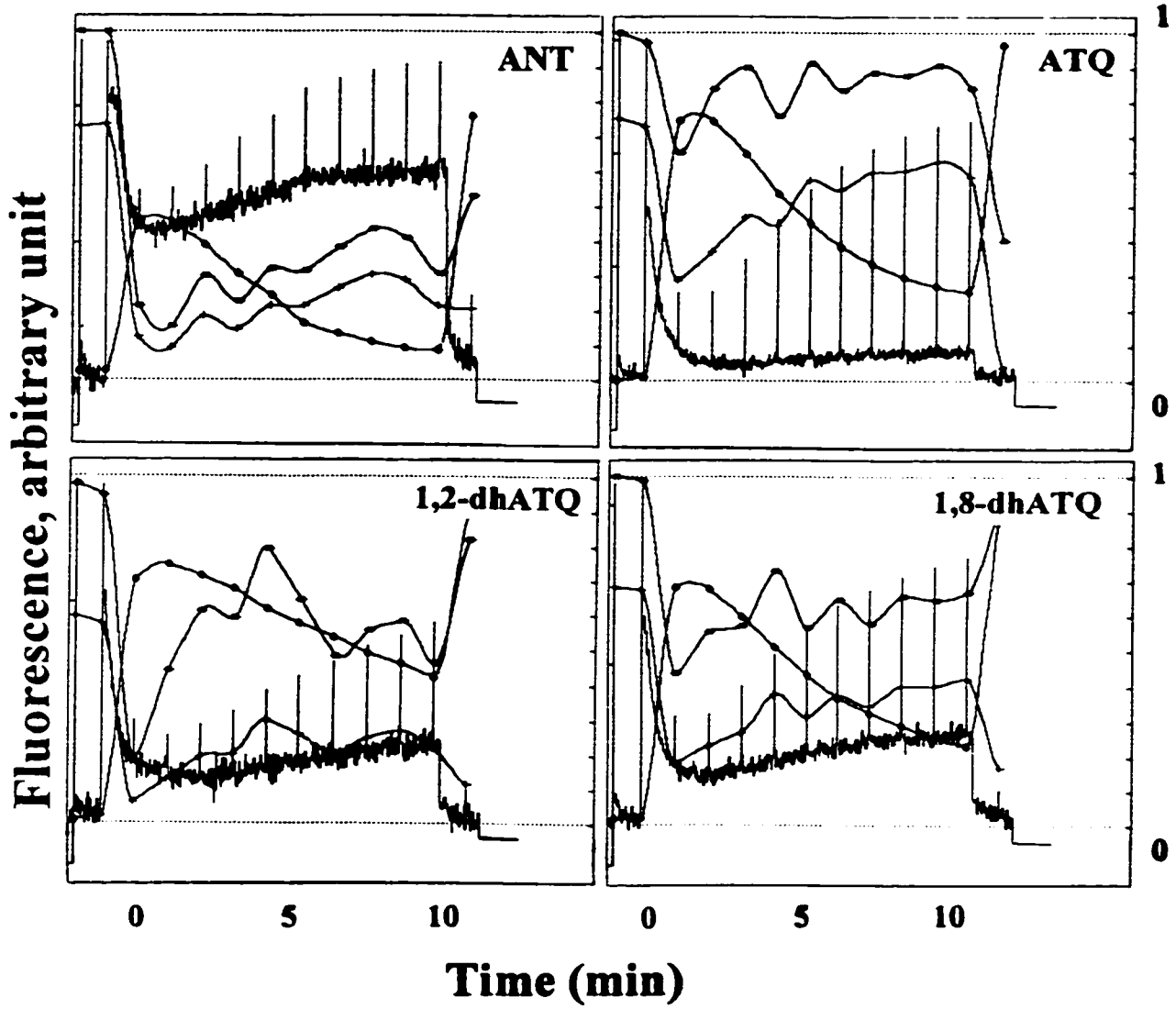

Figure 4.11 Chl *a* fluorescence scans of *L. gibba* treated with ANT, ATQ, 1,2-dhATQ and 1,8-dhATQ obtained with a PAM fluorometer. Plants were exposed to the chemicals under 100 μmol m^{-2} s^{-1} SSR perior measurement. In all cases, chemical concentration was 1 μg/ml. Fluorescence measurements were performed after 30 min dark adaptation as in Figure 4.9.

F_T rose, while F_M' was almost unchanged. This is concomitant with diminished qP and Yield, while qN did not change a great deal. PAM analysis for ATQ shows lower F_T value while F_M' also drops somewhat. This may indicate that ATQ can act as acceptor of electrons from PSI (similar to the action of methyl viologen). For ATQ there is a slight drop in qP and Yield, while qN rises. In the case of 1,2-dhATQ changes in all three photosynthetic parameters were observed. This is due to a drop in F_M' and a rise in F_T. Both photosynthetic yield and qP were significantly diminished, indicating diminished energy storage and closed PSII reaction centres. Analysis for 1,8-dhATQ showed a higher F_T value, while F_M' fell slightly similar to the observations of 2-dhATQ. The results for ANT, 2-hATQ, 1,2-dhATQ and 1,8-dhATQ indicate that the most common effects for ANT and its photoproducts is inhibition of photosynthesis downstream from PSII.

4.3.5 Effects of Photomodified ANTs on PSI and PSII activity in vitro

To complete this investigation on photosynthesis as a site of action for ANT derivatives, photosynthetic electron transport was probed with an oxygen electrode. Thylakoid membranes were isolated from leaf tissue as described in materials and methods and treated in vitro with ANT, ATQ, 2-hATQ and 1,2-dhATQ at concentrations ranging from 0.25 to 20 mg/L. Measurements of O_2 evolution indicated that PSII activity (H_2O –> PBQ) declined with increasing chemical concentration. ANT was the most effective chemical and 1,2-dhATQ was the least effective in inhibiting O_2 production. However, in all cases the concentrations required for inhibition were very high. This loss of oxygen evolution at elevated concentrations may be due to non-specific damage to the thylakoid membrane structure. This is consistent with the fluorescence data, where PSII was not impaired at low concentration.

PSI mediated electron transport activity was measured as O_2 uptake following electron transport from DCPIP to MV. MV passes the electrons to O_2, resulting in oxygen consumption. Treatment of thylakoid with the chemicals caused up to a 30% inhibition of PSI (Figure 4.12). Once again very high concentrations of the chemicals were required. Thus, the in vitro studies show neither PSII nor PSI were inhibited by low concentration of the chemicals. Because the fluorescence data indicates inhibition downstream from PSII for most ANT photoproducts, this would put the site of inhibition general at the cytochrome-b6/f complex.

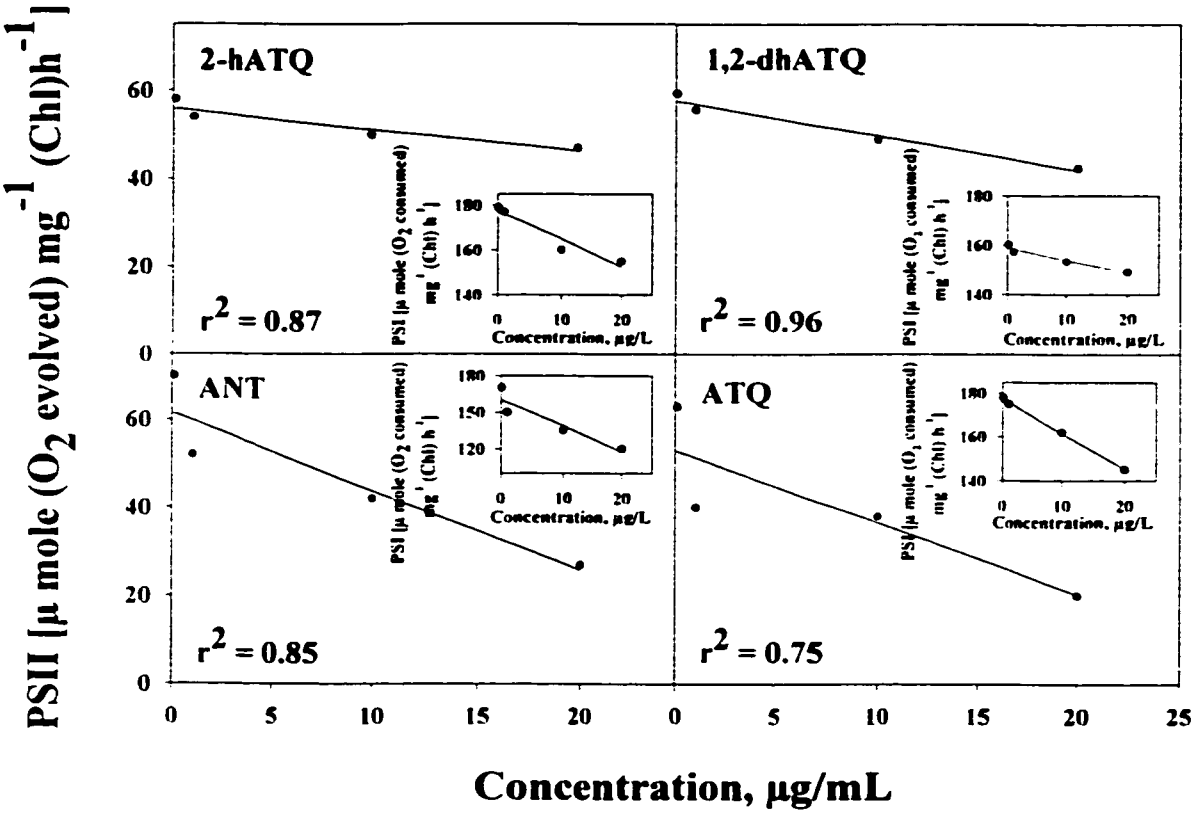

Figure 4.12 PSII and PSI activities of thylakoids examined after exposure to different chemicals. The values are the means of three independent experiments ± SE. For abbreviations see abbreviations and acronyms. PSII measured as amount of oxygen evolution as PSI is measured as amount of oxygen consumption.

4.4 Discussion

Thylakoid membranes are sensitive to environmental stress and organic pollutants. PSII and cytochrome-b6/f appear to be particularly sensitive to a number of factors, including chemical contaminants. As well, other sites in the chloroplasts (e.g. the Calvin cycle) can be inhibited. Because all of these forms of stress affect the function of PSII, directly or indirectly, Chl *a* fluorescence can be used as a tool not only to reveal stress response mechanisms, but also to quantify stress responses under laboratory and field conditions. Activity of PSII (Chl *a* fluorescence) was therefore a very useful measure of contaminant effect in this Chapter. Use of Chl *a* fluorescence and an oxygen electrode showed that intact and photomodified forms of ANT, ATQ and hATQs inhibited photosynthesis in vivo and in vitro.

Intact and photomodified ANT, as well as ATQ and some hATQs inhibit or affect electron transport downstream from PSII. The order of decreasing impact on photosynthesis in *L. gibba* were: 2-hATQ > ATQ > 1,2-dhATQ > ANT > 1-hATQ > 1,3-dhATQ > 1,2,10-thANT > 1,2,4-thATQ > 1,2,5,8-thATQ > 1,5-dhATQ > 2,6-dhATQ > 1,8-dhATQ > 1,4-dhATQ. The variation in sites of impact and direct or indirect effects on photosynthesis, were observed as changes in relative Chl *a* fluorescence. The low toxicity of 2,6-dhATQ was consistent with its low level of photosynthesis inhibition. 2-hATQ as well as 1,8-dhATQ significantly increased F_T and modestly reduced the F_M' signals. This response is associated with blocking of electron transport downstream from PSII, resulting in reduction of the PQ pool. Because these chemicals block the reoxidation of PQH_2, the absorbed energy cannot be used in photochemistry, and it must be non-photochemically dissipated, resulting in increased F_T signal. The F_M' signal decreases could be related to lower photochemical quenching values. Interestingly in case of ATQ, the F_T signal was

lower than in control plants. This may suggest that ATQ is acting as an electron acceptor (similar to MV) (Figure 4.11). Thus, there are two apparent sites of impact. This may explain why mixtures of ANT photoproducts, which contain both ATQ and hATQs, are so toxic.

Overall, the results of the effects on photosynthesis revealed that downstream electron transport from PSII is more sensitive to chemical inhibition. 2-hATQ was the most toxic compound identified, and this was supported by the greatest decrease in photochemical quenching and yield (Table 3.1; Figure 4.9 - 4.11). Photosynthetic activity showed more than 50% reduction in the effective quantum yield upon exposure to 2.0 μg/ml of 2-hATQ for 6 h (Figure 4.9). This is consistent with 2-hATQ causing a lower PSII activity (F_V/F_M) (Figure 4.4 and Table 4.1). However, this is preceded by diminished F_Q/F_M, meaning that PSII is likely damaged after electron transport backs up. The diminished electron transport was also reflected in the decline in maximum quantum yield as the concentration increases from 0.5 μg/ml to 2.0 μg/ml of 2-hATQ. 1,2-dhATQ also showed this inhibitory effects downstream from PSII even though it is not the most toxic of the chemicals tested.

2,6-dhATQ, at a concentration of 2.0 μg/ml, did not significantly depress photosynthesis. The impact of 2,6-dhATQ on PSII needs further investigation, however as it appears to enhance electron transport as indicated by elevated quantum yield. To further understand the effect of 2,6-dhATQ, longer-term exposures may be required. Nonetheless, 2,6-dhATQ also does not cause whole organism toxicity. So it should not be surprising that it does not inhibit photosynthesis.

As mentioned above ATQ seems to accept electrons from PSI in a manner similar to MV. The diminishment of F_Q/F_M may be due to melding of the first two

quenching phases because of very rapid electron transport. In contrast, for most of the chemicals interpretation of the diminishment of F_Q/F_M is that the cytochrome-b6/f complex is inhibited first, then electron transport backs up. This leads to excitation pressure on PSII which damages this photosystem.

Because the impacts of the chemicals on plants in Chl *a* fluorescence and electron transport were measured after a short time, high concentrations of the chemicals were used both in *in vivo* and *in vitro* experiments. For the *in vivo* studies of Chl *a* fluorescence, in some cases the intact and photomodified chemicals were used at concentrations above the maximum solubility of these chemicals. Nonetheless, these high concentrations are comparable to PAH concentrations in contaminated aquatic environmental samples (Neff, 1979; Edwards, 1983; Eadie, 1984). In addition, photomodified hATQs are much more soluble than are intact chemicals (Huang *et al.*, 1995; Mallakin *et al.*, 1999) and at environmentally relevant levels, the photomodified products had strong impacts on bioenergetic pathways (Huang *et al.*, 1997a). For example, the Chl *a* fluorescence quenching data (F_Q/F_M) showed that inhibition of cytochrome-b6/f by photomodified ANT, ATQ and 2-hATQ could be detected at low concentrations (i.e. ~ 0.05 μg/ml).

For the *in vitro* studies of electron transport, the concentrations used (1-20 μg/ml) were higher than those used *in vivo* for few reasons: Thylakoid membranes do not bioconcentrate contaminants as do living plants, very short incubations were used in the *in vitro* assays of electron transport, and the *in vitro* exposure of membranes to the chemical were performed at low temperature (4°C). Even at high concentrations there was not a great deal of inhibition. This may be explained by non-specific damage to membranes.

Photomodified ANT, ATQ and hATQs inhibited photosynthetic activity in SSR. A route for inhibition of PSII in the light is that inhibition of cytochrome-b6/f occurs first and this leads to photoxidative damage to PSII. Electron transport in chloroplasts proceeds from H_2O through PSII to the plastoquinone (PQ) pool, and then through PSI to NADP+ (Hall and Rao, 1987; Greenberg, 1991). When cytochrome-b6/f is inhibited, electron transport from PSII to PSI will also be blocked because the PQ pool will become reduced and remain in that state. The result of a reduced electron acceptor pool will be no electron transport through PSII, and inhibition of PSII will develop due to excitation pressure on PSII complexes (Gray *et al.*, 1994; Virgin *et al.*, 1993; Aro *et al.*, 1994). This will ultimately result in permanent oxidative damage to PSII as a consequence of excitation of Chl without the possibility of transferring the energy into the electron transport chain. Thus, if cytochrome-b6/f is a primary site of inhibition, the electron transport chain backs up such that PSII is also damaged.

The hypothesis that inhibition of PSII occurred following direct inhibition of cytochrome-b6/f was reported previously for ANT and mixtures of photomodified products (Oettmeier *et al.*, 1988; Huang *et al.*, 1997a). The initial fluorescence quenching (F_O), is diminished by ANT, ATQ and many hATQs in SSR (Figures 4.5 and 4.7). Because the compounds did not inhibit O_2 evolution from PSII, the site of inhibition by the hATQs may be inferred to intersystem electron transport, at the cytochrome-b6/f complex. Based on Chl *a* fluorescence and electron transport, we conclude that ANT and hATQs (except ATQ which can act as electron acceptor) inhibit electron transport at the cytochrome-b6/f complex and this causes accumulation of PQH_2.

It has been reported that some quinones directly inhibit PSII (Oettmeier *et al.*, 1988, 1999). Early in the photomodification process of ANT, the photoproducts are

primarily quinones (Chapter 2) (Mallakin *et al.*, 2000), which may exert their impact largely on PSII. As photomodification proceeds and benzoic acids and hydroxyquinones form, cytochrome-b6/f may become the primary site of action. Nonetheless, the effects of the hATQ and ATQ all seem to be downstream from PSII. Interestingly, defence mechanisms are designed to ameliorate damage to PSII (Huang *et al.*, 1997b). Therefore, this kind of damage to thylakoids may be hard to protect against.

Toxicological and inhibitory responses of ANT, ATQ and hATQs have been described in this chapter. Some caused complete inhibition of photosynthesis, while others showed a limited impact. This may suggest that the chemicals in combination can have synergistic effects; this will need further research. The results of these tests provide an indication of the maximum impact for a given dosage; however, additional experiments are required to permit us to understand the response of pulses of chemicals in flowing water. The discovery of F_Q/F_M as a sensitive measure of inhibition of plant function is important for bioindicator development and cytochrome-b6/f activity studies. The mechanistic ramifications of this effect could be plant's inability to maintain and/or establish the thylakoid pH gradients, or inhibition of cytochrome-b6/f activity. Furthermore, Chl *a* fluorescence were correlated with growth inhibition, showing that F_V/F_M and F_Q/F_M have potential as reliable, validated bioindicators of acute and chronic toxicity of photomodified PAHs. The results presented here also demonstrate the feasibility of using PAM fluorometery to measure photosynthesis in *L. gibba*.

Chapter V

Use of Molecular Shape to Model the Photoinduced Toxicity of Hydroxyanthraquinones: Electron Density Shape Features Predict Toxicity[1]

---

[1] This paper is for submission to *Ecotoxicology and Environmental Safety* and authored as Ali Mallakin, Zbigneuf Zimpel, Paul G. Mezey, D. George Dixon, and Bruce M. Greenberg.

5.1 Introduction

Polycyclic aromatic hydrocarbons (PAHs), a group of toxic and mutagenic contaminants, are both ubiquitous and highly hydrophobic (Neff, 1979; Eadie, 1984). Photoinduced processes involving these chemicals are environmentally relevant, and are observed as increased toxicity of PAHs in the presence of simulated solar radiation (Mallakin *et al.*, 1999, Huang *et al.*, 1997a). PAHs strongly absorb solar ultraviolet (UV) radiation, resulting in photomodification usually via oxidation reactions (Mallakin *et al.*, 2000). Recent work has shown that photomodification of ANT results in complex mixtures of photoproducts that are more toxic to *L. gibba* than the parent compounds (Mallakin *et al.*, 1999; Chapter three). It was further demonstrated that photomodified PAHs are biologically damaging to the photosynthetic apparatus (Chapter four). Of course, the different ANT photoproducts have distinctly different toxicities. Consequently, the structures of molecules should contain information concerning their toxicological risks. In this chapter, molecular shape analysis was used to compare the electron densities of the molecules to their toxicities.

Our understanding of environmental toxicology can benefit from molecular shape analysis (Dean, 1987; Mezey, 1986, 1987, 1995; Walker and Mezey, 1995). Molecular shape and numerical evaluation of molecular similarity can be used in quantitative structure activity relationships (QSARs) (Johnson and Maggiora, 1990; Mezey *et al.*, 1996; Mezey, 1998). The nuclear distribution and electron density cloud of a molecule should be able to describe its biological and chemical reactivity. However, because the electron densities of organic molecules also describe their nuclear distribution, in most instances they alone can describe the reactivity of a molecule. The electron density clouds of organic compounds represent fuzzy

molecular bodies that provide a mode for analysing the shapes of molecules (Mezey, 1992; Mezey, 1993; Walker and Mezey, 1995; Mezey and Walker, 1997). If two molecules react differently, these differences should be reflected in their electron density clouds. Theoretically, for reactions of organic molecules in biologically relevant settings, no other quantum considerations of the molecule are required (Mezey, 1993; Carbo, 1995).

Initially, molecular shape studies made use of available software packages for molecular modelling, and applied them to computer generated QSAR modelling for toxicology. Early on, partial fused spheres Van der Waals surfaces were used in QSAR studies (Richards, 1977; Connolly, 1985; Gibson and Scheraga, 1987). However, they only represent a simple description of molecular shape. This can be explained as follows. First, fused-sphere Van der Waals surfaces provide a finite molecular boundary, but the actual charge cloud gradually fades into the vacuum surrounding the molecule (Mezey and Walker, 1997). Second, the electron densities of most atoms in molecules are not spherical. For instance it is not possible to describe π-electron density by spheres centered on the nuclei of atoms (Mezey, 1993; Mezey, 1988, Gibson and Scheraga, 1987; Mezey and Walker, 1997). Aromatic rings cannot be represented completely by fused spheres because the electron density is neither spherical nor cylindrical in any aromatic π-bond. In an aromatic molecule, π-bonds are more reactive than σ-bonds and have important chemical characteristics which are poorly described by the Van der Waals surface approach.

Accurate electron shape density representations of molecules were developed to better describe the toxicity of different molecules (Mezey, 1993; Mezey *et al.*, 1998). This methodology allowed the incorporation of π-orbitals into the electron cloud surfaces. This is a key element in understanding the correlations between toxic

properties and/or biochemical reactivities of molecules, and specific shape features of their electron density clouds. In particular, many environmental contaminants are aromatic (e.g. PAHs and PCBs). Current techniques using a computational microscope method of quantum chemical and *ab initio* molecular descriptions, based on fuzzy density fragments, allow one to generate high-resolution electron density maps of PAHs (Mezey *et al.*, 1996). Previous studies have used these computer generated molecules to develop a QSAR model describing the photoinduced toxicity of intact PAHs (Mezey *et al.*, 1998). It was shown that the computer programs are capable of recognizing and evaluating similarities within a selected molecular family (e.g. PAHs), and correlating local and global shape features with primary toxicological data. This led to the finding that global shape and single-ring shape could be associated with the photosensitization and photomodification activities of intact PAHs, respectively.

To extend the above QSAR work, a suite of anthracene photoproducts (ATQ and hATQs) were selected for development of a shape fragment database for QSAR modeling. In chapter three, the toxicity of different ANT photoproducts under actinic radiation was evaluated. In chapter four, it was shown that toxicity was due in large part to inhibition of photosynthesis. In this chapter, a complete description of the electron shape-density cloud of each molecule is generated at both high and low electron density ranges. Computer modelling is then used to relate the shape density clouds for each molecule to the toxicological data from Chapter three. Further, it is important to determine if the same shape model that describes toxicity at the whole organism level will predict toxicity at the level of photosynthesis.

5.2 Methodology

ANT, ATQ and eleven hATQ molecules were examined. Data on their relative experimental toxicity to *L. gibba* (Mallakin *et al.*, 1999; Chapter three), and the relevant numerical results of the photosynthetic analysis (Chapter four) are listed in Table 5.1. The toxicity data used for modeling were growth inhibition at 0.5 μg/ml and 2 μg/ml. As well, the EC50s for growth inhibition were used for toxicity modeling. This gave three measures of whole organism toxicity to use in modeling. For photosynthesis, diminishment of F_Q/F_M and F_V/F_M were used. The data used were diminishment of F_Q/F_M and F_V/F_M at 0.5 μg/ml and 2 μg/ml, and the EC50s for diminishment of F_Q/F_M and F_V/F_M. The concentration of a test chemicals in water is expressed as μg/ml, or units of test chemicals per 10^6 units of untreated dilution water. Because of the long-standing use of mass-based units for reporting doses or exposure concentration in previous reports (Mallakin 1999, 2000), this unit used in current study. Rather than reporting in units of mg/L or μg/ml, toxicity data obtained with specific chemicals or chemical mixtures may be reported in molar units such as mmol/L or μmol/mL. The use of molar concentrations is very important from a toxicological point of view, as toxic effects are usually a function of the number of molecules present at the target sites, not the mass of those molecules.

This study was a collaboration with Paul Mezey, Zbigneouf Zimpel, and Duane Walker at the University of Saskatchewan. I generated the molecular shape data bases in Dr. Mezey's laboratory using their protocols and computer code (Mezey *et al.*, 1996, 1998). The nuclear geometries of ANT, ATQ and hATQs were optimized using the Gaussian 92 program package running on an Alpha DEC 3000 Unix computer (Frisch *et al.*, 1990). The minimum ground-state energy of each molecule was calculated using the closed-shell Hartree-Fock approximation. The electron

densities for each molecule studied were computed using high-resolution shape fragment databases (Mezey, 1998). The molecular shapes were generated using the shape-group method, in which the molecular shapes were constructed using the contour surfaces of calculated quantum mechanical descriptions of the molecules (Mezey *et al.*, 1998). A numerical comparison of molecular shape codes used for similarity analysis: the similarities of the shapes of three-dimensional molecular bodies were quantified and measured by comparing their numerical shape codes (Mezey, 1990 a,b). The family of one-dimensional Betti numbers is ordered into a matrix, called the (a,b)-map (electron density shape maps). The standard methods of comparing matrices was applied to these (a,b)-maps in order to obtain a numerical measure for molecular similarity (Mezey, 1996). The comparison involves no visual inspection and is carried out automatically by the computer. The direct comparison of electron densities using point-by-point comparisons of electron densities for a set of grid points and the average relative difference between the corresponding density values were implied. These similarity measures can be evaluated for any given range of electron density thresholds as well as for the whole range of the electron density. The algorithmic shape-similarity evaluation by the computer is fully reproducible (Mezey, 1996).

Table 5.1 Toxicity data used for modeling. Toxicity is inhibition of growth of *L. gibba* by ANT and its photoproducts, and presented as normalized inhibition of growth relative to the control plants. Chemicals tested were at concentrations of 0.5 and 2 μg/ml based on amount of the parent compounds. EC50s were calculated from full dose response curves and are given in μg/ml. F_V/F_M and F_Q/F_M values were for diminishment of these parameters relative to the control. Data for 2 μg/ml and 0.5 μg/ml inhibition is relative impairment of fluorescence [F_V/F_M control - F_V/F_M treated] / F_V/F_M control, and [F_Q/F_M control - F_Q/F_M treated] / F_Q/F_M control). EC50 values for diminishment of F_V/F_M and F_Q/F_M were obtained from full dose response curves (Chapter four).

Name of PAH Molecule	Growth Inhibition 0.5 μg/ml	Growth Inhibition 2 μg/ml	Growth Inhibition EC50s	(F_V/F_M)			(F_Q/F_M)		
				EC50s μg/ml	Inhibition 0.5 μg/ml	Inhibition 2 μg/ml	EC50s μg/ml	Inhibition 0.5 μg/ml	Inhibition 2 μg/ml
ANT	0.45	0.96	0.8	1.8	0.48	0.46	0.09	0.74	0.92
ATQ	0.43	0.97	0.5	1.6	0.05	0.49	0.03	0.76	1.00
1-hATQ	0.34	0.50	2.4	3.4	0.11	0.09	0.06	0.75	1.00
2-hATQ	1.00	0.99	0.05	0.4	0.62	0.57	0.02	0.81	1.00
1,2-dhATQ	0.22	0.40	2.8	1.7	0.54	0.46	0.6	0.65	0.68
1,3-dhATQ	0.26	0.45	2.5	3.5	0.21	0.18	0.15	0.05	0.8
1,4-dhATQ	0.07	0.22	6.5	20.0	0.20	0.17	20.0	0.08	0.04
1,5-dhATQ	0.05	0.16	15	13.0	0.25	0.22	13.0	0.09	0.2
1,8-dhATQ	0.22	0.41	2.5	16.0	0.32	0.26	8.0	0.37	0.4
2,6-dhATQ	0.02	0.08	12	15.0	0.04	0.06	7.0	0.27	0.36
1,2,4-thATQ	0.07	0.25	6	7.0	0.09	0.13	0.55	0.42	0.6
1,2,5,8-thATQ	0.11	0.17	9.5	10.0	0.12	0.21	1.00	0.45	0.52
1,2,10-thANT	0.05	0.20	10	5.0	0.14	0.36	1.00	0.49	0.56

To determine the molecular shapes, the internuclear distances of ANT, ATQ and eleven hATQs were optimized using the 6-31G** atomic orbital basis set. The electron density for each molecule and each molecular fragment was deposited to a database obtained from the parent molecules and described in previous papers (Mezey *et al.*, 1996, 1998). The input for the GAUSSIAN calculations was obtained from *. PDB (Photoshop Deluxe Boundary) files generated using Hyperchem® software on an IBM PC computer. Using the shape-group method, (a,b)-maps were computed for each molecule (Mezey *et al.*, 1993). Such (a,b)-maps are universal, discrete representations of the molecular shapes, molecular fragments and whole molecules. The data can be analyzed at different electron densities. In this study, the densities used were 0.1 to 0.001 atomic units (a.u.), where one a.u. corresponds to electron charge per cubic bohr. These data were analyzed in search of correlations between shape and toxicity of chemicals, as well as correlations to inhibition of photosynthetic activity. The goal was to find a correlation between the (a,b)-maps of ANT and the ANT photoproducts and the experimental toxicities. Based on the knowledge of the photoinduced toxicity of PAHs, one-ring and whole-molecule similarities were generated from the (a,b)-maps (Mezey *et al.*, 1998). This was shown previously to be a predictor of toxicity for intact PAHs.

The quality of the above computational analyses was determined from the quantum mechanical computations that resulted in the electron densities. The (a,b)-maps were tested for accuracy using the AVS® software package on a UNIX computer. This was done at the *ab initio* level using a set of atomic orbital basis functions (expansion functions) (Mezey, 1993). The quality of the shape analyses and shape code computations were also determined by the computed electron densities, which were used to generate graphical displays of the molecules (Mezey, 1993).

5.3 Statistical and Correlation Analysis

The linear regressions were fit to test for relationship between molecular shape and toxicity using the MGLH module of SYSTAT (Version 8.0 for Windows, Systat, Evanston, IL, USA). The quality of fit of the regressions (r^2) and the significance of the regressions (p) were determined with SYSTAT. The shape data were also fit to hyperbolic functions based on the toxicity data yielding theoretical toxicities, $Y_{theor} = C_0/1\text{-}C_1X_1$. Where X_1 is the one-ring or whole molecule similarities, and C_0 and C_1 are the regression coefficients. These hyperbolic fits were then plotted against empirical toxicity and tested for correlations.

5.4 Results and Discussion

5.4.1 Generation of Shape Data Bases for ANT and its Photoproducts

The local charge cloud of the carbonyl and hydroxy regions of ANT derivatives, obviously have quite different structures, so they should have different reactivities and toxicities (Mallakin *et al.*, 1999). This will be reflected in their (a,b)-maps. If the shapes were identical, then the reactivities of the two molecules would also be identical. This principle has motivated the introduction of the quantitative shape-activity relations (QShAR), which has been applied previously for several polycyclic aromatic hydrocarbons (PAHs) (Mezey, 1992; Mezey *et al.*, 1995; Mezey *et al.*, 1995; Mezey *et al.*, 1998). Because the electron density clouds are responsible for the toxic action of the molecules, by comparing shape features of toxic molecules with their known activities, one should be able to derive regression equation that can be used to estimate the activities of chemicals based on the analysis of their molecular shapes (Mezey and Walker, 1997; Mezey *et al.*, 1998). The shape group method

provides an automated computational tool for rapidly generating shape maps of molecules (Mezey, 1993; Mezey, 1995). The ANT derivatives provide a good test system to further develop this methodology.

Important for the description of 3D electron densities of molecules are *molecular isodensity contours* (MIDCOs). The nuclear arrangement of a molecule is the dominant factor that determines the molecular electron distribution. For any formal nuclear configuration of a molecule we may assume a 3D coordinate system. For a given nuclear arrangement, the shape group distribution as a function of two parameters, a and b, defines an (a,b)-map for each shape group type. These are then assembled into full shape maps for a given molecule.

To begin the process of generating a shape map, precise structures of ANT, ATQ and the eleven hATQs were constructed with the GAUSSIAN 90 program package (Frisch *et al.*, 1990). Using the GAUSSIAN 90 (Frisch et al., 1990) and GSHAPE 90, the 6-31G** Gaussian basis set was generated for each molecule (Walker *et al.*, 1991). MIDCO maps were then calculated for each molecule. These representations were used below to generate the (a,b)-maps of the molecules that were used to derive the QSARs. If the MIDCOs are of high quality, then the (a,b)-maps will also be good. To test the MIDCOs, visual representations of the molecules were generated. These are shown at high electron density (0.1 a.u) for 12 of the 13 compounds used in this study (Figure 5.1). The quality of the generated electron density was revealed in the quality of the structures that were generated. In the MIDCOs, the hydroxy and oxygen groups of the compounds are clearly distinguishable especially at the higher electron densities (Figure 5.1). The lowest density MIDCO (0.001 a.u.) shows a feature of low density surfaces, in which the fine density structures are lost (Figure 5.2).

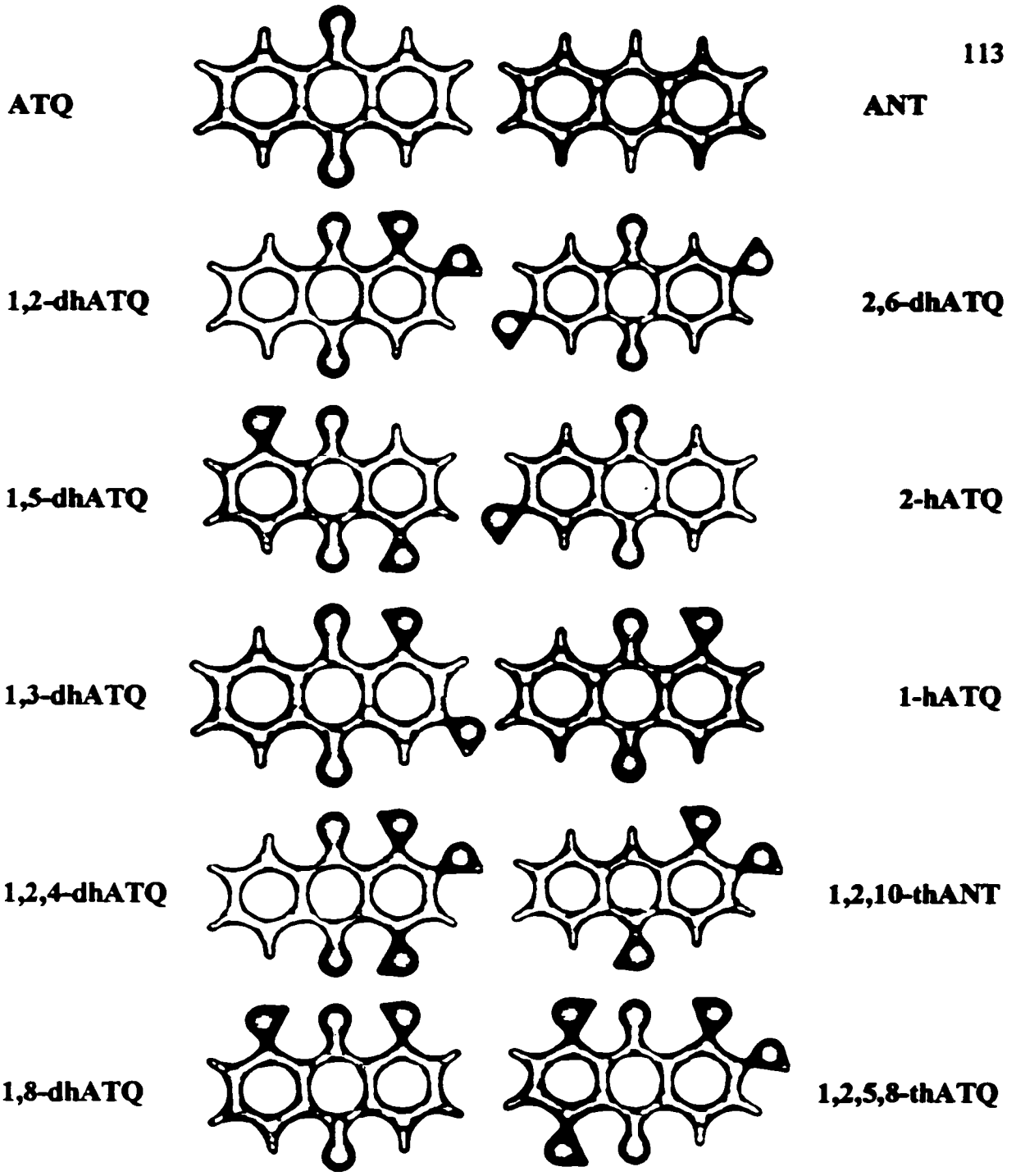

Figure 5.1 The 0.1 au electron density contours of ANT, ATQ and hATQs. Densities were calculated from MIDCOs of each molecule. The contours shown here are representations of these data.

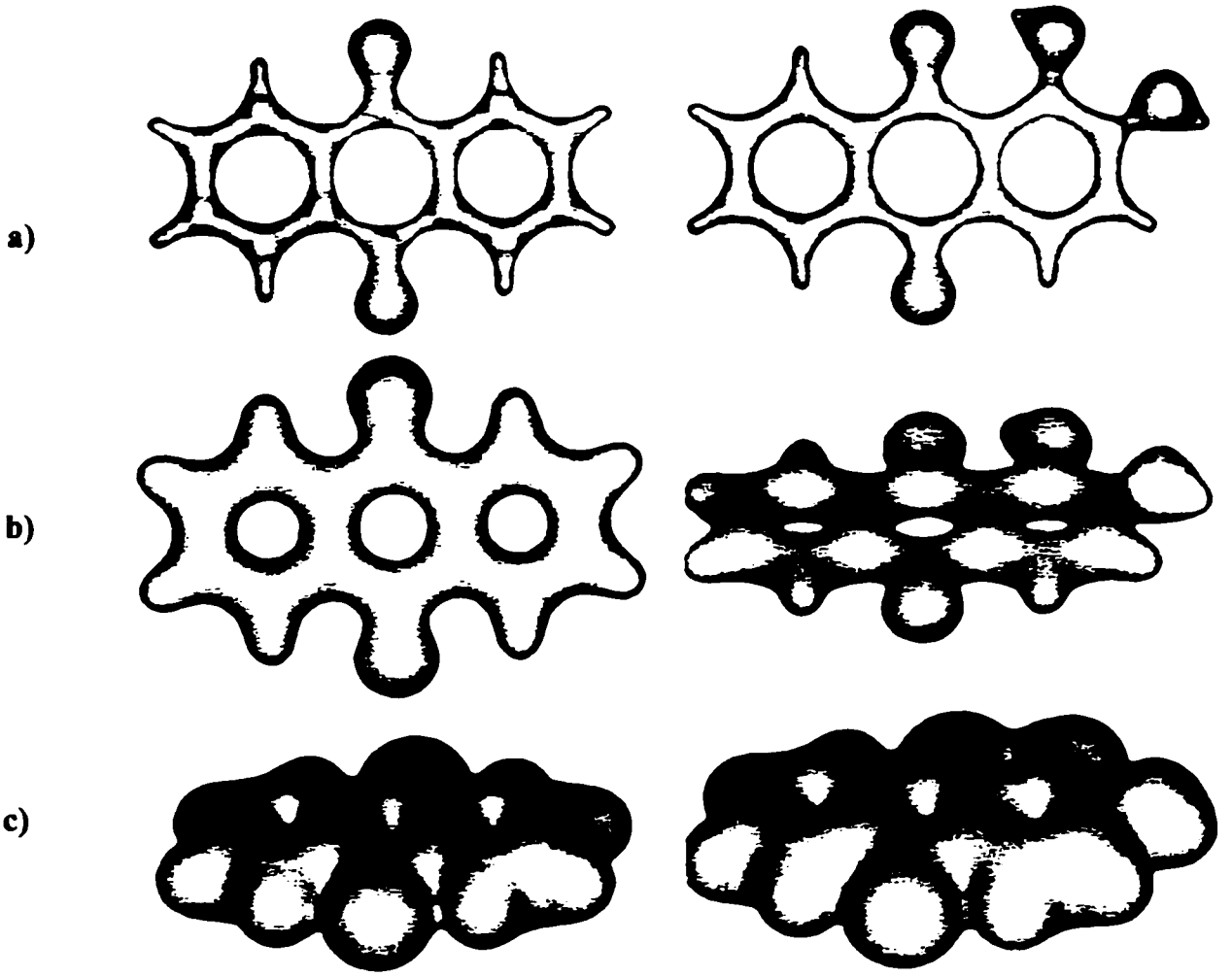

Figure 5.2 Electron densities of ATQ and 1,2-dhATQ are shown at different density thresholds. Those shown are a) 0.1 au, b) 0.01 au and c) 0.001 au. MIDCOs, were used to generate these graphic representations of the molecules.

One can observe the planarity of the molecules (Figure 5.2, 5.3), showing the quality of the computer generated structures. This is demonstrated for ATQ, and 1,2-dhATQ at electron densities of 0.01 and 0.001 a.u. (Figure 5.2). Note, the hydroxy groups adjacent to the carbonyls accurately have the hydrogen towards the oxygen so hydrogen bonding can occur. As well, adjacent hydroxys were found to point away from each other due to steric hindrances. These features were all found based on the MIDCOs.

The above contour surfaces may be regarded as the surface that interacts with other molecules. The *molecular isodensity contour surfaces* (MIDCOs) were used to generate from (a,b)-maps of the molecules (Mezey, 1993). To generate the (a,b)-maps from the above data, a set of Betti numbers were calculated. These are integers that provide a precise numerical characterization of the MIDCO surfaces (Mezey, 1993). The Betti numbers of the shape groups are the topological invariants that serve as the basis of a numerical, non-visual shape characterization. A list of the one-dimensional Betti numbers for the finite number of shape groups of the molecule generates a numerical shape code (Mezey, 1993). A numerical comparison of molecular shape codes can be used for similarity analysis: the similarity of the shapes of three-dimensional molecular bodies can be quantified and used to compare different molecules (Mezey, 1990; Mezey,1993). The one-dimensional Betti numbers for different groups on the molecules are ordered into an n-dimensional array called the (a,b)-map. The standard methods of comparing matrices can be applied to these (a,b)-maps in order to obtain a numerical measure for molecular similarity. This comparison is carried out automatically by the computer. This computation of Betti numbers describes the shape of the entire molecule. These arrays are used to obtain a numerical measure for molecular similarity between molecules (Mezey, 1993) (Appendix 1).

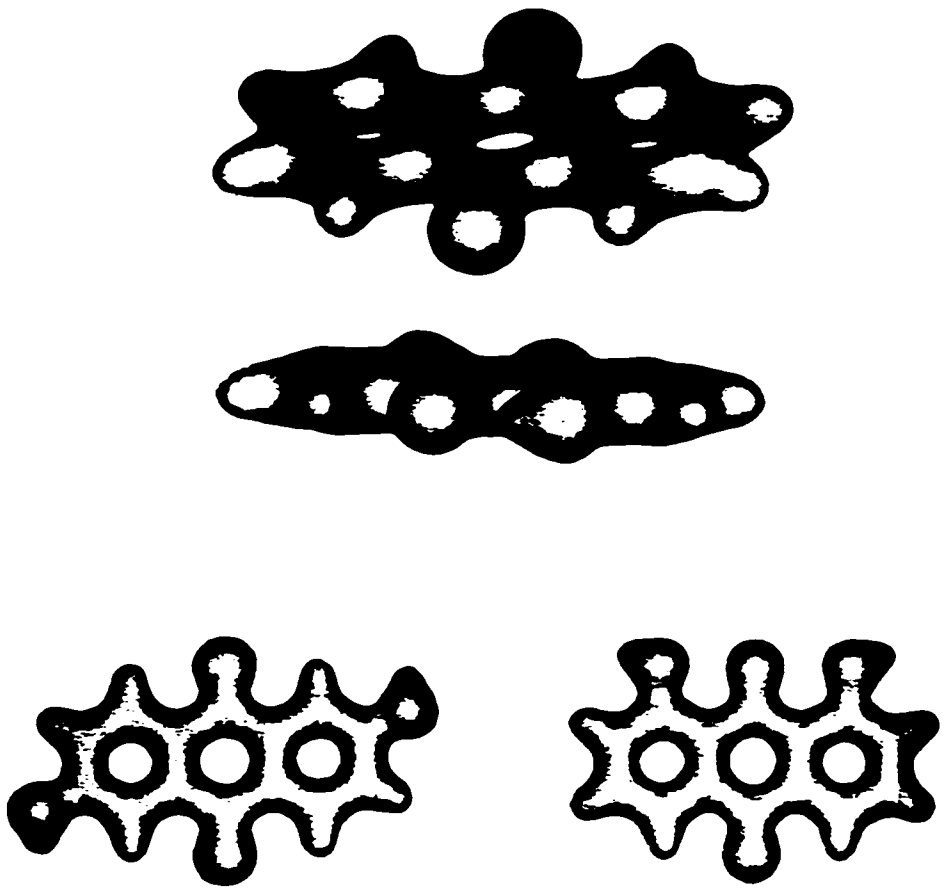

Figure 5.3 The 0.01 au electron density contour of ATQ, 1,8-dhATQ and 2,6-dhATQ molecule showing planarity of the molecules.

A computational method based on additive fuzzy molecular fragments (AFDF) allows a check of the quality of the particular (a,b)-maps. The computational and the *ab initio* quality of the computed electron densities provide confidence in the results for each of the molecules produced. Using the nuclear coordinates, a whole range of possible conformations of *ab initio* quality can be made. In this way the electron density of virtually any conformation can be computed. The AFDF methodologies then determine if the correct conformations of a molecule were generated from the shape code of the fuzzy, three-dimensional structures of the molecules. The use of fuzzy fragments (i.e. electron density clouds without boundaries), eliminates the large 'mismatch' errors typical of fragments with boundaries (Mezey, 1993). The (a,b)-maps were an accurate description of the shape of the electron density clouds based on *ab initio* calculation (data not shown). Thus, these maps could be used to calculate similarity indices. These indices were generated for whole molecules and one-ring molecules (Table 5.2 and Appendix 1).

The (a,b)-maps of ANT, ATQ and 11 hATQs and their fragments were computed to compare their molecular shapes with empirical toxicity data. The quantum chemical accuracy was demonstrated by the *ab initio* quality of the computed electron densities (Walker and Mezey, 1993). The accuracy of the application of the shape method was limited to the 6-31G** basis set since the density fragment database has been constructed at this *ab initio* level (Walker and Mezey, 1993). A similarity comparison of the shapes of a series of ANT derivatives should provide information to permit one to understand the complex nature and relative hazards of these aromatic compounds. A numerical comparison of molecular shape codes was used for shape comparison and similarity analysis (Mezey, 1990; 1993). The similarity of the shapes of three-dimensional molecular bodies was quantified and measured by comparing their numerical shape codes (Table 5.2). To consider the

similarity comparison of the shapes of the molecules, the electron distributions were superimposed. The standard methods of comparing matrices was applied to these (a,b)-maps to obtain a numerical measure for molecular similarity (Mezey, 1993). This comparison does not involve a visual inspection. Rather an algorithmic shape-similarity evaluation was carried out by computer. This is repeated for all possible pairs of fragments in the molecules (Table 5.2 and Appendix 1).

Table 5.2 Results of the numerical shape-analysis and similarities of (a,b)-maps. Whole molecule and fragment similarity for ANT, ATQ and hATQs were analysed. The (a,b)-maps of the whole molecules and their middle rings were compared to the (a,b)-map of 2-hATQ. The degree of similarity with 2-hATQ as a reference structure is shown for each molecule.

Compounds	Whole Molecule Similarity *ED 3-1	Fragment Similarity *ED 3-1
ANT	0.63	0.30
ATQ	0.64	0.81
1-hATQ	0.81	0.73
2-hATQ	1.00	1.00
1,2-dhATQ	0.66	0.71
1,3-dhATQ	0.74	0.75
1,4-dhATQ	0.66	0.71
1,5-dhATQ	0.66	0.69
1,8-dhATQ	0.71	0.71
2,6-dhATQ	0.69	0.63
1,2,4-thATQ	0.65	0.72
1,2,5,8-thATQ	0.57	0.66
1,2,10-thANT	0.62	0.47

*ED 3-1 (Electron Density 10^{-3}-10^{-1}) represents the electron density distribution calculated using *ab initio* Hartree-Fock method at the range of 0.001 to 0.1 au.

The whole molecule and the middle ring fragment of 2-hATQ, the most toxic molecule among the selected chemicals, was compared to the most similar fragments of other compounds. Thus, the (a,b)-maps of 2-hATQ and its fragments were compared to (a,b)-maps of other molecules and their fragments. The whole molecule and central ring similarities are presented in Table 5.2.

When the whole molecule similarity was examined, the range of similarity was as low as 0.57 for 1,2,5,8-thATQ relative to 2-hATQ (1.0). Interestingly, ANT (0.63) and 1,2,10-thANT (0.62) were more similar to 2-hATQ than 1,2,5,8-thATQ, even though they did not have a central quinone ring. As well, at the whole molecule level, 1,2-dhATQ (0.66) was less similar to 2-hATQ than either 1,3-dhATQ (0.74) and 1,8-dhATQ (0.71), even though neither of the latter molecules had a hydroxy at the second position. Three of the five dhATQs had identical whole similarities to 2-hATQ (Table 5.2). However, they were not identical when compared directly to each other (Appendix 1).

The fragment similarities based on the central quinone ring were spread over a larger range; from 0.30 for ANT to 1.0 for 2-hATQ. As would be expected, the two nonquinone molecules (ANT and 1,2,10-thANT) had the least similarity with the reference molecule (2-hATQ). The most similar molecule to 2-hATQ by this measure was ATQ, not one of the hATQs. Once again three of the five dhATQs had identical similarities relative to 2-hATQ, but these were not the same three molecules that had identical similarities to 2-hATQ at the whole molecule level (Table 5.2).

The similarities of (a,b)-maps were now ready to be correlated with experimental toxicities. Correlations were performed in two steps. First the correlations of the (a,b)-maps for the central ring were examined, with respect to the

middle ring of 2-hATQ molecule as reference. Second, the similarities of the (a,b)-maps of the whole molecules were analysed and compared with 2-hATQ molecule (Table 5.2). The similarity measures were then correlated with toxic activities, forming the basis of QSAR models.

5.4.2 Correlation Between Shape Analysis and Toxicity Data

The similarities of the (a,b)-maps of single fragments, with respect to the middle ring of 2-hATQ as a reference, were first examined. 2-hATQ was used as the reference point because it is the most toxic of the chemicals tested. The fragment similarities were compared to the toxicity data from chapter three. Growth inhibition for all 13 chemicals in this study was plotted against the fragment similarities (Figure 5.4). A very weak correlation between the middle ring similarities and toxicity data was observed. However, one can see that ANT and 1,2,10-thANT may be outliers. Thus, these two compounds were excluded in an attempt to obtain a better linear fit for the rest of hATQs examined. The elimination of ANT and 1,2,10-thANT was motivated by their structural differences (they are the only non-quinone molecules) and they had the lowest similarity to 2-hATQ for the single fragment data (Table 5.2). In addition they both can be photomodified rapidly to quinones (Chapter Two). So most of their toxic activity is probably due to the generated quinones. Thus, these two compounds are mechanistically outlier. Use of Spearman's non-parametric analysis showed that 2-hATQ is the real statistical outlier for both regressions (Figure 5.4 A and B). When ANT and 1,2,10-thANT excluded from the graph the regression was improved dramatically ($r^2 = 0.92$), and now molecular shape can be accurately fit to empirical toxicity (Figure 5.4).

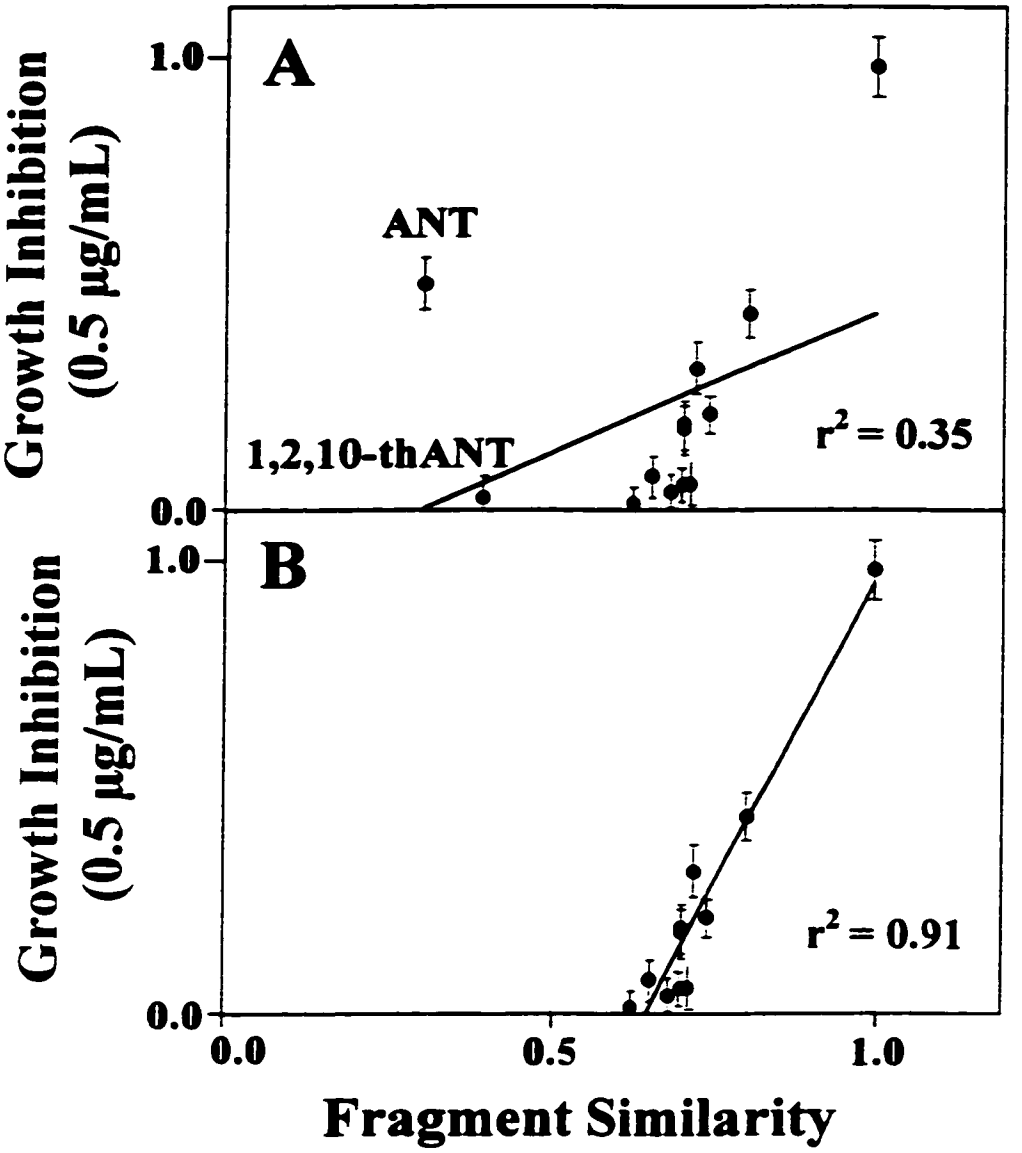

Figure 5.4 A) Correlation between growth inhibition (0.5 µg/mL) and fragment similarity with all 13 chemicals including ANT and 1,2,10-thANT. B) Correlation between growth inhibition (0.5 µg/mL) and fragment similarity without ANT and 1,2,10-thANT. The electron density range used was 10^{-3} to 10^{-1} au.

With the above conditions, a more detailed comparison of shape similarities and toxicity data was performed. Both whole molecule and fragment similarities were used. The chemical concentrations and the shapes of electronic charge clouds have a fundamental role in the initial chemical reactions responsible for their toxicity and correlation analysis. Interestingly, the best correlation between shape similarity and toxicity was for growth inhibition of the chemicals at 0.5 μg/ml, compared to 2 μg/ml and EC50s (Figure 5.5). Nonetheless, the results show that there is a difference in the correlations with toxicity between the whole molecule and fragment similarities.

Higher correlations between fragment similarity and empirical toxicity were observed than between whole molecule similarity and toxicity. Indeed, there are better correlations between fragment similarities than whole molecule similarities for the 2 μg/ml and EC50 data as well (Figure 5.5). However, it is important to realize that the whole molecule similarities were for all 13 chemicals, while single fragment similarities had 2 chemicals removed as discussed above. Indeed, looking at the whole molecule similarity correlation to growth inhibition at 0.5 μg/ml, there are no obvious chemicals that are outliers.

The results from this part of the correlation analysis showed that data sets for growth inhibition at 0.5 and 2 μg/ml showed good correlations to the shape similarity. However there were poor correlations between the EC50 values and the shape data (r^2 = 0.42 and 0.19, Figure 5.5). Note, that the slope is negative. As the shape similarities of fragments and/or whole molecules increase, the EC50s decrease (Figure 5.5). Because the chemicals most similar to 2-hATQ also have lower EC50s (higher toxicity and growth inhibition). The stronger correlation of toxicity with the shape features of the middle ring of these molecules may due to the fact that ANT and 1,2,10-thANT are not in the correlations.

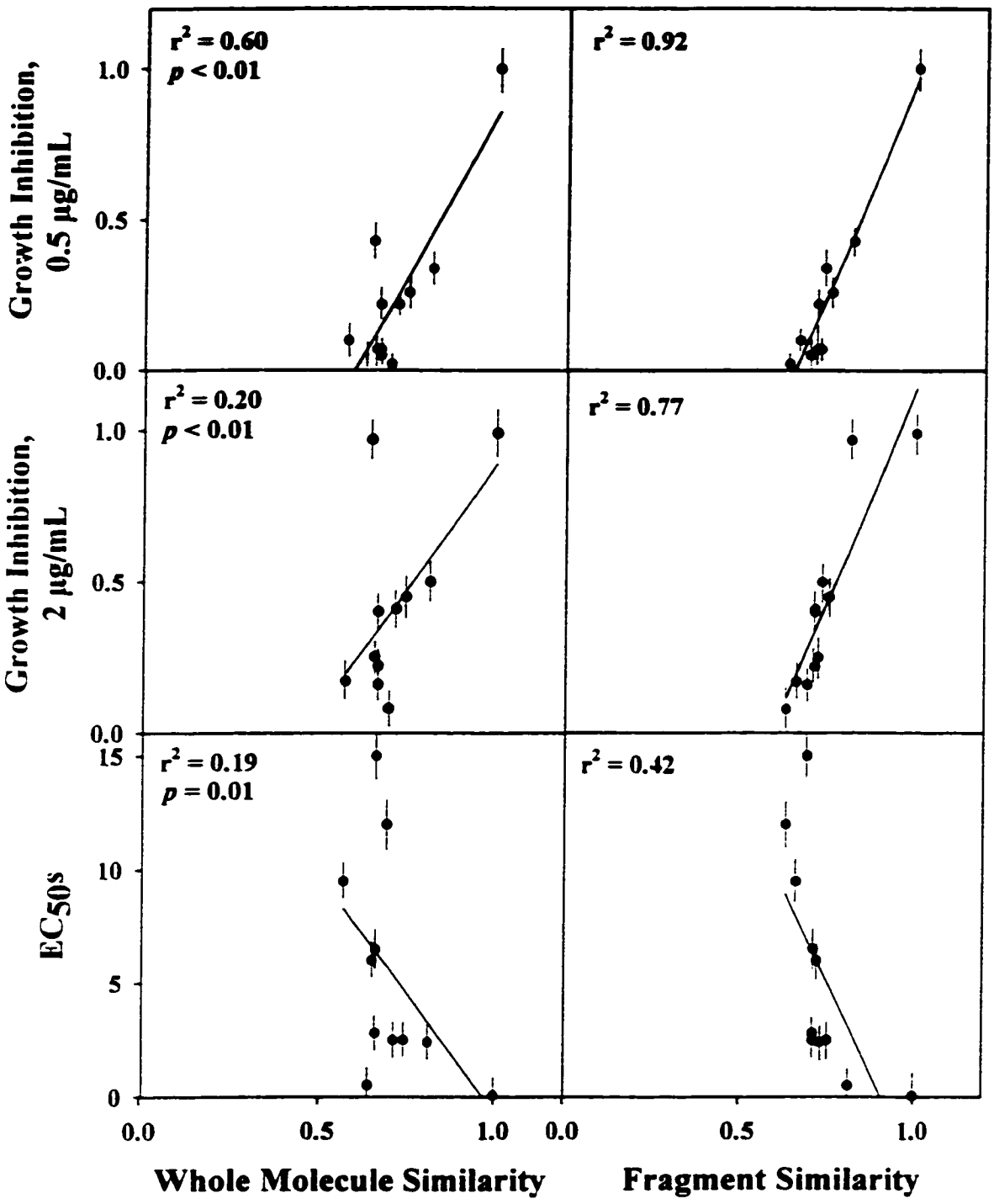

Figure 5.5 Experimental toxicity vs. whole molecule similarity and fragment similarity with a density range of 10^{-3} to 10^{-1} described for ATQ and h-ATQs.

Thus, the low electron density of quinone ring in hATQs and middle ring of ATQ as a potential feature, may explain why toxicity is not being compared to molecules without this feature.

Among the three correlations of whole molecule similarity and empirical toxicity, the results from 0.5 μg/ml growth inhibition again showed higher regression coefficient than 2 μg/ml and EC50s (Figure 5.5). The r^2 for the regressions suggest that use of growth inhibition 0.5 μg/ml is an important measure of toxicity and is amenable to QSAR analysis. Growth inhibition at 2 μg/ml had a weak correlation with whole molecule similarity, however there is one outlier (ANT) presented in the graph which degrades the correlation (Figure 5.5). The EC50's did not correlate well with whole molecular similarity ($r^2 = 0.19$). In this case one can see that the data falls onto a vertical line where the similarities reach at lower value (Figure 5.5). If the data could be spread out via a hyperbolic function the QSAR model might improve (see section 5.4.3).

The identified shape features, local and global shape characteristics, can predict toxicity. With intact PAHs this was attributed to the photosensitization and photomodification activities of the molecules (Mezey *et al.*, 1998). In that model the local and global shapes had to be combined to get a good correlation. In this work, local (fragment) and global shape (whole molecule) could be independently correlated to toxicity. This reflects the fact that the ANT photoproducts do not require photoactivation to be toxic (Chapter three).

Figures 5.5 imply that whole molecule and fragment similarities by themselves in general are weakly correlated with experimental toxicities, although the patterns shown indicate the presence of underlying relations for further modeling. To

determine if this relation could be better revealed, a hyperbolic fit of the shape data to the toxicity data was performed.

5.4.3 Hyperbolic Fit of Molecular Shape and Toxicity Data

The rationale for this approach is to best fit the molecular shape data to the empirical toxicity. A hyperbolic function spreads out one set of data with respect to another and optimises the slope between two sets of data (Mezey *et al.*, 1998). Thus, the hyperbolic function (equation 1) was fit to each empirical toxicity data set to solve the constant C_0 and C_1.

$$Y_{theor} = C_0 / 1 - C_1 X_1 \quad (1)$$

Where X_1 represents either one-ring or whole molecule similarities, and C_0 and C_1 are constants for intercept and slope to fit the shape and toxicity data (Table 5.3). The optimum values of the coefficients C_0, and C_1 are generated by fitting either the fragment or whole molecule similarities against the experimental toxicities. They were calculated for the whole molecule and the fragment shape similarities based on growth inhibition at 0.5 and 2 μg/ml as well as the EC50s (Table 5.3). The correlations of Y_{theor} for ANT and the 12 photoproducts vs the empirical toxicity data were quite strong. The correlations in all cases include all 13 chemicals. The six graphs show how the hyperbolic fit of the shape data to toxicity gives excellent correlations (Figure 5.6). Interestingly, the whole molecule correlations are now as good as those for the fragment similarities (Figures 5.6). Correlations between whole molecule and fragment similarities with empirical toxicity are highly significant ($p <$ 0.005 in all cases). In this inclusive model with use of hyperbolic equation, the adjusted r^2 is high for all the six graphical models. This is especially striking for the

Table 5.3 The numerical shape analysis and theoritical toxicity (hyperbolic dependencies). Theoretical toxicity derived using equation $Y_{theor} = C_0 / 1\text{-}C_1X_1$ from the similarities of (a,b)-maps shape code of the whole PAH molecules and one-ring fragments to the (a,b)-maps of the 2-hATQ molecule and its middle one-ring fragment, respectively.

Compounds	Hyperbolic Dependencies G.I. (0.5 μg/ml) Whole Molecule Similarity W.M.S. (3-1)	Hyperbolic Dependencies G.I. (0.5 μg/ml) Fragment Similarity F.G. (3-1)	Hyperbolic Dependencies G.I. (2.0 μg/ml) W.M.S. (3-1)	Hyperbolic Dependencies G.I. (2.0 μg/ml) F.S. (3-1)	Hyperbolic Dependencies G.I. (EC50s) W.M.S. (3-1)	Hyperbolic Dependencies G.I. (EC50s) F.S. (3-1)
ANT	0.28	0.13	0.6048	0.288	0.504	0.24
ATQ	0.27	0.34	0.6208	0.7857	0.32	0.405
1-hATQ	0.27	0.24	0.405	0.365	1.944	1.752
2-hATQ	0.99	0.99	0.99	0.99	0.05	0.05
1,2-dhATQ	0.14	0.15	0.264	0.284	1.848	1.988
1,3-dhATQ	0.19	0.19	0.333	0.3375	1.85	1.875
1,4-dhATQ	0.05	0.05	0.1452	0.1562	4.29	4.615
1,5-dhATQ	0.03	0.03	0.1056	0.1104	9.9	10.35
1,8-dhATQ	0.15	0.15	0.2911	0.2911	1.775	1.775
2,6-dhATQ	0.01	0.01	0.0552	0.0504	8.28	7.56
1,2,4-thATQ	0.05	0.03	0.1625	0.18	3.9	4.32
1,2,5,8-thATQ	0.06	0.07	0.0969	0.1122	5.415	6.27
1,2,10-thANT	0.03	0.02	0.1725	0.94	6.2	4.7

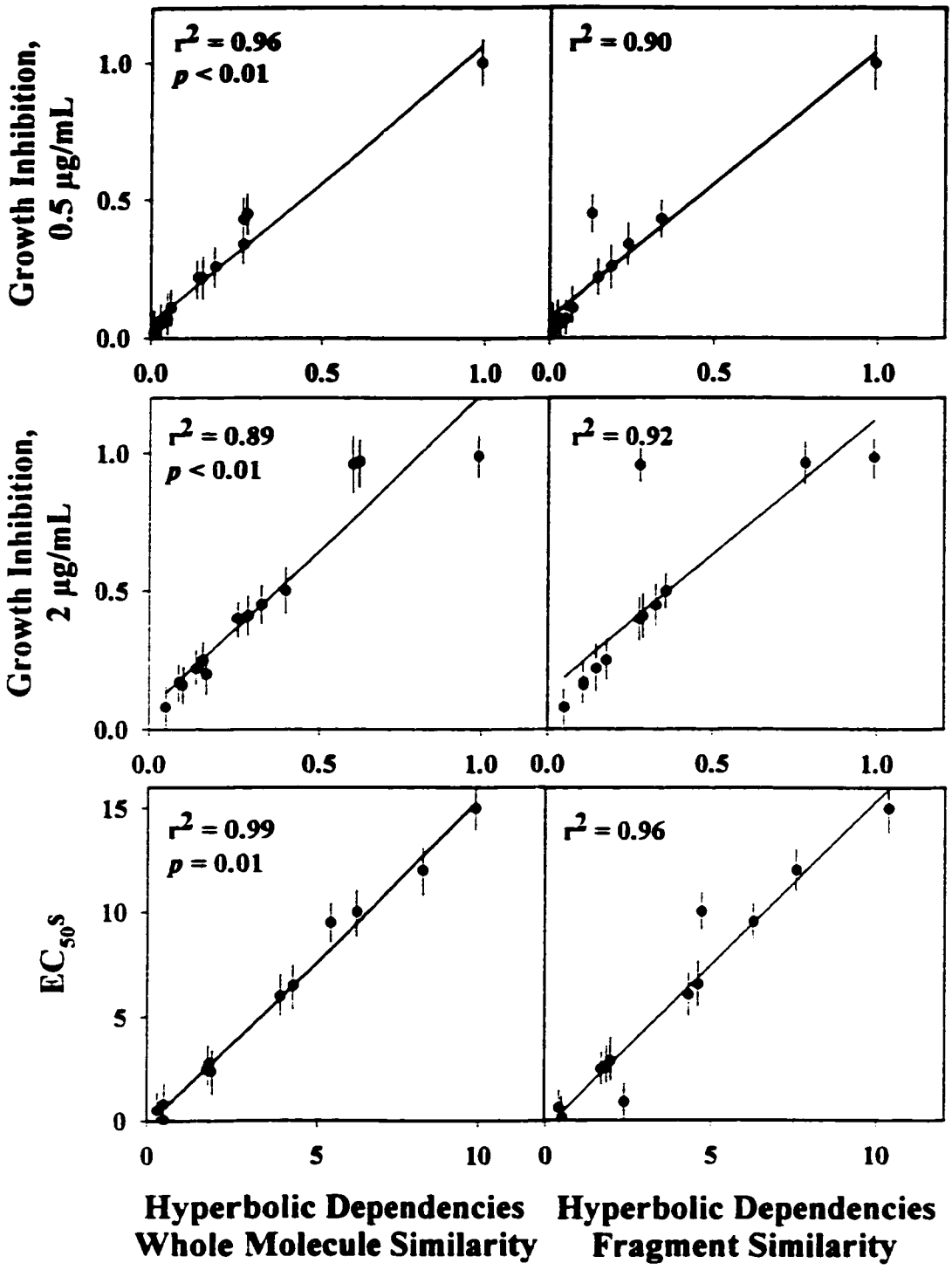

Figure 5.6 The hyperbolic type dependence shows a strong and almost linear relation between similarities of whole molecule and one ring with experimental toxicity. Hyperbolic dependencies for whole molecule and one-ring similarity described for ANT, ATQ and h-ATQs with density range of 10^{-3} to 10^{-1}.

EC50s, which had essentially no correlation to toxicity in Figure 5.5.

The results obtained demonstrate that in this QSAR study before use of hyperbolic fit, the correlations of fragment similarities and toxicity data (growth inhibitions at 0.5, 2 μg/ml and EC50s) were better than the whole molecule (Figure 5.5). After use of hyperbolic fit, equally good correlations of the toxicity data to the whole molecule and fragment shape features were observed. The differences between fragment and whole molecule similarities may relate to the ways in which these moieties interact with biological receptors. This may lie in the possible differences in the structures of the chemicals which are consistent with the production of specific biological effects. The QSAR model studied here is similar to models known as linear free energy relationships or LFERs (Leffer and Grunwald, 1969). For both the fragment and whole molecule similarities analyses, linear regression resulted in models that reflect changes in free energy. This is based on the assumption that the structure of a molecule (i.e., its geometric and electronic properties) dictates its ability to interact with plants and ultimately inhibition of growth.

It is significant that both the whole molecule and fragment similarities correlate with toxicity. The low electronic density in the middle ring is a diagnostic element that may provide a measure of the rapid rate of photooxidation of the molecules. As well, this is the most reactive region of the molecules. Thus, since these molecules appear to be toxic without further activation, it is logical that the central ring is an important determinant in toxicity. Conversely, the whole molecule similarity of ANT and its photoproducts may represent their general ability to bind to biological receptors. This is consistent with the ability of these chemical to bind specific proteins in the photosynthetic apparatus and inhibit electron transport (Chapter four). Thus, it is logical that both local and global shape features can independently be

incorporated into QSARs of toxicity for modified ANT.

The electron density (ED) distribution were calculated for ANT, ATQ and hATQs using the standard *ab initio* Hartree-Fock method at 6-31G** basis set and three different density ranges of (10^{-2} - 10^{-1}, 10^{-3} - 10^{-1}, 10^{-3} - 10^{-2}). Appendix 1 shows a calculated matrix of the similarities of (a,b)-maps for whole molecules and fragments with different density ranges. The ranges and levels of similarity are slightly different for 10^{-3} to 10^{-1}, 10^{-2} to 10^{-1} and 10^{-3} to 10^{-2} au (Appendix 1). Thus each density range should correlate with toxicity. In the above work the density range of 10^{-3} - 10^{-1} au was used, as this density range cover the largest density range of the molecules (Table 5.1). However, it was important to determine if the other density ranges would correlate with toxicity. Thus, the single fragment similarity were plotted against growth inhibition with 0.5 μg/ml (Figure 5.7). Indeed the density range of 10^{-3}-10^{-1} au gave the best correlation to toxicity (Figure 5.7). Thus, for ANT and oxyANTs it is important to have low and high electron density regions in the QSARs.

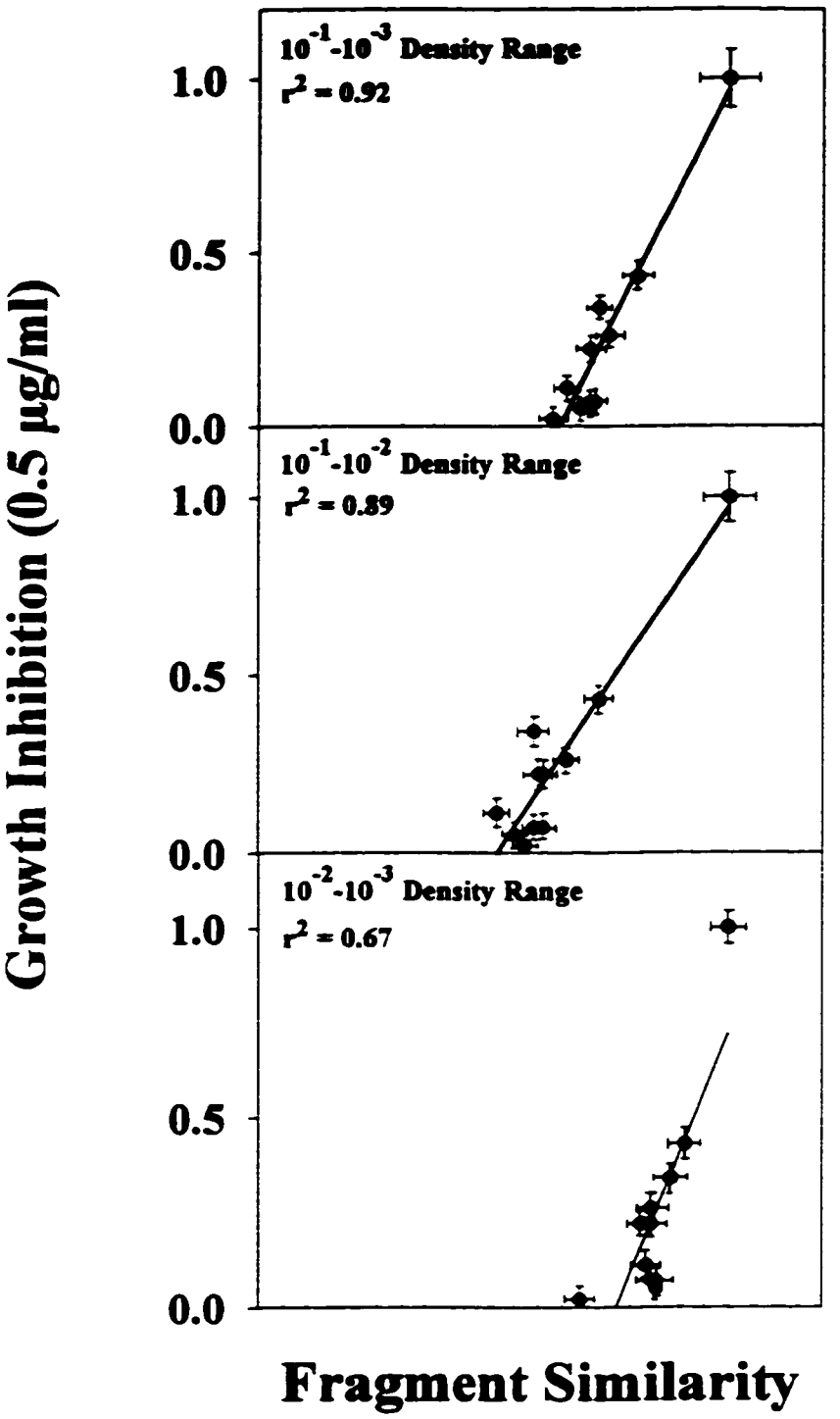

Figure 5.7 Experimental toxicity vs. fragment similarity presented for density range of 10^{-3} to 10^{-1}, 10^{-2} to 10^{-1} and 10^{-3} to 10^{-2}.

5.4.4 Correlation Analysis of Photosynthetic Activity and Molecular Shapes

Because both the one ring and whole molecule similarities of ANT, ATQ and the hATQs showed a good correlation with the empirical whole organism toxicity data, it was of interest to compare the molecular shape data bases to a physiological end point. Further, it was important to determine if the hyperbolic fits for whole organism toxicity would correlate to another endpoint (such as photosynthesis activity) without adjustment of the data. Therefore the hyperbolic fits of shape data in Table 5.3 were plotted against data for inhibition of photosynthesis by the chemicals. Inhibition of photosynthetic activity in vivo with *L. gibba* was assessed by Chl *a* fluorescence induction (Chapter 4). F_V/F_M and F_Q/F_M were used as an indicators of photosynthetic activity vs molecular shape similarity. They were shown in chapter 4 to correlate with whole organism toxicity. The correlation analysis between molecular shape similarity and photosynthetic activity are shown in figures 5.8, 5.9 and 5.10.

The EC50 values for F_V/F_M and F_Q/F_M were plotted against hyperbolic dependencies of one-ring and whole molecule similarity to determine their correlation and predictive capacity. The photosynthetic activity data from chapter 4 (Tables 4.1 and 5.1) were plotted against hyperbolic dependencies acquired for EC50 values from growth inhibition in this study (Table 5.3). A weak correlation between molecular similarity and inhibition of photosynthetic activity was obtained when the F_Q/F_M was used in the regression (Figure 5.8 (A-B); $r^2 = 0.613, 0.602$, $p < 0.01$). Hence, this model has some predictive capacity for inhibition of photosynthesis by ANT, ATQ and the hATQs. A better relationship was apparent when F_V/F_M was used (Figure 5.8; $r^2 = 0.737, 0.741$). A theoretical basis exists for the dependence of photosynthetic activity and molecular similarity.

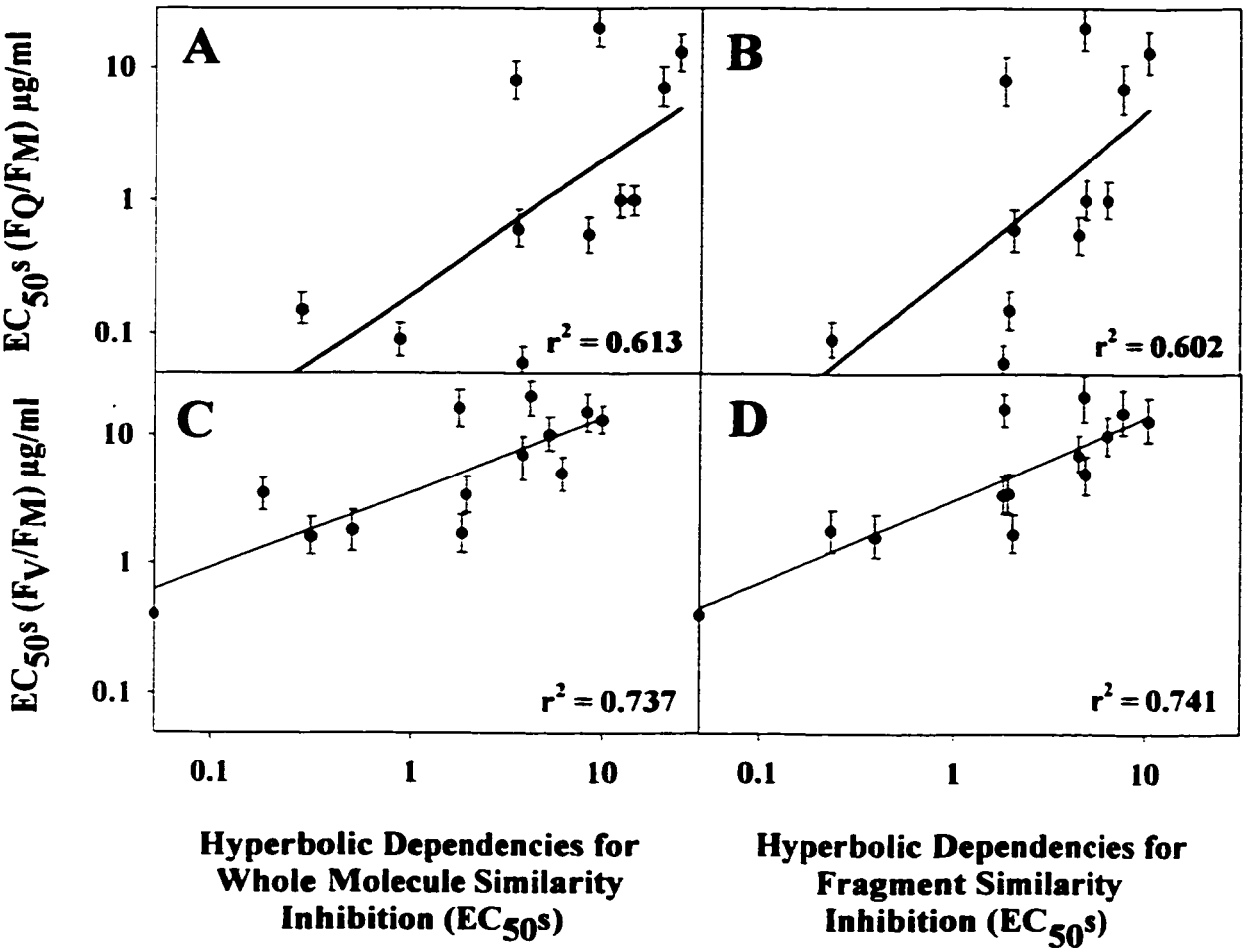

Figure 5.8 Correlations of (a,b)-maps for one-ring and whole molecule similarities vs F_V/F_M and F_Q/F_M. Hyperbolic fit of the similarities for the EC50s for inhibition of growth were used on the X axis. The relevant photosynthesis data is plotted on the Y axis. A) Correlation of F_Q/F_M with hyperbolic dependencies of whole molecular similarity. B) Correlation analysis of F_Q/F_M with hyperbolic dependencies of one-ring similarity. C) Correlation of F_V/F_M hyperbolic dependencies of vs whole molecular similarity. D) F_V/F_M vs hyperbolic dependencies of one-ring similarity.

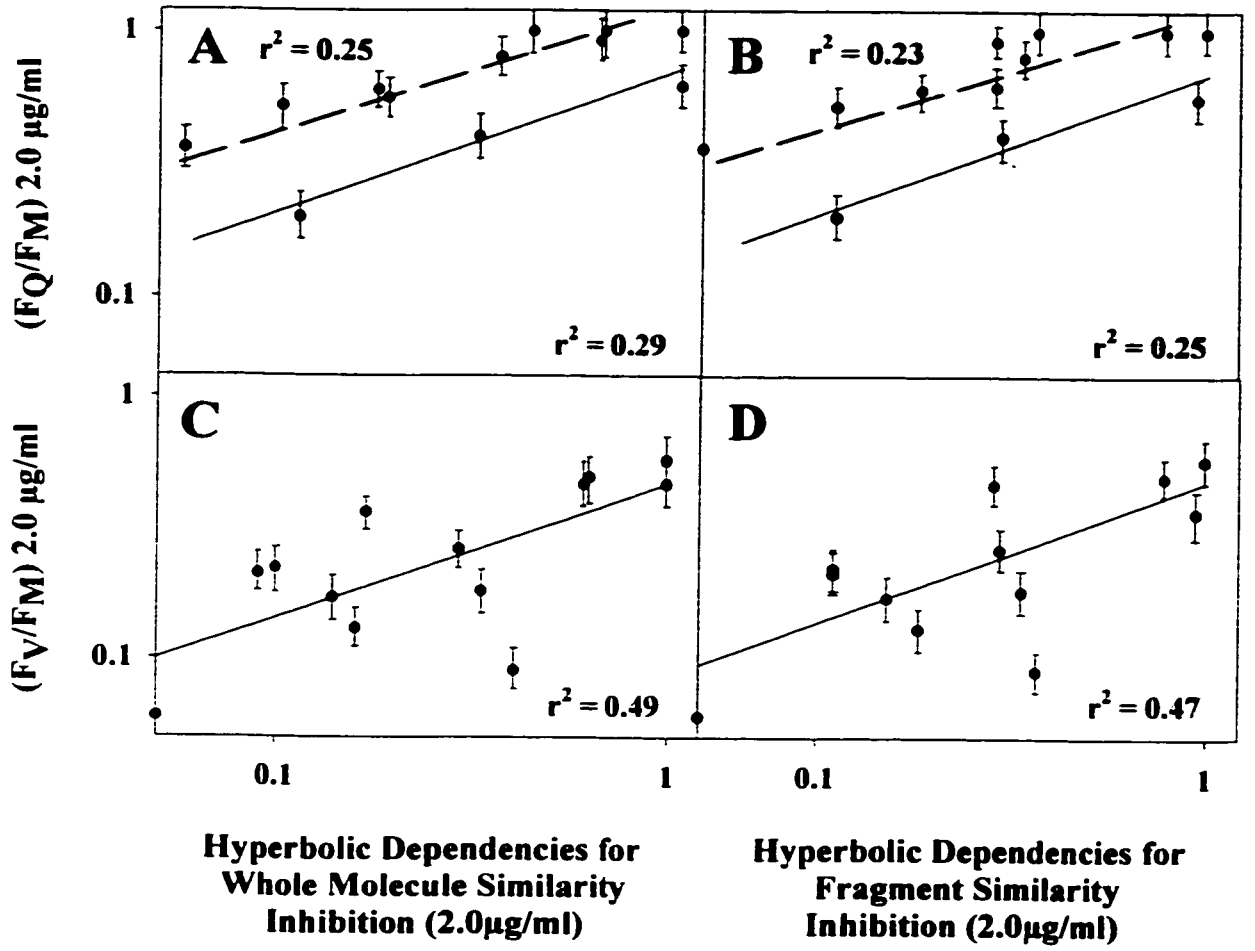

Figure 5.9 Computed correlation of similarities of (a,b)-maps of one-ring and whole molecule vs F_V/F_M and F_Q/F_M measured at 2 µg/ml chemical concentrations. A) Correlation of F_Q/F_M with hyperbolic dependencies of whole molecular similarity. B) Correlation analysis of F_Q/F_M with hyperbolic dependencies of one-ring similarity. C) Correlation of F_V/F_M hyperbolic dependencies of vs whole molecular similarity. D) F_V/F_M vs hyperbolic dependencies of one-ring similarity.

This is because F_V/F_M was found to be a better indicator of acute toxicity than F_Q/F_M and EC50s is also a measure of acute toxicity. Nonetheless, it is important that the two data sets for F_Q/F_M and F_V/F_M have reasonably strong correlation coefficients (Figure 5.8), as both F_Q/F_M and F_V/F_M were found to be excellent bioindicators of effects.

The results of analysis with the chemicals at 2 μg/ml revealed again that F_V/F_M had higher correlations to the shape data than F_Q/F_M (Figure 5.9), even though the F_Q/F_M is more sensitive indicator of photosynthetic activity. The correlation of F_Q/F_M with hyperbolic dependencies for whole molecule and fragment similarity at 2 μg/ml is not statistically significant and provide a low level of regression coefficient (r^2 = 0.29 and 0.25). However, it is interesting that there are three outliers in these correlations that when removed from the data sets result in increased r^2 values (1,2-dhATQ, 1,5-dhATQ and 1,2,4-thATQ) (Figure 5.9). It is unclear why these do not fit well in the regression. Again F_V/F_M, which was found to have better fits than F_Q/F_M for EC50 data, had better correlations for the 2 μg/ml than F_Q/F_M (Figures 5.8 and 5.9).

The analysis relationship between photosynthetic activities at 0.5 μg/ml and chemical shape revealed reasonably strong correlations (Figure 5.10). Interestingly, the FQ/FM correlations are now slightly better than those for FV/FM. This is consistent with F_Q/F_M which bring a better measure of chronic toxicity (Chapter four). Thus, at lower concentration of chemicals one would expect to have a better fit to the shape data.

The results of previous studies (Huang *et al.*, 1997; Krylov *et al.*, 1997; Mezey *et al.*, 1998) and the work related here show that molecular similarities of hATQs

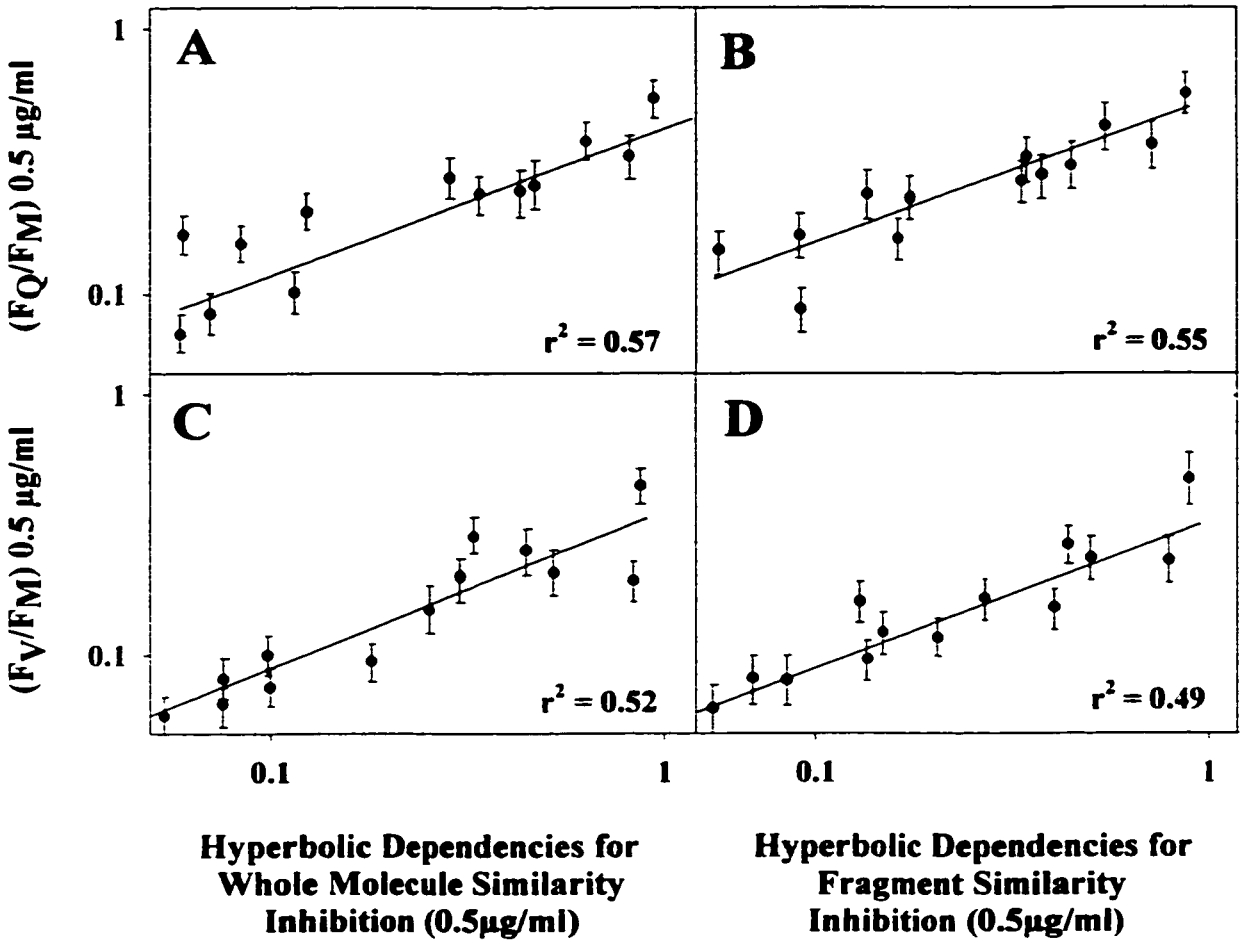

Figure 5.10 Computed correlation of similarities of (a,b)-maps of one-ring and whole molecule vs F_V/F_M and F_Q/F_M measured at 0.5 µg/ml chemical concentrations. A) Correlation of F_Q/F_M with hyperbolic dependencies of whole molecular similarity. B) Correlation analysis of F_Q/F_M with hyperbolic dependencies of one-ring similarity. C) Correlation of F_V/F_M hyperbolic dependencies of vs whole molecular similarity. D) F_V/F_M vs hyperbolic dependencies of one-ring similarity.

correlate with indicators of photosynthetic activity (F_V/F_M and F_Q/F_M) (Figure 5.7). The global and local shape features correlated equally well with the photosynthesis data. This is again consistent with direct action of these chemicals on the photosynthetic apparatus (see Chapter four). Importantly, this part of the research showed that a QSAR model based on whole organism toxicity correlated well with inhibition at the putative site of action of these chemicals. This lends further credence to the supposition that the primary site of these compounds in plants is the photosynthetic apparatus.

The interaction of hazardous chemicals with biological organisms is very complicated. Thus, an attempt at modeling relationships between chemical structures and photosynthetic activity without considering internal and environmental factors will fail to explain the impacts. Understanding the reaction mechanisms is a fundamental feature in predicting toxicity of contaminants and impairment of photosynthesis. These correlations provide the results for elucidating which interactions between a given chemical and the biological activity (inhibition of photosynthesis) have the greatest impact on the hazards of the contaminants in the environment. If these correlations between the shape of chemicals and the biological activity are fully understood, toxicity of contaminants in the environment can be predicted based on the chemical and biological properties of these reactions.

Appendix 1

Similarities of (a,b)-maps for whole molecules and fragments with different electron density range.

SIMILARITIES OF AB-MAPS FOR "A" FRAGMENTS: RANGE 10^{-2} - 10^{-1}

	1)	2)	3)	4)	5)	6)	7)	8)	9)	10)	11)	12)	13)
1) ANT	1.00	0.25	0.23	0.26	0.22	0.22	0.23	0.23	0.26	0.29	0.26	0.24	0.36
2) ATQ	0.25	1.00	0.60	0.73	0.56	0.62	0.56	0.52	0.66	0.67	0.74	0.48	0.32
3) 1 hATQ	0.23	0.60	1.00	0.59	0.72	0.68	0.69	0.66	0.62	0.61	0.64	0.64	0.33
4) 2 hATQ	0.26	0.73	0.59	1.00	0.60	0.66	0.59	0.55	0.61	0.57	0.61	0.51	0.32
5) 1,2 dhATQ	0.22	0.56	0.72	0.60	1.00	0.67	0.67	0.66	0.52	0.54	0.62	0.63	0.33
6) 1,3 dhATQ	0.22	0.62	0.68	0.66	0.67	1.00	0.54	0.48	0.62	0.68	0.61	0.50	0.36
7) 1,4 dhATQ	0.23	0.56	0.69	0.59	0.67	0.54	1.00	0.74	0.48	0.49	0.53	0.73	0.32
8) 1,5 dhATQ	0.23	0.52	0.66	0.55	0.66	0.48	0.74	1.00	0.47	0.48	0.49	0.80	0.33
9) 1,8 dhATQ	0.26	0.66	0.62	0.61	0.52	0.62	0.48	0.47	1.00	0.71	0.67	0.47	0.36
10) 2,6 dhATQ	0.29	0.67	0.61	0.57	0.54	0.68	0.49	0.48	0.71	1.00	0.63	0.49	0.35
11) 1,2,4 thATQ	0.26	0.74	0.64	0.61	0.62	0.61	0.53	0.49	0.67	0.63	1.00	0.50	0.32
12) 1,2,45,8 thATQ	0.24	0.48	0.64	0.51	0.63	0.50	0.73	0.80	0.47	0.49	0.50	1.00	0.30
13) 1,2,10 thANT	0.36	0.32	0.33	0.32	0.33	0.36	0.32	0.33	0.36	0.35	0.32	0.30	1.00

SIMILARITIES OF AB-MAPS FOR WHOLE MOLECULES: RANGE 10^{-2} - 10^{-1}

	1)	2)	3)	4)	5)	6)	7)	8)	9)	10)	11)	12)	13)
1) ANT	1.00	0.66	0.65	0.58	0.61	0.62	0.63	0.58	0.68	0.62	0.63	0.54	0.50
2) ATQ	0.66	1.00	0.69	0.64	0.62	0.64	0.62	0.59	0.69	0.69	0.58	0.54	0.50
3) 1 hATQ	0.65	0.69	1.00	0.85	0.66	0.73	0.71	0.68	0.75	0.73	0.69	0.60	0.65
4) 2 hATQ	0.58	0.64	0.85	1.00	0.65	0.77	0.62	0.60	0.74	0.74	0.65	0.59	0.63
5) 1,2 dhATQ	0.61	0.62	0.66	0.65	1.00	0.81	0.72	0.76	0.79	0.79	0.79	0.66	0.61
6) 1,3 dhATQ	0.62	0.64	0.73	0.77	0.81	1.00	0.75	0.74	0.87	0.85	0.73	0.65	0.59
7) 1,4 dhATQ	0.63	0.62	0.71	0.62	0.72	0.75	1.00	0.87	0.76	0.75	0.74	0.74	0.60
8) 1,5 dhATQ	0.58	0.59	0.68	0.60	0.76	0.74	0.87	1.00	0.76	0.78	0.73	0.77	0.62
9) 1,8 dhATQ	0.68	0.69	0.75	0.74	0.79	0.87	0.76	0.76	1.00	0.85	0.72	0.61	0.56
10) 2,6 dhATQ	0.62	0.69	0.73	0.74	0.79	0.85	0.75	0.78	0.85	1.00	0.72	0.67	0.58
11) 1,2,4 thATQ	0.63	0.58	0.69	0.65	0.79	0.73	0.74	0.73	0.72	0.72	1.00	0.73	0.62
12) 1,2,45,8 thATQ	0.54	0.54	0.60	0.59	0.66	0.65	0.74	0.77	0.61	0.67	0.73	1.00	0.59
13) 1,2,10 thANT	0.50	0.50	0.65	0.63	0.61	0.59	0.60	0.62	0.56	0.58	0.62	0.59	1.00

SIMILARITIES OF AB-MAPS FOR "A" FRAGMENTS: RANGE 10^{-1} - 10^{-1}

	1)	2)	3)	4)	5)	6)	7)	8)	9)	10)	11)	12)	13)
1) ANT	1.00	0.29	0.28	0.30	0.28	0.27	0.28	0.28	0.29	0.29	0.30	0.29	0.37
2) ATQ	0.29	1.00	0.75	0.81	0.71	0.72	0.70	0.69	0.74	0.70	0.80	0.64	0.47
3) 1 hATQ	0.28	0.75	1.00	0.73	0.80	0.76	0.77	0.76	0.72	0.65	0.76	0.72	0.50
4) 2 hATQ	0.30	0.81	0.73	1.00	0.71	0.75	0.71	0.69	0.71	0.63	0.72	0.66	0.47
5) 1,2 dhATQ	0.28	0.71	0.80	0.71	1.00	0.75	0.77	0.76	0.67	0.62	0.76	0.72	0.49
6) 1,3 dhATQ	0.27	0.72	0.76	0.75	0.75	1.00	0.66	0.64	0.73	0.72	0.72	0.63	0.51
7) 1,4 dhATQ	0.28	0.70	0.77	0.71	0.77	0.66	1.00	0.82	0.63	0.57	0.71	0.80	0.48
8) 1,5 dhATQ	0.28	0.69	0.76	0.69	0.76	0.64	0.82	1.00	0.63	0.56	0.68	0.82	0.48
9) 1,8 dhATQ	0.29	0.74	0.72	0.71	0.67	0.73	0.63	0.63	1.00	0.72	0.75	0.61	0.51
10) 2,6 dhATQ	0.29	0.70	0.65	0.63	0.62	0.72	0.57	0.56	0.72	1.00	0.66	0.57	0.51
11) 1,2,4 thATQ	0.30	0.80	0.76	0.72	0.76	0.72	0.71	0.68	0.75	0.66	1.00	0.66	0.48
12) 1,2,45,8 thATQ	0.29	0.64	0.72	0.66	0.72	0.63	0.80	0.82	0.61	0.57	0.66	1.00	0.47
13) 1,2,10 thANT	0.37	0.47	0.50	0.47	0.49	0.51	0.48	0.48	0.51	0.51	0.48	0.47	1.00

SIMILARITIES OF AB-MAPS FOR WHOLE MOLECULES: RANGE 10^{-1} - 10^{1}

	1)	2)	3)	4)	5)	6)	7)	8)	9)	10)	11)	12)	13)
1) ANT	1.00	0.63	0.62	0.63	0.63	0.64	0.68	0.61	0.67	0.63	0.64	0.55	0.55
2) ATQ	0.63	1.00	0.68	0.64	0.60	0.62	0.59	0.60	0.66	0.63	0.57	0.55	0.51
3) 1 hATQ	0.62	0.68	1.00	0.81	0.69	0.72	0.67	0.68	0.73	0.69	0.66	0.58	0.62
4) 2 hATQ	0.63	0.64	0.81	1.00	0.66	0.74	0.66	0.66	0.71	0.69	0.65	0.57	0.62
5) 1,2 dhATQ	0.63	0.60	0.69	0.66	1.00	0.79	0.76	0.76	0.78	0.76	0.73	0.61	0.61
6) 1,3 dhATQ	0.64	0.62	0.72	0.74	0.79	1.00	0.76	0.74	0.81	0.81	0.73	0.62	0.61
7) 1,4 dhATQ	0.68	0.59	0.67	0.66	0.76	0.76	1.00	0.80	0.75	0.74	0.73	0.67	0.61
8) 1,5 dhATQ	0.61	0.60	0.68	0.66	0.76	0.74	0.80	1.00	0.76	0.77	0.70	0.67	0.58
9) 1,8 dhATQ	0.67	0.66	0.73	0.71	0.78	0.81	0.75	0.76	1.00	0.78	0.69	0.58	0.57
10) 2,6 dhATQ	0.63	0.63	0.69	0.69	0.76	0.81	0.74	0.77	0.78	1.00	0.71	0.63	0.59
11) 1,2,4 thATQ	0.64	0.57	0.66	0.65	0.73	0.73	0.73	0.70	0.69	0.71	1.00	0.68	0.65
12) 1,2,45,8 thATQ	0.55	0.55	0.58	0.57	0.61	0.62	0.67	0.67	0.58	0.63	0.68	1.00	0.63
13) 1,2,10 thANT	0.55	0.51	0.62	0.62	0.61	0.61	0.61	0.58	0.57	0.59	0.65	0.63	1.00

SIMILARITIES OF AB-MAPS FOR "A" FRAGMENTS: RANGE 10^{-3} - 10^{-2}

	1)	2)	3)	4)	5)	6)	7)	8)	9)	10)	11)	12)	13)
1) ANT	1.00	0.32	0.31	0.33	0.33	0.31	0.34	0.34	0.32	0.30	0.34	0.34	0.39
2) ATQ	0.32	1.00	0.91	0.91	0.86	0.84	0.86	0.87	0.83	0.73	0.86	0.81	0.62
3) 1 hATQ	0.31	0.91	1.00	0.88	0.89	0.86	0.86	0.87	0.82	0.71	0.90	0.82	0.65
4) 2 hATQ	0.33	0.91	0.88	1.00	0.84	0.84	0.85	0.85	0.82	0.69	0.84	0.83	0.64
5) 1,2 dhATQ	0.33	0.86	0.89	0.84	1.00	0.85	0.87	0.87	0.81	0.70	0.92	0.81	0.64
6) 1,3 dhATQ	0.31	0.84	0.86	0.84	0.85	1.00	0.79	0.79	0.85	0.77	0.83	0.77	0.67
7) 1,4 dhATQ	0.34	0.86	0.86	0.85	0.87	0.79	1.00	0.91	0.78	0.66	0.89	0.87	0.64
8) 1,5 dhATQ	0.34	0.87	0.87	0.85	0.87	0.79	0.91	1.00	0.79	0.65	0.87	0.87	0.63
9) 1,8 dhATQ	0.32	0.83	0.82	0.82	0.81	0.85	0.78	0.79	1.00	0.74	0.82	0.77	0.68
10) 2,6 dhATQ	0.30	0.73	0.71	0.69	0.70	0.77	0.66	0.65	0.74	1.00	0.69	0.65	0.67
11) 1,2,4 thATQ	0.34	0.86	0.90	0.84	0.92	0.83	0.89	0.87	0.82	0.69	1.00	0.82	0.64
12) 1,2,45,8 thATQ	0.34	0.81	0.82	0.83	0.81	0.77	0.87	0.87	0.77	0.65	0.82	1.00	0.64
13) 1,2,10 thANT	0.39	0.62	0.65	0.64	0.64	0.67	0.64	0.63	0.68	0.67	0.64	0.64	1.00

SIMILARITIES OF AB-MAPS FOR WHOLE MOLECULES: RANGE 10^{-1} - 10^{-2}

	1)	2)	3)	4)	5)	6)	7)	8)	9)	10)	11)	12)	13)
1) ANT	1.00	0.61	0.63	0.67	0.66	0.67	0.77	0.65	0.67	0.65	0.67	0.57	0.60
2) ATQ	0.61	1.00	0.67	0.65	0.60	0.59	0.60	0.63	0.64	0.58	0.58	0.57	0.52
3) 1 hATQ	0.63	0.67	1.00	0.77	0.72	0.71	0.66	0.71	0.74	0.67	0.66	0.59	0.61
4) 2 hATQ	0.67	0.65	0.77	1.00	0.71	0.76	0.72	0.74	0.72	0.67	0.68	0.59	0.64
5) 1,2 dhATQ	0.66	0.60	0.72	0.71	1.00	0.78	0.81	0.78	0.79	0.76	0.68	0.57	0.62
6) 1,3 dhATQ	0.67	0.59	0.71	0.76	0.78	1.00	0.78	0.77	0.77	0.77	0.75	0.60	0.65
7) 1,4 dhATQ	0.77	0.60	0.66	0.72	0.81	0.78	1.00	0.75	0.76	0.76	0.73	0.61	0.63
8) 1,5 dhATQ	0.65	0.63	0.71	0.74	0.78	0.77	0.75	1.00	0.78	0.80	0.69	0.60	0.54
9) 1,8 dhATQ	0.67	0.64	0.74	0.72	0.79	0.77	0.76	0.78	1.00	0.72	0.68	0.57	0.59
10) 2,6 dhATQ	0.65	0.58	0.67	0.67	0.76	0.77	0.76	0.80	0.72	1.00	0.72	0.62	0.61
11) 1,2,4 thATQ	0.67	0.58	0.66	0.68	0.68	0.75	0.73	0.69	0.68	0.72	1.00	0.64	0.69
12) 1,2,45,8 thATQ	0.57	0.57	0.59	0.59	0.57	0.60	0.61	0.60	0.57	0.62	0.64	1.00	0.65
13) 1,2,10 thANT	0.60	0.52	0.61	0.64	0.62	0.65	0.63	0.54	0.59	0.61	0.69	0.65	1.00

References

Albert, A. 1985. Selective Toxicity, 7th ed. Chapman & Hall, London.

American Society for Testing and Materials (ASTM). 1991. Standard guide for conducting static toxicity tests with *Lemna gibba* G3. In *Annual Book of ASTM standards*. Vol.14, Committee E-47 on Biological Effects and Environmental Fate, Aquatic Toxicology, E 1415-91. ASTM, Philadelphia.

American Society for Testing and Materials (ASTM). 1995. Standard guide for using lighting in laboratory testing. Committee E-47 on Biological Effects and Environmental Fate, E 1733-95. *In Annual Book of ASTM Standards*, Volume 11.05. Philadelphia.

Anderson, J. 1987. Molecular Organization of Thylakoid Membranes. *In* J. Amesz (ed), Photosynthesis. Elsevier Science Publishers. **4**, 273-297.

Ankley, G.T., D.A Benoit, J.C. Balough, T.B. Reynoldson, K.E. Day, and R.A. Hoke. 1994. Evaluation of potential confounding factors in sediment toxicity tests with three freshwater benthic invertebrates. *Environ. Toxicol. Chem.* **13**, 627-635.

Arfsten, D.P., D.J. Schaffer, and D.C. Mulveny. 1996. The effects of near ultraviolet radiation on the toxic effects of polycyclic aromatic hydrocarbons in animal and plants: A review. *Ecotoxicol. Environ. Saf.* **33**, 1-24.

Aro, E.M., S. McCaffery and J.M. Anderson. 1994. Recovery from photoinhibition in peas (*Pisum Sativum L.*) acclimated to varying growth irradiances. *Plant Physiol.* **104**, 1033-1041.

Babu, T.S., S.C. Sabat and P. Mohanty. 1992. Heat induced alterations in the photosynthetic electron transport and emission properties of the cyanobacterium *Spirulina platensis. J. Photochem. Photobiol. B: Biol.* **12**, 161-171.

Baek, S.O., R.A. Field, M.E. Goldstone, P.W. Kirk, J.N. Lester and R. Perry. 1991. A review of atmospheric polycyclic aromatic hydrocarbons: sources, fate and behaviour. *Water, Air and Soil Pollut.* **60**, 279-300.

Baker, N.R., T.M. East, and S.P. Long. 1983. Chilling damage to photosynthesis in young *Zea mays.* II. Photochemical function of thylakoids *in vivo. J. Exp. Bot.* **34**, 189-197.

Barnthouse L., and J. Brown. 1994. Issue paper on conceptual model development. *In* Ecological Risk Assessment Issue Papers, EPA/630/R-94/009, U.S. Environmental Protection Agency, Washington, D.C.

Basu, D.K., and J. Saxena. 1978. Polynuclear aromatic hydrocarbons in selected U.S. drinking waters and their raw water sources. *Environ. Sci. Technol.* **12**, 795-798.

Benenati, F. 1990. Keynote address: plants-keystone to risk assessment. *In* W. Wang. J.W. Gorsuch, W.R. Lower (eds), Plants for Toxicity Assessment, ASTM STP 1091, American Society of Testing and Materials, Philadelphia.

Bierman, V.J., Jr. 1990. Equilibrium and biomagnification partitioning of organic chemicals in benthic animals. *Environ. Sci. Technol.*, **24**, 1407-1412.

Bjorseth, A. 1983. **Handbook of polycyclic aromatic hydrocarbons.** Marcel Dekker, New York.

Blumer, M. 1965. **Organic pigments: their long-term fate,** *Science*. **149,** 722-726.

Blumer, M. 1976. **Polycyclic aromatic compounds in nature.** *Sci. Amer.* **234,** 35-45.

Bolhar-Nordenkampf, H.R. and G. Oquist. 1993. Chlorophyll fluorescence as a tool in photosynthesis research. *In* D.O. Hall, J.M.O. Scurlock, H.R. Bolhar-Noredenkampf, R.C. Leegood, S.P. Long (eds), Photosynthesis and Protection in a Changing Environment: A Field and Laboratory Manual, Chapman and Hall, London.

Borneff, J., F. Selenka, H. Kunte, and A. Maximos. 1968. Experimental studies on the formation of polycyclic aromatic hydrocarbons in plants. *Environ. Res.* **2,** 22-29.

Brisou, J. 1969. Biosynthesis of 3,4-benzopyrene and anaerobiosis. *C.R. Soc. Biol.* (Paris) **163,** 772-774.

Brody, M.S., Y. Valette, and M.E. Troyer. 1993. Ecological risk assessment case study: modeling future losses of bottomland forest wetlands and changes in wildlife habitat within a louisiana basin. *In* A Review of Ecological Assessment Case Studies from a Risk Assessment Perspective, EPA/630/R-92/005,U.S. Environmental Protection Agency, Washington, D.C.

Butler, G.C. 1978. **Principles of Ecotoxicology.** SCOPE 12. New York, Wiley.

Calamari, D. (ed). 1993. **Chemical exposure predictions.** Chelsea, MI: Lewis.

Call, D.J., L.T. Brooke, M.L. Knuth, S.H. Poirer, and M.D. Hoglund. 1985. Fish subchronic toxicity prediction model for industrial organic chemicals that produce narcosis. *Environ. Toxicol. Chem.* **4**, 335-341.

Carbo, R. (ed). 1995. Molecular similarity and reactivity: from quantum chemical to phenomenological approaches. Kluwer Academic.

Cavalieri, E.L., and E.G. Rogan. 1990. Radical caution in aromatic hydrocarbon carcinogenesis. *Free Rad. Res. Commun.* **11**, 77-87.

Chaphekar, S.B. 1991. An overview on bio-indicators. *J. Environ. Biol.* **12**, 163-168.

Chessels, M., D.W. Hawker and D.W. Connell. 1992. Influence of solubility in lipid on bioconcentration of hydrophobic compounds. *Ecotoxicol. Environ. Safety.* **23**, 260-273.

Connell, D.W. 1988. Bioaccumulation potential of persistent organic chemicals with aquatic organisms. *Rev. Environ. Contam. Toxicol.* **101**, 117-154.

Cook, R.H., R.C. Pierce, P.B. Eaton, R.C. Lao, F.I. Onuska, J.F. Payne, and E. Vavasour. 1983. Polycyclic aromatic hydrocarbons in the aquatic environment: formation, sources, fate and effects on aquatic biota. NRCC 18981, National Research Council of Canada, Ottawa, Ontario, Canada.

Cooke, M. and A.J. Dennis. 1983. PAHs: Formation, Metabolism and Measurement, Battelle Press, Columbus, OH.

Culley, D.D. Jr., E. Rejmankova, J. Kvet and J.B. Frye. 1981. Production, chemical quality and use of duckweeds (*lemnaceae*) in aquaculture, waste management and animal feeds. *J. world Maricult. Soc.* **12**, 27-49.

Dean, P.M. 1987. Molecular foundation of drug-receptor interaction, Cambridge. University Press.

Dearden J.C. and R.M. Nicholson. 1991. Correlation of biodegradability with atomic charge difference and superdelocalizability. *In* K.L.E. Kaiser (ed), QSAR in Environmental Toxicology-II. Reidel, Dordrecht. pp. 83-89.

Delistraty, D. 1986. Growth and photosynthetic response of a freshwater alga, *Selenastrum capricornutum*, to an oil shale by-product water. *Bull Environ. Contam. Toxicol.* **36(1)**, 114-121.

Djomo, J.E., P. Garrigues and J.F. Narbonne. 1996. Uptake and depuration of polycyclic aromatic hydrocarbons from sediment by the Zebrafish (*Brachydanio rerio*). *Environ. Toxicol. Chem.* **15**, 1177-1181.

Draber, D. and A. Trebst. 1986. Inhibitors of photosystem II and the topology of the herbicide and Q_B binding polypeptide in the thylakoid membranes. *Photosynth. Res.* **10**, 381-392.

Drever J.I. 1988. The geochemistry of natural waters, 2nd ed. Englewood Cliffs, NJ: Prentice-Hall.

Duxbury, C.L., D.G. Dixon, and B.M. Greenberg. 1997. The effects of simulated solar radiation on the bioaccumulation of polycyclic aromatic hydrocarbons by the duckweed *Lemna gibba*. *Environ. Toxicol. Chem.* **16,** 1739-1748.

Eadie, B.J. 1984. Distribution of PAHs in Great Lakes, *In* J.O. Nriagu (ed), *Advances in Environmental Science and Technology*. John Wiley and Sons. **14,** 195-211.

Edwards, N.T. 1983. Polycyclic aromatic hydrocarbons (PAH's) in the terrestrial environment-a review. *J. Environ. Qual.* **12,** 427-441.

Fasset, C.N. 1972. *A Manual of Aquatic Plants*, 6th edn. Univ. Wisconsin Press, Madison. 405 pp.

Ferraro, S.P, H. Lee, R.J. Ozretich, and D.T. Specht. 1990. Predicting bioaccumulation potential: a test of a fugacity based model. *Arch. Environ. Contam. Toxicol.* 19, 386-394.

Fletcher, J.S., F.L. Johnson, J.C. McFarlane. 1990. Influence of greenhouse versus field testing and taxonomic differences on plant sensitivity to chemical treatment. *Environ. Toxicol. Chem.* 9, 769-776.

Foote, C.S. 1979. Mechanisms of photooxidation. In Singlet Oxygen, Wasserman HH, Murray RW, Eds., Academic Press, New York, pp. 135-146.

Foote, C.S. 1987. Type I and II mechanisms in photodynamic action. p. 22-38, *In* J.R. Heitz and K.R. Downum (eds), light-activated pesticides. ACS symposium series

339. American Chemical Society, Washington, DC.

Foote, C. S. 1991. **Definition of type I and type II photosensitized oxidation.** *Photochem. Photobiol.* **54, 659.**

Gauger, W.K., J.J. Kilbane, R.L. Kelly and V.J. Srivastava. 1990. **Enhancement of microbial degradation of hydrocarbons in soil and water,** p. 171-203. *In* C. Akin, J. Smith (eds), **Gas, oil, coal and environmental biotechnology, Institute of Gas technology, Chicago, Illinois, USA.**

Gaur JP, and A.K. Singh. 1990. Growth, photosynthesis and nitrogen fixation of Anabaena doliolum exposed to assam crude extract. *Bull Environ. Contam. Toxicol.* **44(3),** 494-500.

Gensemer, R.W., L. Ren, K. Day, K.E. Solomon, and B.M. Greenberg. 1996. Fluorescence induction as a biomarker of creosote phototoxicity to the aquatic macrophyte *Lemna gibba. In* D. Bengtson, and Henschel D.S. (eds), Environmental Toxicology and Risk Assessment: Biomarkers and Risk Assessment, ASTM STP 1306. American Society for Testing and Materials. pp. 163-176.

Gensemer, R.W., D.G. Dixon, and B.M. Greenberg. 2000. Using chlorophyll *a* fluorescence induction to detect the onset of anthracene photoinduced toxicity in *Lemna gibba*, and the mitigating effects of humic acid. Limnology and Oceanography (in press).

Gobas, F.A., L. Lovett-Doust and G.D. Haffner. 1991. A comparitive study of the bioconcentration and toxicity of chlorinated hydrocarbons in aquatic macropytes and

fish. *In* J.W. Gorsuch, W.R. Lower, M.A. Lewis and W. Wang (eds), Plants for toxicity assessment: second volume. STP 1115. American Society for testing and materials, Philadelphia, PA. pp. 178-193.

Goerlitz, D.F., D.E. Trouitman, E.M. Godsy and B.J. Franks. 1985. Migration of woodpreserving chemicals in contaminated groundwater in a sand aquifer at Pensacola, Florida. *Environ. Sci. Technol.* **19**, 955-961.

Graef, W. and H. Diehl. 1966. The natural normal levels of carcinogenic PCAH and the reasons therepf. *Arch. Hyg. Bacteriol.* **150**, 49-59; ca 65, 7604.

Gray, G.R., S.R. Boese, and N.O.A. Huner. 1994. A comparison of low temperature growth vs low temperature shifts to induce resistance to photoinhibition in spanish (*Spinacia oleracea*). *Plant Physio.* **90**, 560-566.

Gray, G.R., L.V. Savitch, A.G. Ivanov and N.P.A. Huner. 1996. Photosystem II excitation pressure and development of resistance to phoyoinhibition: II. Adjustment of photosynthetic capacity in winter wheat and winter rye. *Plant Physiol.* **110**, 61-71.

Greaves, J.A., B.G. Blair, R.M. Russotti, E.A. Law, and N.P. Cloud. 1992. Measurement of chlorophyll fluorescence kinetics in photosynthesis research with a new portable microprocessor and computer operated instrument. CF-1000 Instruction Manual, Morgan Instruments, Inc. Andover, pp. 43-62.

Greenberg, B.M. 1991. Photosynthesis. *In* Y.H. Hui (ed), Encyclopedia of Food Science and Technology. Vol 2. Wiley-Interscience, New York, NY, USA. pp. 2065-2073.

Greenberg, B. M., X-D. Huang, and D.G. Dixon. 1992. Applications of the aquatic higher plant *Lemna gibba* for ecotoxicological assessment. *J. Aquat. Ecosyst. Health* 1, 147-155.

Hall, D.O. and K.K. Rao. 1987. Photosynthesis. E. Arnold, London. UK.

Hall, A. T., and J.T. Oris. 1991. Anthracene reduces reproductive potential and is maternally transferred during long-term exposure in fathead minnows. *Aquatic. Tox.* 19, 249-264.

Halliwell, B., and J.M.C. Gutteridge. 1985. Free Radicals in Biology and Medicine. Clarendon, Oxford, UK.

Hansch C. and A.J. Leo. 1979. Substituent constants for correlation analysis in chemistry and biology. Wiley, New York.

Hansch, C. 1989. Comparative structure-activity relationships. *In* J.L. Fauchere (ed), Quantitative Structure-Activity Relationships in Drug Design. Alan R. Liss, New York. pp.23-30.

Harvey, R.G. 1985. Polycyclic hydrocarbons and carcinogenesis. ACS symposium series 293. *Am. Chem. Soc.*, Washington, D.C.

Hawkins, W.E., W.W. Walker, R.M. Overstreet , J.S. Lytle, and T.F. Lytle. 1990. Carcinogenic effects of some polynuclear aromatic hydrocarbons on the Japanese medaka and guppy in waterborne exposures. *Sci. Total Environ.* 94, 155-167.

Henderson, S. T. 1977. Daylight and its spectrum, Adam Hilger, Bristol, U.K.

Hermens J.L.M., J. De Bruijn, J. Pauly, and W. Seinen. 1987. QSAR studies for fish toxicity data of organophosphorus compounds and other classes of reactive organic compounds, p: 135-152. *In* K.L.E. Kaiser (ed), QSAR in Environmental Toxicology II. Reidel, Dordrecht.

Hermens J.L.M. 1989. Quantitative structure-activity relationships of environemntal pollutants, *In* O. Hutzinger (ed), Handbook of Environmental Chemistry, Vol. 2E. Springer-Verlag, Berlin. pp.111-162.

Hinga, K.R., M.E.Q. Pilson, R.F. Lee, J.W. Farrington, K. Tjessem and A.C. Davis. 1980. Biogeochemistry of benzoanthracene in an enclosed marine ecosystem. *Environ. Sci. Technol.* **14**, 1137-1143.

Hinman, M.L., and S.J. Klaine. 1992. Uptake and translocation of selected organic pesticides by the rooted aquatic plant *Hydrilla verticillata* Royle. *Environ. Sci. Technol.* **26**, 609-613.

Hill, B.H., B.H. McFarland, L. Parrish , and W.T. Willingham. 1993. Introduced tiles versus natural substrates for the assessment of metal impacts on periphyton communities in a Rocky Mountain.. *Bull N. Am. Benthol Soc.* **10**, 191.

Hill, B.H., J.M. Lazorchak, F.H. McCormick, and W.T. Willingham. 1997. The effects of elevated metals on benthic community metabolism in a Rocky Mountain stream. *Environ. Pollut.*

Hillman, W.S. and D.D. Culley, Jr. 1978. The uses of duckweed. *Amer. Sci.* **66**, 442-451.

Hites, R.A., R.E. LaFlamme and J.W. Farington. 1977. Sedimentary polycylic aromatic hydrocarbons: the historical record. *Science.* **198**, 829-831.

Hobson, J. F., D.E. Carter, and D.V. Lightner. 1984. Toxicity of a phthalate ester in the diet of a penaied shrimp. *J. Toxicol. Environ. Health.* **13(4-6)**, 959-968.

Huang, X-D., D.G. Dixon and B.M. Greenberg. 1993. Impacts of UV radiation and photomodification on the toxicity of PAHs to the higher plant *Lemna gibba* (Duckweed). *Environ. Toxicol. Chem.* **12**, 1067-1077.

Huang, X-D., D.G. Dixon, and B.M. Greenberg. 1995. Increased polycyclic aromatic hydrocarbon toxicity following their photomodification in natural sunlight: Impacts on the duckweed *Lemna gibba* L.G-3. *Ecotoxicol. Environ. Saf.* **32**, 194-200.

Huang, X-D., B.J. McConkey, T.S. Babu and B.M. Greenberg. 1997a. Mechanism of photoinduced toxicity of photomodified anthracene to plants: inhibition of photosynthesis in the aquatic higher plant *Lemna gibba* (Duckweed). *Environ. Toxicol. Chem.* **8**, 1707-1715.

Huang, X-D., S.N. Krylov, L. Ren, B.J. McConkey, D.G. Dixon, and B.M. Greenberg. 1997b. Mechanistic quantitative structure-activity relationship model for the photoinduced toxicity of polycyclic aromatic hydrocarbons: II. An empirical model for the toxicity of 16 PAHs to the duckweed *Lemna gibba* L. G-3. *Environ.*

Toxicol. Chem. **16**, 2296-2303.

Hughes, J.S., M.M. Alexander and K. Balu. 1988. An evaluation of appropriate expressions of toxicity in aquatic plant bioassays as demonstrated by the effects of atrazine on algae and duckweed. *In* W.J. Adams, G.A. Chapman and W.G. Landis (eds), Aquatic Toxicology and Hazard Assessment, Vol. 10 *Amer. Soc. Test. Materials*, STP. **971**, 531-547.

Imlay, J., and I. Fridovich. 1992. Exogenous Quinones directly inhibit the respiratory NADH dehydrogenase in *E. coli. Arch. biochem. biophysic.* **296**, 337-346.

James, A. (ed). 1993. An introduction to water quality modeling, 2nd ed. New York: Wiley.

Johnson, A.C. and D. Larsen. 1985. The distribution of polycyclic aromatic hydrocarbons in the surficial sediments of Penbscot Bay (Maine, USA) in relation to possible sources and to other sites worldwide. *Mar. Environ. Res.* **15**, 1-16.

Johnson, M.A. and G.M. Maggiora (eds) 1990. Concepts and application of molecular similarity, Wiley.

Jones, T.W., and L. Winchel. 1984. Uptake and photosynthesis inhibition by atrazine and its degradation products on four species of submerged vascular plants. *J. Environ. Qual.* **13**, 243-247.

Jones, K.C., J.A. Stratford, K.S. Waterhouse, E.T. Furlong, W. Giger, R.A. Hites, C.H. Schaffnert and A.E. Jonston. 1989. Increases in the polunuclear

aromatic hydrocarbon content of an agricultural soil over the last century. *Environ. Sci. Technol.* **23**, 95-101.

Jones, K.C., G. Sanders, S.R. Wid, V. Burnett and A.E. Johnston. 1992. Evidence for a decline of PCBs and PAHs in rural vegetation and air in the United Kingdom. *Nature*. **356**, 137-140.

Jorgensen, S.E. (ed). 1990. Modelling in ecotoxicology modelling. Developments in environmental modelling, 9. New York: Elsevier.

Judy, B.M., W.R. Lower, and M.W. Thomas. 1990a. The chlorophyll fluorescence assay as a rapid indicator of herbicide toxicity. *Proc. South Weed Sci. Soc.* **43**, 358-365.

Judy, B.M., W.R. Lower, C.D. Miles, M.W. Thomas, and G.F. Krause. 1990b. Chlorophyll Fluorescence of a higher plant as an Assay for Toxicity Assessment of Soil and Water, ASTM STP 1091, *In* W. Wang, J.W. Gorsuch, W.R. Lower (eds). American Society for Testing and Materials, Philadelphia.

Judy, B.M., W.R. Lower, F.A. Ireland, and G.F. Krause. 1991. A seedling chlorophyll fluorescence toxicity assay. *In* J.W. Gorsuch, W.R. Lower, W. Wang, M.A. Lewis, (eds), Plants for Toxicity Assessment: Second Volume, ASTM STP 1115, American Society for Testing and Materials, West Conshohocken, PA.

Kaiser, K.L.E. 1984. QSAR in Environmental Toxicology. Reidel, Dordrecht.

Karickhoff, S.W., D.S. Brown and T.A. Scott. 1979. Sorption of hydrophobic pollutants on natural sediments. *Water Res.* **13**, 241-248.

Katz, M., C. Chan, H. Tosine and T. Sakuma. 1979. Relative rates of photochemical and biological oxidation in vitro of polynuclear aromatic hydrocarbons. *In* P.W. Jones and P. Leber (eds), Polynuclear Aromatic Hydrocarbons. Ann Arbor Science, Ann Arbor, MI, USA. pp. 171-189.

Kautsky, H., and A. Hirsch. 1934. Chlorophyllfluoreszenz und kohlensaureassimilation. Das fluoreszenzverhalten gruner pflanzen. *Biochem. Zeitschrift.* **274**, 423-434

Kennish, M.J. 1992. Ecology of estuaries: anthropogenic effects. Boca Raton, FL: CRC Press.

Kim, S-T and A. Sancar. 1993. Photochemistry, photophysics and mechanism of pyrimidine dimer repair by DNA photolyase. *Photochem. Photobiolo.* **57**, 895-904.

Knorr, M. and D. Schenk. 1968. Synthesis of polycyclic aromatic compounds by bacteria. *Arch. Hyg. Bacteriol.* **152**, 282-285.

Krause, G.H. and E. Weis. 1984. Chlorophyll fluorescence as a tool in plant physiology. II. Interpretation of fluorescence signals. *Photosynth. Res.* **5**, 139-157.

Krull, J.N. 1969. Factors affecting die-offs in shallow water areas. *Amer. Midl. Natur.* **82**, 293-295.

Krylov, S.N., X-D. Haung, L.F. Zeiler, D.G. Dixon and B.M. Greenberg. 1997. Mechanistic quantitative structure-activity relationship model for the photoinduced toxicity of polycyclic aromatic hydrocarbons: I. Physical model based on chemical kinetics in a two-compartment system. *Environ. Toxi. Chem.* **16(11)**, 2283-2295.

Kubinyi, H. 1993. Hansch analysis and related approaches. VCH, Weinheim.

Kubinyi, H, and O.H. Kehrhahn. 1978. Quantitative structure activity relationships. IV. Nonlinear dependence of biological activity on hydrophobic character: calculation procedures for the bilinear model. *Arzneim. Forsch. Drug. Res.*, **28**, 598-601.

Kuivasniemi, K, V. Eloranta, and J. Knuuitinen. 1985. Acute toxicity of some chlorinated phenolic compuds to selenastrum capricornutum and phytoplankton. *Arch Environ. Contam. Toxicol.* **14**, 43-49.

Lakowics,. J.R. 1983. Principles of fluorescence spectroscopy. Plenum, New York, NY, USA.

Lamparczyk, H., R.J. Ochocka, J. Grzybowski, J. Halkiewicz and A. Radecki. 1988. Parameters related to pollution by n-alkanes and PAH in baltic water and sediments. *Marine Pollution Bulletin.* **19**, 222-226.

Landolt, E. and R. Kandeler. 1987. *The family of Lemnaceae*. Veroff. Geobot. Inst. Eidg. Tech. Hochschule, Zurich.

Landrum, P.L., L.W. Hayton, H.H. Lee, L.S. McCarty, D. Mackay and J.M. Mckim. 1994. Chapter 3: Synopsis of discussion session on the kinetics behind

environmental bioavailability. Bioavailability: Physical, Chemical, and Biological Interactions, edited by J.L. Hamelink, P.F. Landrum, H.L. Bergman, and W.H. Benson, p. 203-219. SETAC Pellston Workshop Series. Boca Raton, FL: Lewis.

Lanno, R.P., B.E. Hickie, and D.G. Dixon. 1989. Feeding and nutritional considerations in aquatic toxicology. *Hydrobiologia* **188/189**, 525-531.

Larson, R.A., and M.R. Berenbaum. 1988. Environmental phototoxicity "solar ultraviolet radiation affects the toxicity of natural and man-made chemicals". *Enviro. Sci. Tech.* **22(4)**, 354-360.

Lavorel, J. and A-L Etienne. 1977. In vivo chlorophyll fluorescence. In Primary processes of photosynthesis Elsevier, Amsterdam. pp. 203-268.

Lee, L.M., M.V. Novotny and K.O. Bartle. 1981. Analytical chemistry of polycyclic aromatic compounds. Academic Press.

Leffler, J.E., and E. Grunwald. 1969. Rates of Equilibria of organic reactions. Wiley, New York.

Leo, A. 1975. Calculation of partition coefficients useful in the evaluation of the relative hazards of various chemicals in the environment. *In* G.D. Veith and D.E. Konasewich (eds), structure-activity correlations in studies of toxicity and bioconcentration with aquatic organisms. Great lakes Research Advisory Board, Windsor, Ontario. pp. 151-176.

Leo, A. 1991. **Calculating the hydrophobicity of chlorinated hydrocarbon solutes.** *Sci. Total Environ.* **109/110, 121-130.**

Libes, S.M. 1992. **An introduction to marine biogeochemistry.** New York: Wiley.

Lichtenthaler, H.K. and U. Rinderle. 1987. **The role of chlorophyll fluorescence** in the detection of stress conditions in plants. *Crit. Rev. Anal. Chem.* **19, S29-S83.**

Lipnick, R.L., C.S. Pritzker, and D.L. Bentley. 1987a. Application of QSAR to model the toxicology of industrial organic chemicals to aquatic organisms and mammals, *In* D. Hadzi and B. Jerman-Blazic (ed), Progress in QSAR. Elsevier, Amsterdam.

Lipnick, R.L. K.R. Watson, and A.K. Strausz. 1987b. A QSAR study of the acute toxicity of some industrial organic chemicals to goldfish. Narcosis, electrophile and proelectrophile mechanisms. *Xenobiotica*, 17, 1011-1025.

Lipnick, R.L., J.L. Bentley, D.L. Bentlry, and R.C. Myers. 1993. A QSAR based study of the eye irritation of simple alcohols. *Toxicologist.* **13(1), 444.**

Lipnick, R.L. 1995. Strucrure-Activity Relationships, *In* G.M. Rand (ed), Fundamentals of aquatic toxicology: effects, environmental fate, and risk assessment, second edition, Taylor and Francis Ltd. Washington, D.C.

Lovett Doust, L., J. Lovett Doucet, and M. Schmidt. 1993. In praise of plants as biomonitors-send in the clones. *Function Ecol.* **7, 754-758.**

Lovett Doust, J., M. Schmidt, and L. Lovett Doucet. 1994. Biological assessment

of aquatic pollution: a review, with emphasis on plants as biomonitors. *Biol. Rev.* **69**, 147-186.

Lower, W.R., A.G. Underbrink, A.F. Yanders, K. Roberts, T.K. Raney, G. Lombard, D.D. Hemphill, and T. Clevenger. 1984. New methodology for assessing mutagenicity of water and water related sediments. Proceeding of the Second International Conference on Ground –Water Quality Research, Tulsa, OK. pp. 194-196.

Lyman, W.J. 1995. Transport and transformation processes. *In* G.M. Rand (ed), Fundamentals of aquatic toxicology: effects, environmental fate, and risk assessment, second edition, Taylor and Francis Ltd. Washington, D.C.

Mackay, D. and S. Paterson. 1990. Fugacity models, *In* W. Karcher and J. Devilles (eds), Practical Applications of Quantitative Structure-Activity Relationships (QSAR) in Environmental Chemistry and Toxicology. Kluwer Publishing, Dordrecht.pp. 433-460.

Mackay, D. 1991. Multimedia environmental models. The fugacity approach. Boca Raton, FL: Lewis.

Mackay, D., W.Y. Shiu, and K.C. Ma. 1992a. Illustrated handbook of physical-chemical properties and environmental fate for organic chemicals. Vol. II. Polynuclear aromatic hydrocarbons, polychlorinated Dioxins, and Dibenzofurans. Boca Raton, FL: Lewis.

Mackay, D., H. Puig, and L.S. McCarty. 1992b. An equation describing the time

course and variability in uptake and toxicity of narcotic chemicals to fish. *Environ. Toxicol. Chem.* **11**, 941-951.

Malkin, S., W. Bilger, and U. Schreiber. 1994. The relationship between millisecond luminescence and fluorescence in tabacco leaves during the induction period. *Photosyn. Res.* **39**, 57-66.

Mallakin, A., B.J. McConkey, G. Miao, B. Mckibben, V. Snieckus, D.G. Dixon and B.M. Greenberg. 1999. Impacts of structural photomodification on the toxicity of environmental contaminants: anthracene photooxidation products. *Ecotox. Environ. Safe.* **43**, 204-212.

Mallakin, A., D.G. Dixon and B.M. Greenberg. 2000. Pathway of anthracene modification under simulated solar radiation. *Chemosphere,* **40(12)**, 131-137.

Manny, B.A., and D. Kenaga. 1991. The Detroit River: effects of contaminants and human activities on aquatic plants and animals and their habitats. *Hydrobiologia,* **219**, 269-279.

Martin, Y.C., E. N. Bush, and J.J. Kyncl. 1990. Quantitative description of biological activity. *In* C. Hansch (ed. Board chairman), Comprehensive Medical Chemistry, Vol. 4. Pergamon Press, Oxford.

May, W.S., S.P. Wasik, and D.H. Freeman. 1978. Determination of the solubility behaviour of some polycyclic aromatic hydrocarbons in water. *Anal. Chem.* **50**, 175-179.

McCarty, J.F., and L.R. Shugart. 1990. Biomarkers of environemntal contamination. **Boca Raton, FL: Lewis.**

McCarty, L.S., D. Mackay, A.D. Smith, G.W. Ozburn, and D.G. Dixon. 1992. Residue-based interpretation of toxicity and bioconcentration QSARs from aquatic bioassays: neutral narcotic organics. *Environ. Toxicol. Chem.* **11**, 917-930.

McConkey, B.J., C.L. Duxbury, D.G. Dixon, and B.M. Greenberg. 1997. Toxicity of a PAH photooxidation product to the bacteria *Photobacterium phosphoreum* and the duckweed *Lemna gibba*: effects of phenanthrene and its primary photoproduct, phenanthrenequinone. *Environ. Toxicol. Chem.* **16**, 892-899.

Mckee, P., A. Burt, D. McCurvin, D. Hollinger, D. Sutherland and W. Neaves. 1990. Levels of dioxins, furans and other organic contaminants in harbour sediments near a wood preserving plant using pentachlorophenol and creosote. *Chemosphere.* **20**, 1679-1685.

McVey, M., and B.A. Macler. 1993. Ecological risk assessment case study: selenium effects at Kesterson Reservoir. *In* A review of Ecological Assessment Case Studies from a Risk Assessment Perspective, EPA/630/R-92/005, U.S. Environmental Protection Agency, Washington, D.C.

Means, J.C., S.G. Wood, J.J. Hasett, and W.L. Banwart. 1980. Sorption of polynuclear aromatic hydrocarbons by sediments and soils. *Environ. Sci. Technol.* **14**, 1524-1529.

Mekenyan, O. G., G.T. Ankley, G.D. Veith, and D.J. Call. 1994. QSAR for photoinduced toxicity: I. Acute lethality of polycyclic aromatic hydrocarbons to *Daphnia magna*. *Chemosphere* **28**, 567-582.

Mezey, P.G. 1986. Theory of reaction mechanisms and molecular design. *J. Mol. Struct., Theochem*, **138**, 13-21.

Mezey, P.G. 1987. The shape of molecular charge distributions: group theory without symmetry. *J. Comput. Chem.* **8**, 462-469.

Mezey, P.G. 1990. Topological Quantum Chemistry. *In* H. Weinstein and G. Naray-Szabo (eds), reports in molecular theory. CRC Press, Boca Raton, Vol. 1, pp 156-183.

Mezey, P.G. 1992. Dynamic shape analysis of biomolecules using topological shape codes. *In* J. Bertan (ed), The role of computational models and theories in biothechnology. Kluwer Academic Publishers, Dordrecht, pp 83-104.

Mezey, P.G. 1993. Shape in Chemistry; An Introduction To Molecular Shape and Topology. VCH Publishers, Inc.

Mezey, P. G. 1995. Methods of molecular shape-similarity analysis and topological shape design. *In* P.M. Dean (ed.), Molecular Similarity in Drug Design. Chapman & Hall-Blackie Publishers, Glasgow, U.K., pp. 241-268.

Mezey, P. G., Z. Zimpel, P. Warburton, P.D. Walker, D. Irvine, D. G., Dixon and B.M. Greenberg. 1996. A high-resolution shape-fragment MEDLA database for toxicological shape analysis of PAHs. *J. Chem. Inf. Comp. Sci.* **36**, 602-611.

Mezey, P.G. and P.D. walker. 1997. Fuzzy molecular fragments in drug research. *Drug Discovery Today (Elsevier Trend Journal).* **2,** 6-11.

Mezey, P.G., Z. Zimpel, P. Warburton, P.D. Walker, D.G. Irvine,X-D. Huang, D.G. Dixon and B.M. Greenberg. 1998. Use of QShAR to model the photoinduced toxicity of PAHs: Electron density shape features accurately predict toxicity. *Environ. Toxicol. Chem.* **17,** 1207-1215.

Miles, D. 1990. The role of chlorophyll Fluorescence as a Bioassay for Assessment of Toxicity in Plants., ASTM STP 1091, *In* W. Wang, J.W. Gorsuch, W.R. Lower (eds), American Society of Testing and Materials, Philadelphia.

Mihelic, J.R. and R.G. Luthy. 1991. Sorption and microbial degradation of naphthalene in soil-water suspension under denitrification conditions. *Environ. Sci. Technol.* **25,** 169-177.

Montgomery, J.H. and L.M. Welkom. 1990. Ground water chemicals desk reference. Levis Publ.

Morgan, D.D., D. Warshawsky, and T. Atkinson. 1977. The relationship between carcinogenic activities of polycyclic aromatic hydrocarbons and their singlet, triplet, and singlet-triplet splitting energies and phosphorescence lifetimes. *Photochem. Photobiol.* **25,** 31-38.

Morgan, P. and R.J. Watkinson. 1989. Hydrocarbon degradation in soils and methods for soil biotreatment. *Crit. Rev. Biotechnol.* **8,** 305-333.

Morselli, L., and S. Zappoli. 1988. PAH determination in samples of environmental interest. *Sci. Total Environ.* **73**, 257-266.

Muir, D.C.G., G.P. Rawn and N.P. Grift. 1985. Fate of the pyrethroid insecticide deltamethrin in small ponds: a mass balance study. *J. Agric. Food Chem.* **33**, 603-609.

Nakatani, H.Y., and Barber J. 1977. An improved method for isolating chloroplasts retaining their outer membranes. *Biochim Biophys Acta.* **461(3)**, 500-512.

Nakhimovsky, L. 1989. Handbook of low temperature electronic spectra spectra of polycyclic aromatic hydrocarbons. Elsevier, Amsterdam, The Netherland.

Neff, J.M. 1979. Polycyclic Aromatic Hydrocarbons in the Aquatic Environment: Sources, Fate and biological Effects. Applied Science, London, UK.

Nendza, M. 1991. QSARs of bioconcentration: validity assessment of log P_{ow}/log BCF correlations. *In* R. Nagel and R. Loskill (eds), Bioaccumulation in Aquatic Systems: Contributions to the Assessment. VCH, Weinheim, pp. 43-66.

Nestler, J. 1974. Characteriazation of wood-preserving coal tar creosote by gas-liquid chromatography. *Anal. Chem.* **46**, 46-53.

Newsted, J. L., and J.P. Giesy. 1987. Predictive models for photoinduced acute toxicity of polycyclic aromatic hydrocarbons to *Daphnia magna*, Strauss (Cladocera, Crustacea). *Environ. Toxicol. Chem.* **6**, 445-461.

Nikolaou, K., P. Masclet, and G. Mouvier. 1984. Sources and chemical reactivity

of polynuclear aromatic hydrocarbons in the atmosphere-A critical review. *Sci. Total Environ.* **32**, 103-132.

Oettmeier, W., K. Masson and A. Donner. 1988. Anthraquinone inhibitors of photosystem II electron transport. *FEBS Lett.* **321**, 259-262.

Oettmeier, W. 1999. Herbicide resistance and supersensitivity in photosystem II. *Cell Mol Life Sci.* **55(10)**, 1255-1277.

Ogren, E., and N.R. Baker. 1985. Evaluation of a technique for the measurement of chlorophyll fluorescence from leaves exposed to continous light. *Plant Cell Environ.* **8**, 539-547.

Oquist, G., and R. Wass. 1988. A portable microprocessor operated instrument for measuring chlorophyll kinetics in stress physiology. *Physiol. Plant.* **73**, 211-217.

Oris, J.T., and J.P. Giesy. 1985. The photoenhanced toxicity of anthracene to juvenile sunfish (Lepomis spp.). *Aquat. Toxicol.*, **6**, 133-146.

Outridge, P.M. and B.N. Noller. 1991. Accumulation of toxic trace elements by fresh-water vascular plants. *Rev. Environ. Contam. Toxicol.* **121**, 1-63.

Papageorgiou, G. 1975. Chlorophyll fluorescence: an intrinsic probe of photosynthesis. *In* Bioenergetics of Photosynthesis, Academic Press, New York. pp. 319-371.

Pearlman, R.S., S.H. Yalkowsky and S. Banerjee. 1984. Water solubilities of

polycyclic aromatic and heteroaromatic compounds. *J. Phys. Chem. Ref. Data.* **13**, 555-562.

Peterson, H.G., N. Nyholm. 1993. Algal bioassays for metal toxicity identification. *Water Pollut. Res. J. Can.* **28**,129-153.

Pierce, R.C., S.P. Mathur, D.T. Williams, and M.J. Boddington. 1980. Phthalate esters in the aquatic environment. National Research Council Canada, NRCC publication number 17583, 180.

Powles, S.B. 1984. Photoinhibition of photosynthesis induced by visible light. *Annu Rev. Plant. Physiol.* **35**, 14-44.

Purcell, W.P., E.G. Bass, and J.M. Clayton. 1973. Strategy of Drug Design: A Guide to Biological Activity. New York: Wiley-Interscience.

Radding, S.B., T. Mill, C.W. Gould, D.H. Liu, H.L. Johnson, D.C. Bomberger and C.V. Fojo. 1976. The environmental fate of selected polynuclear aromatic hydrocarbons. Prepared for EPA, Washington, D.C.

Rand, G.M., P.G. Wells, and L.S. McCarty. 1995. Introduction to aquatic toxicology,. *In* G.M. Rand (ed), Fundamentals of aquatic toxicology: effects, environmental fate, and risk assessment, second edition, Taylor and Francis Ltd. Washington, D.C.

Readman, J.W., R.F.C. Mantoura and M.M. Rhead. 1984. The physico-chemical speciation of polycyclic aromatic hydrocarbons (PAH) in aquatic system. *Fresenius*

Z. Anal. Chem. **319**, 126-131.

Ren, L., X-D, Huang, B.J. McConkey, and D.G. Dixon. 1994. Photoinduced toxicity of three polycyclic aromatic hydrocarbons (fluoranthene, pyrene, naphthalene) to the duckweed *Lemna gibba* L.G-3. *Ecotoxicol. Environ. Saf.* **28**, 160-171.

Richards, F.M. 1977. *Annu. Rev. Biophys. Bioeng.* **6**, 151.

Robinson, J., and J.M. Cooper. 1970. Method of determining oxygen concentration in biological media, suitable for calibration of the oxygen electrode. *Anal. Biochem.* **33**: 390-399.

Rodgers, Jr., J.H., D.S. Cherry and R.K. Guthrie. 1978. Cycling of elements in duckweed (*Lemna perpusilla*) in an ash settling basin and swamp drainage system. *Water Res.* **12**, 765-770.

Sabljic A. 1990. Topological indices and environmental chemistry, *In* W. Karcher and J. Devillers (eds), Practical Applications of Quantitative Structure-Activity Relationships (QSAR) in Environmental Chemistry and Toxicology, Dordrecht: Kluwer. pp. 61-82.

Samiullah, Y. 1990. Prediction of the environmental fate of chemicals. New York: Elsevier Applied Science.

Scheehan, P., F. Korte, W. Klein, and P. Bourdeau. 1984. Effects of pollutants at the ecosystem level. SCOPE 22. Chichester, Wiley.

Schoney, R., T. Codey, D. Warshawsky, and M. Radike. 1988. Metabolism of mutagenic polycyclic aromatic hydrocarbons by photosynthetic algal species. *Mutat. Res.* 197, 289-302.

Schreiber, U., L. Grobermann, and W. Vidaver. 1975. A potable, solid state fluorometer for the measurement of chlorophyll fluorescence induction in plants. *Rev. Sci. Instrum.* 46, 538-542.

Schreiber, U. 1986. Detection of rapid induction kinetics with a new type of high frequency modulated chlorophyll fluorometer. *Photosynth . Res.* 9, 262-272.

Schrimer, K., J.S. Herbrick, B.M. Greenberg, D.G. Dixon, and N.C. Bols. 1999. The use of fish gill cells in culture to evaluate the cytotoxicity and photocytotoxicity of intact and photomodified creosote. *Environ. Toxicol. Chem.* 18(6), 1277-1297.

Scully, N.M., D.R.S. Lean, D.J. McQueen, and W.J. Cooper. 1995. Photochemical formation of hydrogen peroxide in lakes: Effects of dissolved organic carbon and ultraviolet radiation. *Can. J. Fish. Aqua. Sci.* 52(12), 2675-2681.

Shiaris, M.P. 1989. Seasonal biotransformation of naphthalene, phenanthrene, and benzo(a)pyrene in surficial estuarine sediments. *Appl. Environ. Microbiol.* 55, 1319-99.

Shimp, R.J., R.J. Larson, and R.S. Boethling. 1990 Use of biodegradation data in chemical assessment. *Environ. Toxicol. Chem.* 9, 1369-1377.

Sims, R.C. and M.R. Overcash. 1983. Fate of polycyclic aromatic compounds

(RNAs) in soil-plant systems. Residue Reviews. 88, 2-6.

Sims, J.L., R.C. Sims, and J.E. Matthews. 1990. Approach to bioremediation of contaminated soil. *Hazard. Waste. Hazard. Mater.* 7, 117-149.

Southworth, G.R. 1977. Transport and transformation of anthracene in natural waters: Process rate studies. Oak Ridge, Tennessee: Department of Energy (ORNL).

Smith, J.H., W.R. Mabey, N. Bohonos, B.R. Holt, S.S. Lee, T-W. Chou, D.C. Bomberger and T. Mill. 1978. Environmental pathways of selected chemicals in freshwater system; part II: laboratory Studies. US Environmental Protection Agency, Athens, Ga. EPA-600/7-78-074.

Stevens, B, R.D. Small, Jr, and S.R. Perez. 1974. The photoperoxidation of unsaturated organic molecules. XIII. O2AG quenching by alpha-tocopherol. Photochem Photobiol. **20(6)**, 515-7517.

Stucki G. and M. Alexander. 1987. Role of dissolution rate and solubility in biodegradation of aromatic compounds. *Appl. Environ. Microbiol.* **53**, 292-297.

Suess, M.J. 1976. The environmental load and cycle of polyaromatic hydrocarbons. *Sci. Total Environ.* **6**, 239-250.

Tanford, C. 1980. The Hydrophobic Effect: Formation of micelles and biological membranes, 2nd ed. New York: Wiley-Interscience.

Taylor, P.J. 1990. Hydrophobic properties of drugs. Comprehensive Medicinal

Chemistry, *In* C. Hansch (ed Board chairman), Vol.4.Oxford: Pergamon.

Thomas, R.G. 1982. Volatilization from water. Handbook of Chemical Property Estimation Methods, chapter 15. New York: McGraw-Hill.

Thompson, R.H. 1971. Naturally occurring quinones. 2nd ed. London, Butterworths Scientific Publ.

Trebst A, and E. Harth. 1974. Structure-activity-relationship of inhibitors of photosynthetic electron flow. Herbicidal N-alkylated-ureas and ringclosed N-acylamides as inhibitors of photosystem II. *Z Naturforsch [C]. Z Naturforsch [C]* 29(5-6), 232-235.

Tridech, S., A.J. Englande, Jr., M.J. Herbertt and R.F. Wilkinson. 1981. Tertiary wastewater treatment by the application of vascular aquatic plants. *Chem. Water Reuse.* 2, 521-539.

Turbak, S.C., S.B. Olson, and G.A. McFeters. 1986. Comparison of algal assay systems for detecting waterborne herbicides and metals. *Water. Res.* 20, 91-96.

Turner, J.E., M.W. English, T.W. Schultz and N.J. Kvaak. 1988. QSAR88, Oak Ridge, TN: U.S. Dept. of Energy, NTIS CONF-880520-(DE8813180).

Tute, M.S. 1990. History and objectives of quantitative drug design. Comprehensive Medicinal Chemistry, *In* C. Hansch (ed board chairman), Vol. 4, pp.1-31.

U.S. Code of Federal Regulations. 1991. Title 40, Part 423, Appendix A - 129

Priority pollutants, July 1, 1991.

Valvani S.C. and S.H. Yalkowsky. 1980. Physical chemical properties of drugs, *In* S..H. Yalkowsky; A.A. Sinkula and S.C. Valvani.(eds), New York: Marcel Dekker.

Van kooten, O. and J.F.H. Snel. 1990. The use of chlorophyll fluorescence nomenclature in plant stress physiology. *Photosynth. Res.* **25**, 147-150.

Veith, G.D., D.J. Call, and L.T. Brooke. 1983. Structure-toxicity relationships for the fathead minnow, *Pimephales promelas*: narcotic industrial chemicals. *Can. J. Fish. Aquat. Sci.* **40**, 743-748.

Versteeg, D.J. 1990. Comparison of short- and long-term toxicity test results for the green alga, Selenastrum capricornutum. *In* W. Wang, J.W. Gorsuch, W.R. Lower (ed), ASTM STP 1091, Plants for Toxicity Assessment, American Society for Testing and Materials, Philadeplphia.

Virgin, I., B. Andersson, and E-M. Aro. 1993. Photoinhibition of photosystem II. Inactivation, protein damage and turnover. *Biochim. Biophys. Acta.* **1143**, 113-134.

Walker, P.D., G.A. Arteca and P.G. Mezey. 1991. A complete shape characterization for molecular charge densities represented by Guassian-type functions. *J. Comput. Chem.* **12**, 220-230.

Walker, P.D. and P.G. Mezey. 1993. Molecular electron density lego approach to molecule building. *J. Amer. Chem. Soc.* **115**, 12423-12430.

Walker, P.D. and P.G. Mezey. 1994. *Ab initio* quality electron densities for proteins: A MEDLA Approach. *J. Amer. Chem. Soc.* **116,** 12022-12032.

Walker, P.D. and P.G. Mezey. 1995. Towards similarity measures for macromolecular bodies: MEDLA test calculations for substituted benzene systems. *J. Comput. Chem.* **16,** 1238-1249.

Walsh, G.E., E.D. Weber, T.L. Simon, L.K. Brashers, and J.C. Moore. 1991. Use of marsh plants for toxicity testing of water and sediment. *In* J.W. Gorsuch, Lower W.R., Lewis, M.A., Wang W. (eds), Plants for Toxicity Assessment: *Second Volume*, ASTM STP 1115, American Society of Testing and Materials, Philadelphia.

Wang, X., and V. Snieckus. 1990. Regioselective synthesis of substituted anthraquinones by tandem directed *ortho* metalation-metal halogen exchange. *Synlett* 6, 313-316.

Wang, W. 1991. Higher plants (common duckweed, lettuce and rice) for effluent toxicity assessment. *In* J.W. Gorsuch, Lower W.R., Lewis, M.A., Wang W. (eds), Plants for Toxicity Assessment: *Second Volume*, ASTM STP 1115, American Society of Testing and Materials, Philadelphia.

Wang W. and K. Freemark. 1995. The use of plants for environmental monitoring and assessment. *Ecotoxicol. Environ. Saf.* **30,** 289-301.

Weinstein, L.H., J.A. Laurence, R.H. Mansl, K. Walti. 1990. The use of native and cultivated plants as bioindicators and biomonitors of pollution damage. *In* Wang, W., J.W. Gorsuch, W.R. Lower (eds), Plants for Toxicity Assessment, ASTM STP

1091, American Society of Testing and Materials, Philadelphia.

Wild, S.D., J.P. Obbard, C.I. Munn, M.L. Berrow and K.C. Jones. 1991. The long term persistence of polynuclear aromatic hydrocarbons (PAHs) in an agricultural soil amended with metal-contaminated sewage sludges. *Sci. Total Environ.* **101**, 235-253.

Wild, S.D., D.J. Mitchell, C.M. Yelland and K.C. Jones. 1992. Arrested municipal solid waste incinerator fly ash as a source of polynuclear aromatic hydrocarbons (PAHs) to the environmnet. *Waste Mgmt. Res.* **10**: 99-111.

Young, R.H. and D.R. Brewer. 1976. The mechanism of quenching of singlet oxygen. *In* A.P. Schaap, ed., *Singlet Molecular Oxygen.* Dowden, Hutchinson & Ross, Stroudsburg, PA.

Zepp, R.G., and P.F. Schlotzhauer. 1979. Photoreactivity of selected aromatic hydrocarbons in water. p. 141-158, *In* P.W. Jones and P. leber (eds), Polynuclear Aromatic Hydrocarbons. Ann Arbor Science Publishers, Ann Arbor, MI.